VARIATIONAL AND AUXILIARY FIELD MONTE CARLO FOR THE HUBBARD AND HUBBARD-HOLSTEIN MODELS:

AN ACCURATE FINITE-SIZE SCALING AND A ”SIGN PROBLEM” SOLUTION

A THESIS SUBMITTED IN FULFILLMENT OF THE REQUIREMENTS

FOR THE DEGREE OF DOCTOR OF PHILOSOPHY

IN

CONDENSED MATTER THEORY

Author:	Advisor:
Seher Karakuzu	Prof. Sandro Sorella

October 2018

ABSTRACT

VARIATIONAL AND AUXILIARY FIELD MONTE CARLO FOR THE HUBBARD AND HUBBARD-HOLSTEIN MODELS:

AN ACCURATE FINITE-SIZE SCALING AND A ”SIGN PROBLEM” SOLUTION

Seher Karakuzu
Ph.D. in Condensed Matter Theory
Advisor: Prof. Sandro Sorella
October 2018

Understanding the properties of strongly correlated materials is a tough work since most of the times analytical tools cannot be applied due to the complicated nature of the problem. Here we apply quantum Monte Carlo techniques in order to tackle one of the most important and unknown phenomena of many materials: the mechanism of superconductivity. We study the Hubbard-Holstein model which is one of the most simple theoretical models including strong correlation and electron-phonon coupling. By using twist-averaging boundary conditions we eliminate finite-size errors in the Monte Carlo simulations. With this useful tool we first solve the Hubbard-Holstein model by variational Monte Carlo by reporting the phase diagram of the model for different phonon frequencies at half filling. Then we investigate the phase separation away from half filling. Finally we try to attack the problem with an essentially unbiased method based on the auxiliary field quantum Monte Carlo technique and accelerated Langevin dynamics. By curing the sign problem via Cauchy integration in the complex plane where the auxiliary fields have been defined, we report the effect of the electron-phonon coupling on some observables such as magnetization, spin and charge structure factors. We show preliminary results that are already meaningful to understand the nature of the transition between magnetism and charge order in the model at half filling.

Keywords: Hubbard-Holstein Model, Twist averaging, Variational Monte Carlo, Auxiliary Field Quantum Monte Carlo, Molecular Dynamics, Path Integral Monte Carlo, Langevin Dynamics.

PUBLICATION LIST

- M. Dagrada, S. Karakuzu, V. Vildosola, M. Casula, and S. Sorella, Exact special twist method for quantum monte carlo simulations, Phys. Rev. B., 24, 245108 (2016).

- S. Karakuzu, L. F. Tocchio, S. Sorella and F. Becca, "Superconductivity, charge-density waves, antiferromagnetism, and phase separation in the Hubbard-Holstein model" , Phys. Rev. B., 96, 205145 (2017) .

- S. Karakuzu, K. Seki, S. Sorella , "Study of the superconducting order parameter in the negative-U 2D-Hubbard model by grand-canonical twist-averaged boundary conditions", Phys. Rev. B., 98, 075156 (2018) .

- S. Karakuzu, K. Seki, S. Sorella , "Solution of the "sign problem" for the half filled Hubbard-Holstein model" ,arXiv:1808.07759.

Acknowledgement

I would like to thank my advisor Prof. Sandro Sorella for his support, guidance and for the time he spent for me during my PhD.

I would like to thank Prof. Michele Casula and Prof. Seiji Yunoki for taking the time to read my thesis and for their valuable feedback.

Contents

Chapter 1

Introduction

Understanding the interplay between electron-electron and electron-phonon interactions is a very challenging task. There has been an intense work in the condensed-matter community, since the early developments of many-body approaches to describe metals, insulators, and superconductors [1]. It is known that the low-temperature properties of several materials are controlled by the competition or sometimes the cooperation between electron-electron and electron-phonon interaction terms. For example, high-temperature superconductors, such as Cuprates and Iron based superconductors have phase diagrams as shown in the Fig. 1.1. In both kind of materials there exists a clear evidence of strong electron-electron correlation. On the other hand, it has been observed that the role of phonons could be not entirely negligible, as suggested by the kinks in the electron dispersion [2] or by the signatures of the isotope effect [3, 4]. In alkali-doped fullerides, which are often known to be phononic superconductors, it has been observed the existence of a superconducting phase close to a Mott transition [5, 6]. Therefore, this particular feature suggests that both the Coulomb repulsion and the electron-phonon coupling are taking place in the mechanism of superconductivity. They are both strong and cooperate to establish a strongly-correlated superconductor. Similarly, in pnictide superconductors [7], such as LaOFeAs, and in aromatic superconductors, such as potassium-intercalated picene [8], there are evidences that, in addition to the strong electron-electron correlation, there is also a non-negligible electron-phonon where electrons couple with the lattice degrees of freedom.

In a short and simple summary, electron-electron repulsion generates spin fluctuations that mediate a non-local pairing among electrons and may give rise to d-wave superconductivity. On the other hand, electron-phonon coupling directly mediates a local attraction among electrons which results in an s-wave superconductor. In addition to that, a strong electron correlation may also lead to spin-density waves and a magnetically ordered state, which competes with superconductivity; instead, a local attraction may also generate charge localization, i.e., charge-density-wave (CDW) or dimerized (Peierls) states. Therefore, it is a very complicated task to obtain the properties of a system in which both interactions are relatively strong and competing each other. Among many theoretical models, in this respect, the Hubbard-Holstein model represents a good prototypical one that includes both electron-electron interaction and also electron-phonon coupling.

1.1 Hubbard-Holstein Model

The Hubbard-Holstein model is one of the simplest models including both electron-electron interaction and also electron-phonon coupling. It incorporates the electron-electron interaction as an on-site Coulomb repulsion U (the Hubbard term) [9] and the electron-phonon coupling g between electrons and dispersionless Einstein phonons with energy ω_0 (the Holstein terms) [10], and also a kinetic term for electrons:

$$\mathcal{H} = -t \sum_{\langle i,j \rangle,\sigma} (c^{\dagger}_{i,\sigma} c_{j,\sigma} + \text{h.c.}) + U \sum_{i} n_{i,\uparrow} n_{i,\downarrow} + \omega_0 \sum_{i} b^{\dagger}_{i} b_{i} + g_0 \sum_{i} n_i (b^{\dagger}_{i} + b_{i}),$$

where $\langle i, j \rangle$ indicate nearest-neighbor sites (on a square lattice); moreover, on a given site i, $c^{\dagger}_{i,\sigma}$ ($c_{i,\sigma}$) creates (destroys) an electron with spin σ, $b^{\dagger}_{i}$ (b_{i}) creates (destroys) a phonon, and $n_i = \sum_{\sigma} n_{i,\sigma} = \sum_{\sigma} c^{\dagger}_{i,\sigma} c_{i,\sigma}$ is the electron density. In analogy, we also define the phonon density on the site i by $m_i = b^{\dagger}_{i} b_{i}$. Of course, this model gives a simplified description of real solids, since both the

Coulomb repulsion and the electron-phonon interaction are assumed to be local. In addition, the latter term is modeled by coupling the lattice displacement $x_i \propto (b_i^\dagger + b_i)$ to the electron *density* n_i.

The physical properties of the Hubbard-Holstein model are determined by the parameters ω_0/t and g_0/t independently. However, it is useful to define the quantity $\lambda = 2g_0^2/\omega_0$, which is often considered to be the strength of the electron-phonon coupling. When $\omega_0/t \to \infty$, i.e in the antiadiabatic limit where the phonons have a large energy, this parameter measures the effective electron-electron attraction since in this case the retarded interaction mediated by phonons becomes instantaneous. Indeed, for $\omega_0 \gg t$ there is an exact mapping from the Holstein model to the negative-U Hubbard model with $U_{\rm att} = -\lambda$. Therefore, the Hubbard-Holstein model reduces to the Hubbard model with a renormalized on-site interaction, i.e., $U_{\rm eff} = U - \lambda$. On the other hand when w_0 is of the order of the electron hopping t such an exact mapping between the two models does no longer holds. Therefore, in the general case with a finite phonon energy, the multidimensional parameter space of the Hubbard-Holstein model with U/t, g_0/t, ω_0/t, as well as the electron density n results in an extremely rich physics and various approaches have been used to understand its ground-state properties.

One can also write the model in terms of the phonon position and momentum degrees of freedom by the following transformation:

$$\hat{X} = \frac{1}{\sqrt{2}}(b_i^\dagger + b_i), \tag{1.1}$$

and

$$\hat{P} = i\frac{1}{\sqrt{2}}(b_i^\dagger - b_i), \tag{1.2}$$

The resulting expression of the Hamiltonian is written as follows:

$$\mathcal{H} = -t\sum_{\langle i,j\rangle,\sigma}(c_{i\sigma}^\dagger c_{j\sigma} + h.c) + \frac{U}{2}\sum_j (n_j-1)^2 + g\sum_j \hat{X}_j(n_j-1) + \frac{w_0}{2}\sum_j\left(\hat{X}_j^2 + \hat{P}_j^2\right). \tag{1.3}$$

with $g = \sqrt{2}g_0$. Therefore, for this representation we have the coupling constant as $\lambda = g^2/w_0$.

Another way of introducing the electron-phonon coupling has been considered within the Su-Schrieffer-Heeger model [11], in which the lattice displacements are coupled to the hopping term rather than to the local density. The Su-Schrieffer-Heeger model is more suitable to describe materials with delocalized phonons, whereas the Holstein model can be used as a good approximation for molecular solids in which there are local phonon modes like in the case of fullerene molecules doped with alkali-metal atoms.

1.2 Numerical Simulations

Computer simulations are very useful tools available to solve very complicated problems. In many theoretical models, such as the Hubbard-Holstein model, that cannot be solved through analytical treatments, the use of computer simulations are most common. The phase diagram of the Hubbard-Holstein model has been studied using several techniques such as, Gutzwiller approximation [12], variational Monte Carlo (VMC) [13], dynamical mean-field theory (DMFT) [14, 15, 16], finite-temperature determinant quantum Monte Carlo (DQMC) [17, 18, 19], also in 1D [20], but no unbiased zero temperature calculation is known in 2D. In this thesis we will make an attempt to understand the ground state properties of the 2D Hubbard-Holstein model by using numerical tools. First, we will apply variational monte carlo method and then auxiliary field quantum monte carlo with accelerated Langevin dynamics. All these techniques, mainly developed in this thesis, will be explained in details in the upcoming chapters.

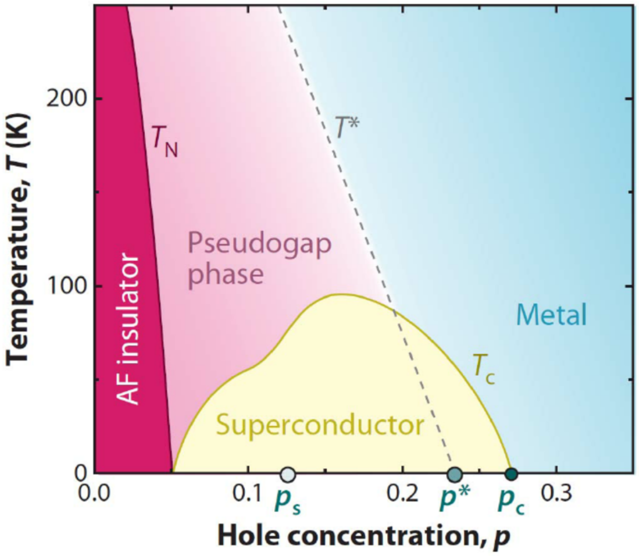

(a) L. Taillefer , Ann. Rev. , 1, 51-70 (2010).

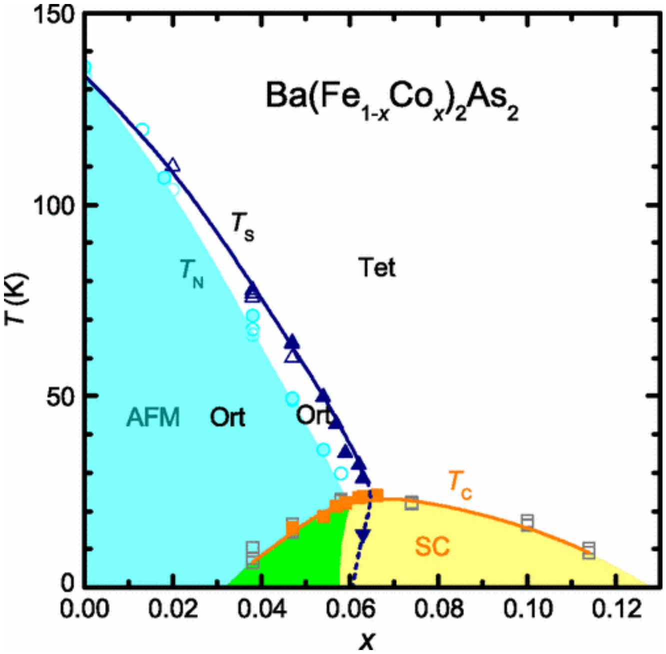

(b) S. Nandi et all. Phys. Rev. Lett. 104, 057006 (2010).

Figure 1.1: An example of the phase diagram of Cuprates (top) and Iron-based supercondcutors (bottom).

1.3 Outline of the Thesis

In the 2nd Chapter an overview of Variational Monte Carlo (VMC) and stochastic reconfiguration techniques will be given. The variational Ansatz for the Hubbard and the Hubbard-Holstein models will be introduced.

In Chapter 3 technical details about auxiliary field quantum Monte Carlo (AFQMC) and the accelerated first order Langevin dynamics will be discussed. Some benchmark tests and results will be reported for the pure Holstein model via accelerated Langevin Dynamics. After introducing the Hubbard interaction we will consider the corresponding Hubbard-Holstein model by employing for the first time to our knowledge an exact integration scheme allowing the elimination of the phonon degrees of freedom. The resulting complex integration in the electronic fields will be moved to the real axis via the Cauchy theorem. Then, some benchmark results will be introduced for the pure Hubbard model.

In Chapter 4 twist averaging boundary conditions in grand canonical ensembles will be introduced and applied to the negative-U Hubbard model both by VMC and AFQMC methods. Some benchmark comparisons and results will be reported for the negative-U Hubbard model at half filling and at finite doping and in the weak coupling regime.

In Chapter 5 the VMC method will be applied to the Hubbard-Holstein model by using twist averaged boundary conditions. The phase diagram of the model will be reported at half filling for different phonon frequencies and phase separation will be investigated at finite hole doping.

In Chapter 6 the accelerated first order Langevin dynamics will be applied to the Hubbard-Holstein model. Therefore, stochastically exact ground state properties in the thermodynamic limit of the model will be reported without sign problem for the first time.

In Chapter 7 the thesis will be concluded by discussing the main outcomes of this PhD thesis.

Chapter 2

Variational Monte Carlo

The most important and successful algorithm for computing large multi dimensional integrals is certainly the Monte Carlo (MC) method. For many physical problems it is very hard to do analytical integrations due to the very large number of degrees of freedom. However, by using MC one can perform these hard integrations via stochastic sampling over configuration space. A configuration space provides information about degrees of freedom in the system. For example, for the system of spinless particles the configuration space $|x\rangle$ is given by the positions of the particles. Another example is the system of electrons in which the configuration space can provide information about both the spin and the positions of electrons in the system. The MC method is determined by well defined stochastic algorithms, usually named Markov process. According to this method one can change randomly the degrees of freedom like spin or positions of the particles in the configuration space. After this operation the change (the move) is accepted or rejected according to the Metropolis acceptance criterium [21]. The main ingredient of Variational Monte Carlo (VMC) is a trial wave function and the fact that the expectation value of a Hamiltonian over any trial wave function provides an upper bound for the exact ground state energy.

$$E = \frac{\langle \Psi_T | \mathcal{H} | \Psi_T \rangle}{\langle \Psi_T | \Psi_T \rangle} \geq E_0. \tag{2.1}$$

Therefore, in VMC the main aim is to construct a trial state which is close to the exact ground state wave function. In VMC the wave function should at least have the same qualitative properties of the system of interest. For the fermionic system, such as electrons, the wave function should satisfy the anti-symmetry properties of the electrons. Thereby one can represent a part of the wave function as a Slater determinant which can be constructed from the ground state of a mean field Hamiltonian. A correlator or a projector to fix the particle number is also generally added as a Jastrow term taking into account the correlation between the electrons. Therefore, the general trial wave function $|\psi_T\rangle$ to be considered can be written as:

$$|\psi_T\rangle = \mathcal{P}|\mathcal{D}\rangle, \tag{2.2}$$

where $\mathcal{P}$ is the projector over a fixed particle number and/or correlator, whereas $\mathcal{D}$ is the uncorrelated antisymmetric determinant part. Expectation value of any operator can be calculated as

$$\langle \mathcal{O} \rangle = \frac{\langle \psi_T|\mathcal{O}|\psi_T\rangle}{\langle \psi_T|\psi_T\rangle} = \sum_x \mathcal{O}_x P_x, \tag{2.3}$$

where $P_x = \frac{|\psi_T(x)^2|}{\sum_x |\psi_T(x)^2|}$ is the probability distribution and $\mathcal{O}_x = \frac{\langle x|\mathcal{O}|\psi_T\rangle}{\langle x|\psi_T\rangle}$ is the local estimator of the operator $\mathcal{O}$ at a given configuration $|x\rangle$. A new configuration $|x'\rangle$ is generated via Markov chain by changing a degree of freedom in the $|x\rangle$ and this change is accepted or rejected via Metropolis Algorithm i.e. $P_{x\to x'} =$ min $[1, |\frac{\psi_T(x')^2}{\psi_T(x)^2}|]$. After thermalization, i.e., for large enough number of Metropolis steps N_{step}, $\bar{\mathcal{O}} \approx \frac{1}{N_{step}} \sum_{n=1}^{N_{step}} \mathcal{O}_{x_n}$ as a consequence of the central limit theorem. In order to calculate the statistical error one can use the $jackknife$ method by dividing the whole data set into M blocks each containing L_{bin} data set such that $M * L_{bin} = N_{step}$ and calculating the average of the ith block by excluding the ith block.

$$\bar{\mathcal{O}}_i = \frac{1}{L_{bin}(M-1)} \sum_{j \notin i}^{N_{step}} \mathcal{O}_j, \tag{2.4}$$

the standard deviation of the total average $\bar{\mathcal{O}}$ is obtained as follows

$$\sigma^2 = \frac{M-1}{M} \sum_{i=1}^{M} (\bar{\mathcal{O}} - \bar{\mathcal{O}}_i)^2. \tag{2.5}$$

2.0.1 Stochastic Reconfiguration

A general many-body wave function is constructed using several parameters and each of these parameters can be optimized stochastically by minimizing the energy of the system. By changing slightly the set of variational parameters α to α' the change of the trial wave function, within the linear approximation, can be written as follows

$$|\Psi_T(\alpha')\rangle \simeq \delta_{\alpha_0}|\Psi_T(\alpha)\rangle + \sum_{k=1}^{p} \delta_{\alpha_k} \frac{\partial}{\partial_{\alpha_k}} |\Psi_T(\alpha)\rangle, \tag{2.6}$$

$$|\Psi_T(\alpha')\rangle = \sum_{k=0}^{p} \delta_{\alpha_k} O_k |\Psi_T(\alpha)\rangle, \tag{2.7}$$

$O_0 = 1$ and O_k are the logarithmic derivatives defined for any configuration $|x\rangle$. Therefore, the local estimator of the operator O_k can be formulated as

$$O_k(x) = \frac{\partial \ln\langle x|\Psi_T(\alpha)\rangle}{\partial \alpha_k}. \tag{2.8}$$

Likewise, one can use the projection method which is the application of the Hamiltonian operator iteratively onto the trial wave function to extract the ground state wave function. For one iteration we have

$$\frac{\langle\Psi_T|(\Lambda - \mathcal{H})\mathcal{H}(\Lambda - \mathcal{H})|\Psi_T\rangle}{\langle\Psi_T|(\Lambda - \mathcal{H})^2|\Psi_T\rangle} \approx \frac{\langle\Psi_T|\mathcal{H}|\Psi_T\rangle}{\langle\Psi_T|\Psi_T\rangle} - \frac{1}{\Lambda}\Big(\frac{\langle\Psi_T|\mathcal{H}^2|\Psi_T\rangle}{\langle\Psi_T|\Psi_T\rangle} - \big(\frac{\langle\Psi_T|\mathcal{H}|\Psi_T\rangle}{\langle\Psi_T|\Psi_T\rangle}\big)^2\Big). \tag{2.9}$$

for large enough Λ. Therefore, the energy after projection will be automatically lower than before. With this in mind we can apply the projection to our unchanged wave function and obtain the new projected wave function $|\Psi_T(\alpha)^P\rangle$ as follows

$$|\Psi_T(\alpha)^P\rangle = (\Lambda - \mathcal{H})|\Psi_T(\alpha)\rangle. \tag{2.10}$$

At this point, in order to ensure to obtain a lower energy, we impose that Eq.(2.7) and Eq.(2.10) are equal s.t.

$$(\Lambda - \mathcal{H})|\Psi_T(\alpha)\rangle = \sum_{k=0}^{p} \delta_{\alpha_k} O_k |\Psi_T(\alpha)\rangle. \tag{2.11}$$

By projecting each side with the k' component we obtain

$$\langle \Psi_T(\alpha)|O_{k'}(\Lambda - \mathcal{H})|\Psi_T(\alpha)\rangle = \sum_{k=0}^{p} \delta_{\alpha_k} \langle \Psi_T(\alpha)|O_{k'}O_k|\Psi_T(\alpha)\rangle, \tag{2.12}$$

for k'=0

$$\langle \Psi_T(\alpha)|(\Lambda - \mathcal{H})|\Psi_T(\alpha)\rangle = \delta_{\alpha_0} + \sum_{k=1}^{p} \delta_{\alpha_k} \langle \Psi_T(\alpha)|O_k|\Psi_T(\alpha)\rangle, \tag{2.13}$$

and for k' $\neq 0$

$$\begin{aligned} \langle \Psi_T(\alpha)|O_{k'}(\Lambda - \mathcal{H})|\Psi_T(\alpha)\rangle &= \delta_{\alpha_0} \langle \Psi_T(\alpha)|O_{k'}|\Psi_T(\alpha)\rangle \\ &+ \sum_{k=1}^{p} \delta_{\alpha_k} \langle . \Psi_T(\alpha)|O_{k'}O_k|\Psi_T(\alpha)\rangle \end{aligned} \tag{2.14}$$

after substituting the δ_{α_0} in the previous equation we obtain

$$\begin{aligned} &\sum_{k=1}^{p} \delta_{\alpha,k} \Big[\langle \Psi_T(\alpha)|O_{k'}O_k|\Psi_T(\alpha)\rangle - \langle \Psi_T(\alpha)|O_{k'}|\Psi_T(\alpha)\rangle \langle \Psi_T(\alpha)|O_k|\Psi_T(\alpha)\rangle \Big] \\ &\qquad = \langle \Psi_T(\alpha)|\mathcal{H}|\Psi_T(\alpha)\rangle \langle \Psi_T(\alpha)|O_{k'}|\Psi_T(\alpha)\rangle - \langle \Psi_T(\alpha)|O_{k'}\mathcal{H}|\Psi_T(\alpha)\rangle. \end{aligned} \tag{2.15}$$

by defining the covariance matrix as

$$S_{kk'} = \Big[\langle \Psi_T(\alpha)|O_{k'}O_k|\Psi_T(\alpha)\rangle - \langle \Psi_T(\alpha)|O_{k'}|\Psi_T(\alpha)\rangle \langle \Psi_T(\alpha)|O_k|\Psi_T(\alpha)\rangle \Big], \tag{2.16}$$

and the quantities

$$f_{k'} = \langle \Psi_T(\alpha)|H|\Psi_T(\alpha)\rangle \langle \Psi_T(\alpha)|O_{k'}|\Psi_T(\alpha)\rangle - \langle \Psi_T(\alpha)|O_{k'}\mathcal{H}|\Psi_T(\alpha)\rangle, \tag{2.17}$$

such that we arrive at differential equation

$$f_{k'} = \sum_{k=1}^{p} \delta_{\alpha_k} S_{kk'}. \tag{2.18}$$

One can easily prove that the quantities defined above are proportional to the generalized forces which are the derivatives of the energy

$$\begin{aligned} f_{k'} = -\frac{1}{2}\frac{\partial E(\alpha)}{\partial \alpha_{k'}} = -\frac{1}{2}\Big(&\frac{\langle \Psi T|O_{k'}\mathcal{H} + \mathcal{H}O_{k'}|\Psi_T\rangle}{\langle \Psi_T|\Psi_T\rangle} + \\ &\frac{\langle |\Psi_T|H|\Psi_T\rangle \big(\langle \Psi_T|O_{k'}|\Psi_T\rangle + \langle \Psi_T|O_{k'}|\Psi_T\rangle\big)}{|\langle \Psi_T|\Psi_T\rangle|^2} \Big). \end{aligned} \tag{2.19}$$

where $E(\alpha) = \frac{<\Psi_T|H|\Psi_T>}{<\Psi_T|\Psi_T>}$. Therefore, when there is no variation in the variational parameters, i.e. the forces are zero, this implies that we are at the minimum of the energy landscape. In the case of steepest descent (SD), the energy is optimized by changing the parameters according to the calculated forces

$$\alpha_k \longrightarrow \alpha_k + \Delta t f_k. \tag{2.20}$$

However, in the SR algorithm the variational parameters are obtained after inverting the Eq.(2.18) such that the new parameters are changed as

$$\alpha_k \longrightarrow \alpha_k + \Delta t \sum_i S_{ki}^{-1} f_i. \tag{2.21}$$

The advantage of the SR algorithm is that all the variational parameters are changed in a correlated way. In addition to that, since the change in the parameters is related to the inverse of the covariance matrix, the parameters change in the directions such that the variance of the parameters are small which allows a more stable algorithm compared to standard SD algorithm. More details about the SR method can be found at [22, 21].

Computing the logarithmic derivatives, O_k, for any configuration needs some attention. Calculation of these terms for any kind of variational parameters such as the ones in the Jastrow part or in the Slater determinant can be found at [21] in detail.

2.1 Variational Wave Functions

As already emphasized in the previous section, the key ingredient of VMC is the construction of a proper wave function which can represent the ground state of the model of interest in a reliable and computationally affordable way. Generally the variational wave function is a correlated Ansatz including several variational parameters which have to be optimized by minimizing the energy of the system to approach the ground state, for example, by means of the SR approach described above. In the upcoming sections we describe the correlated Ansatz that we use to approximate the ground state of strongly correlated lattice models such as Hubbard and Hubbard-Holstein Models which we have introduced in the introduction.

2.1.1 Variational wave function for Hubbard Model

In order to study the negative/positive-U Hubbard Model,while employing the VMC method, we can construct a Jastrow-Slater wavefunction of the form

$$|\Psi\rangle = \mathcal{J}\mathcal{P}|\Psi_{\mathrm{T}}\rangle, \tag{2.22}$$

where $\mathcal{P}$ is the projector fixing the particle number and $\mathcal{J}$ is the density-density Jastrow correlator defined by

$$\mathcal{J} = \exp\left(-\frac{1}{2}\sum_{i,j} v_{i,j} n_i n_j\right), \tag{2.23}$$

where $n_i = \sum_\sigma n_{i\sigma}$ is the total number of particles in the ith site and $v_{i,j}$ depend only on the distance between the lattice sites in order to satisfy the translational and rotational invariance properties of the variational wave function. It has been shown that, for the Hubbard model, it is particularly important to consider a Jastrow factor where the pseudopotential $v_{i,j}$ is non zero even when the two lattice points are at very large distance d, since in this way the correct low-energy description, i.e correct charge fluctuations at small momenta are captured [23, 24].

Monte Carlo integration is done over the configuration space as described before. In the system of interest electrons have defined positions and spins along the quantization axis $S_i^z = \pm 1/2$ which is the z-direction in our case. In order to generate new configurations, one can perform Markov chains by considering the moves (hoppings) defined by the Hamiltonian of the system of interest. Therefore, the moves should consists of the hopping terms in the Hamiltonian such as the kinetic part or the exchange part if present in the Hamiltonian. With this limitation the VMC conserves the total number of particles N and the total projection $S_{\mathrm{tot}}^z = \sum_i S_i^z = 0$ of the spin in the chosen quantization axis. Thus, these kind of projections are implicitly assumed in the Hubbard Hamiltonian defined in Eq. (3.7). While sampling the most probable configurations in order to get the ground state of the Hubbard model, it is also possible to consider the moves which change the number of particles (remaining in the $S^z_{\mathrm{tot}} = 0$ subspace). Therefore, by means of charge fluctuations one can extend the sampling from canonical ensemble (CE) to grand canonical ensemble (GCE) by enlarging the Hilbert space, where the former consists of local moves conserving the particle number while the latter includes moves allowing fluctuations of the particle number.

When we allow the particle fluctuations during the Markov chains, i.e. when the grand canonical ensemble (GCE) is sampled, a fugacity term $\exp(-f \sum\limits_i n_i)$ has to be added to Eq. (2.23) in order to control the particle number. At half filling the fugacity is determined by the condition that Eq. (2.23) remains unchanged (up to a constant) for the particle-hole symmetry:

$$c_{i\sigma} \to (-1)^{x_i+y_i} c^{\dagger}_{i-\sigma} \tag{2.24}$$

where x_i, y_i are the lattice coordinates of the site i. This implies that $f = \frac{1}{N}\sum_{i,j} v_{i,j}$ after a straightforward calculation.

In some part of this thesis we will focus mainly on the attractive version of the Hubbard Hamiltonian, i.e., we will study the negative-U Hubbard model. Negative-U Hubbard model is known to be SU(2) symmetric at half-filling, i.e., there exist both the superconducting (SC) order and charge density wave (CDW) order. On the other hand, away from half-filling the system is known to have uniform SC order. In order to study the ground state properties of the negative-U Hubbard model the antisymmetric part of the wavefunction, $|\Psi_{\mathrm{T}}\rangle$, is chosen to be the ground state of a mean-field (MF) Hamiltonian $\mathcal{H}_{\mathrm{MF}}$ that contains the electron hopping, chemical potential and singlet s-wave pairing terms;

$$\begin{aligned} \mathcal{H}_{\mathrm{MF}} &= -t \sum_{\langle i,j\rangle,\sigma} \left(c^{\dagger}_{i\sigma} c_{j\sigma} + \mathrm{h.c.} \right) - \mu_{\mathrm{BCS}} \sum_{i\sigma} n_{i\sigma} \\ &+ \Delta_0 \sum_i \left(c^{\dagger}_{i\uparrow} c^{\dagger}_{i\downarrow} + \mathrm{h.c.} \right), \end{aligned} \tag{2.25}$$

where μ_{BCS}, and Δ_0 are variational parameters. Such a Hamiltonian can be written in terms of a $2N$x$2N$ matrix, where N is the number of lattice sites, after the particle hole transformation on the spin-down particles,i.e.

$$c_{i\uparrow} = c_{i\uparrow} \qquad c_{i\downarrow} = c^{\dagger}_{i\downarrow} \tag{2.26}$$

After this operation one can write the mean field Hamiltonian as follows

$$\mathcal{H}_{\text{MF}} = \mathbf{c}^{\dagger}\mathbf{H}_0\mathbf{c} \tag{2.27}$$

where $\mathbf{H}_0$ is a $2N$x$2N$ matrix and $\mathbf{c}$ is $2N$x1 vector with its first N elements correspond to spin up and the rest to spin down. We can diagonalize the $\mathcal{H}_{\text{MF}}$ and the eigenvalues are written in the diagonal matrix $\Lambda = \mathbf{U}^{\dagger}\mathbf{H}_0\mathbf{U}$. With this operation we can write the mean field Hamiltonian in terms of new creation and annihilation operators as follows

$$\mathcal{H}_{\text{MF}} = \mathbf{c}^{\dagger}\mathbf{U}\Lambda\mathbf{U}^{\dagger}\mathbf{c} \tag{2.28}$$

Therefore, for a system of N_e number of electrons we can write a non interacting wave function by using the one particle eigenstates of the Hamiltonian:

$$|\Psi_T\rangle = \prod_{i=1}^{N_e}(\sum_{j=1}^{2N} U_{ji}c^{\dagger}_{j})|0\rangle \tag{2.29}$$

where the 1st index of U is the orbital index and the second one is the particle index. The ground state wave function is then constructed by occupying the lowest eigenvalue orbitals and all the variational parameters $v_{i,j}$, μ_{BCS}, and Δ_0 are optimized via the stochastic-reconfiguration technique explained before.

2.1.2 Variational wave function for the Hubbard-Holstein Model

In this section, we describe the correlated many body variational wave function that we have used in the numerical calculations for the Hubbard-Holstein model. In addition to the electrons we have also phonon degrees of freedom in the model. Therefore, the configuration space that we sample is composed of both electronic and phononic configurations. The variational Ansatz should include information also about the phononic correlations in addition to the terms we have used also for the Hubbard model. We have used also in this case a Jastrow-Slater trial function defined by:

$$|\Psi_T\rangle = \mathcal{J}^{ee}\mathcal{J}^{ep}\mathcal{P}(N_e)|\Phi_T^{el}\rangle \otimes |\Phi_T^{ph}\rangle. \tag{2.30}$$

Here, $|\Phi_T^{el}\rangle$ is the ground state of a quadratic mean-field Hamiltonian that contains electron hopping and pairing of singlet type as follows:

$$\begin{aligned}\mathcal{H}_{\mathrm{MF}} &= -t\sum_{\langle i,j\rangle,\sigma} c^{\dagger}_{i,\sigma}c_{j,\sigma} + \mathrm{h.c.} - \mu\sum_{i,\sigma} c^{\dagger}_{i,\sigma}c_{i,\sigma} \\ &+\sum_{i,\sigma}(-1)^{R_i}\left[\Delta_{\mathrm{CDW}} + \Delta_{\mathrm{AF}}(-1)^{\bar{\sigma}}\right]c^{\dagger}_{i,\sigma}c_{i,\sigma} \\ &+\Delta_{\mathrm{SC}}\sum_{i} c^{\dagger}_{i,\uparrow}c^{\dagger}_{i,\downarrow} + \mathrm{h.c.},\end{aligned} \tag{2.31}$$

where μ, Δ_{CDW}, Δ_{AF}, and Δ_{SC} are parameters that are optimized in order to minimize the variational energy via the stochastic reconfiguration method described in the previous section. $\mathbf{R}_i = (X_i, Y_i)$ indicate the coordinates of the site i in the square lattice, and $\bar{\sigma} = +1\,(-1)$ for up (down) electrons. This parametrization of the wave function provides a quite easy and flexible description of the ground state since one can allow any order of interest in the wave function and compare the energies of different states to understand, at least qualitatively, the possible orders in the ground state wave function .For example, if one allows a CDW order (when $\Delta_{\mathrm{CDW}} \neq 0$ and $\Delta_{\mathrm{AF}} = \Delta_{\mathrm{SC}} = 0$), or antiferromagnetic Néel order (when $\Delta_{\mathrm{AF}} \neq 0$ and $\Delta_{\mathrm{CDW}} = \Delta_{\mathrm{SC}} = 0$), or superconducting order (when $\Delta_{\mathrm{SC}} \neq 0$ and $\Delta_{\mathrm{CDW}} = \Delta_{\mathrm{AF}} = 0$) one can compare the energies of these states and pin the order that is most likely to occur in the exact ground state. Moreover, it is possible to construct states with coexisting orders. The mean-field Hamiltonian described above can easily be diagonalized to define the uncorrelated electronic state $|\Phi_T^{el}\rangle$, which has the following form:

$$|\Phi_T^{el}\rangle = e^{\left(\sum_{i,j} f_{i,j}c^{\dagger}_{i,\uparrow}c^{\dagger}_{j,\downarrow}\right)}|0\rangle, \tag{2.32}$$

where the pairing function $f_{i,j}$ depends upon the variational parameters of the mean-field Hamiltonian. The projector $\mathcal{P}(N_e)$ is used to fix the total number of electrons N_e in the system.

The uncorrelated phononic part in the wave function is then given by:

$$|\Phi_T^{ph}\rangle = e^{\mu_{ph}\sum_i n_i^{ph}} e^{b^\dagger_{k=0}}|0\rangle \tag{2.33}$$

where μ_{ph} is the fugacity term which controls the total number of phonons, n_i^{ph} is the total number of phonons on ith site and $|0\rangle$ is the vacuum state of phonons. After expanding the exponential one can write the wave function as:

$$|\Phi_T^{ph}\rangle = \sum_{N_b} e^{\mu_{ph}\sum_i n_i^{ph}} \frac{\left(b^\dagger_{k=0}\right)^{N_b}}{N_b!}|0\rangle, \tag{2.34}$$

where $b^\dagger_{k=0} = 1/\sqrt{N}\sum_i b_i^\dagger$ creates a phonon in the $k=0$ momentum state (N is the number of sites). Here, N_b denotes the total number of phonons. Denoting by $|n_1^{ph},\ldots,n_N^{ph}\rangle$ the (normalized) configuration with n_i^{ph} phonons on the site i, the uncorrelated phononic wave function can be written as:

$$|\Phi_T^{ph}\rangle = \sum_{n_1^{ph},\ldots,n_N^{ph}} \frac{e^{\mu_{ph}\sum_i n_i^{ph}}}{\sqrt{n_1^{ph}!\ldots n_N^{ph}!}}|n_1^{ph},\ldots,n_N^{ph}\rangle. \tag{2.35}$$

For a fixed phonon configuration $|x_{ph}\rangle = |n_1^{ph}n_2^{ph}n_3^{ph}.....n_N^{ph}\rangle$ the overlap of the phononic wave function with the given configuration is given by:

$$\langle x_{ph}|\Phi_T^{ph}\rangle = \frac{e^{\mu_{ph}\sum_{i=1}^N n_i^{ph}}}{\sqrt{n_1^{ph}!n_2^{ph}!n_3^{ph}!....n_N^{ph}!}}. \tag{2.36}$$

Finally, the terms $\mathcal{J}^{ee}$, and $\mathcal{J}^{ep}$ are density-density Jastrow correlators for the electron-electron and electron-phonon correlations, respectively and are written as follows:

$$\mathcal{J}^{ee} = \exp\left(-\frac{1}{2}\sum_{i,j} v_{i,j}^{ee} n_i n_j\right), \tag{2.37}$$

$$\mathcal{J}^{ep} = \exp\left(-\sum_{i,j} v_{i,j}^{ep} n_i n_j^{ph}\right), \tag{2.38}$$

where $v^{ee}_{i,j}$, and $v^{ep}_{i,j}$ are long ranged variational parameters as pseudo-potentials, including the on site terms, that are taken to be translationally invariant such that they depend only upon the distance between ith and jth site, i.e., $|\mathbf{R}_i - \mathbf{R}_j|$. As before we will optimize each of these parameters independently via SR method to reach the lowest possible energy which describes the ground state of the system. We have considered that all the pseudo-potentials are taken to be symmetric,i.e. for example, $v^{ee}_{i,j} = v^{ee}_{j,i}$ and this is valid for all parameters in all Jastrow correlators. It has been observed that the electron-phonon Jastrow term is fundamental to obtain an accurate description when finite electron-phonon coupling term g/t is used in the Hamiltonian. As for the Hubbard model described in the previous section, the long range electron-electron Jastrow factor is fundamental to capture the correct charge fluctuations of the ground state [23, 24].

As mentioned before, the configuration space that is sampled along the Markov chain is defined by specifying both electron and phonon occupations on each site such that we work in a basis where the number of phonons n^{ph}_i is specified on each lattice site, and also the number of electrons with spin-up and spin-down configurations $n_{i,\sigma}$. The uncorrelated phononic part is given by Eq. (2.35) and contains a single variational parameter μ_{ph} to control the total phonon number. We do not need to include any cutoff in the number of phonons which comes as one of the most important advantages of our wave function. With this representation it is very easy to identify the nature of the ground state by just looking at the optimized variational parameters. For example, obtaining a finite Δ_{AF} immediately implies that the state displays AF order. It is worth to mention that the present approach allows us to easily capture metastable states, with given physical properties: for example, by fixing $\Delta_{\mathrm{AF}} = 0$, it is possible to obtain the best paramagnetic state, even if the region of interest displays an antiferromagnetically ordered ground state.

In the Markov chain, we update the phonon configurations by adding or removing one particle randomly at a given random site. In this way we are compatible also with some of the terms of the Hamiltonian. Therefore, the Metropolis algorithm for this wave function is defined as follows

creation of a phonon at site i:

The configuration after creating a single particle at site i is $|x'\rangle = |n_1^{ph} n_2^{ph} n_3^{ph} ....n_i^{ph} + 1...n_N^{ph}\rangle$ and the ratio of the two configuration $|x'\rangle$ and $|x\rangle$ is

$$\frac{\langle x'|\mathcal{J}^{ep}|\Phi_T^{ph}\rangle}{\langle x|\mathcal{J}^{ep}|\Phi_T^{ph}\rangle} = \frac{\frac{e^{\mu_{ph}\sum_{i=1}^{N} n_i^{ph}}}{\sqrt{n_1^{ph}!n_2^{ph}!n_3^{ph}!..(n_i^{ph}+1)!..n_N^{ph}!}}}{\frac{e^{\mu_{ph}\sum_{i=1}^{L} n_i^{ph}}}{\sqrt{n_1^{ph}!n_2^{ph}!n_3^{ph}!..n_i^{ph}!..n_N^{ph}!}}}\mathcal{R}_l^{+} = \frac{e^{\mu_{ph}}}{\sqrt{n_i^{ph}+1}}\mathcal{R}_l^{+}. \tag{2.39}$$

destruction of a phonon at site i:

The configuration after desrtoying a single particle at site i is $|x'\rangle = |n_1^{ph} n_2^{ph} n_3^{ph} ....n_i^{ph} - 1...n_N^{ph}\rangle$ and the ratio of the two configuration $|x'\rangle$ and $|x\rangle$ is

$$\frac{\langle x'|\mathcal{J}^{ep}|\Phi_T^{ph}\rangle}{\langle x|\mathcal{J}^{ep}|\Phi_T^{ph}\rangle} = \frac{\frac{e^{\mu_{ph}\sum_{i=1}^{N} n_i^{ph}}}{\sqrt{n_1^{ph}!n_2^{ph}!n_3^{ph}!..(n_i^{ph}-1)!..n_N^{ph}!}}}{\frac{e^{\mu_{ph}\sum_{i=1}^{L} n_i^{ph}}}{\sqrt{n_1^{ph}!n_2^{ph}!n_3^{ph}!..n_i^{ph}!..n_N^{ph}!}}}\mathcal{R}_l^{-} = e^{-\mu_{ph}}\sqrt{n_i^{ph}}\mathcal{R}_l^{-}. \tag{2.40}$$

Energy calculation of the phononic part:

The calculation of the energy matrix elements for the e-ph coupling term can be computed as follows

$$\frac{\langle x|b_i^{\dagger}|\mathcal{J}^{ep}|\Phi_T^{ph}\rangle}{\langle x|\mathcal{J}^{ep}|\Phi_T^{ph}\rangle} = \sqrt{n_i^{ph}}\frac{\langle x'|\Phi_T^{ph}\rangle}{\langle x|\Phi_T^{ph}\rangle}\mathcal{R}_l^{+} = e^{-\mu_{ph}} n_i^{ph}\mathcal{R}_l^{+}. \tag{2.41}$$

$$\frac{\langle x|b_i|\mathcal{J}^{ep}|\Phi_T^{ph}\rangle}{\langle x|\mathcal{J}^{ep}|\Phi_T^{ph}\rangle} = \sqrt{n_i^{ph}+1}\frac{\langle x'|\Phi_T^{ph}\rangle}{\langle x|\Phi_T^{ph}\rangle}\mathcal{R}_l^{-} = e^{\mu_{ph}}\mathcal{R}_l^{-}. \tag{2.42}$$

where $\mathcal{R}_i^{+}$ and $\mathcal{R}_i^{-}$ are the ratio of the Jastrow terms when a phonon is created or destroyed at site i respectively.

$$\mathcal{R}_i^+ = \exp\left[-\sum_l (v_{l,i}^{ep} n_i)\right], \tag{2.43}$$

$$\mathcal{R}_i^- = \exp\left[+\sum_l (v_{l,i}^{ep} n_i)\right]. \tag{2.44}$$

Note that when there is a term related to the electron hopping, one has to include also the ratios of the electron-electron Jastrow and also the electron-phonon Jastrow since this process will change both these Jastrow terms. More details about electron-electron Jastrow ratio and update calculations can be found at [21].

Chapter 3

Auxiliary Field Quantum Monte Carlo

The auxiliary field quantum Monte Carlo (AFQMC) method is based on the idea that the imaginary-time propagation $e^{-\beta\mathcal{H}}|\Psi_{\mathrm{T}}\rangle$ of a trial wave function $|\Psi_{\mathrm{T}}\rangle$ with a long-enough projection time β can project out the exact ground-state wave function $|\Psi_0\rangle$, provided that the trial wave function is not orthogonal to the exact ground-state wave function, i.e., $\langle\Psi_{\mathrm{T}}|\Psi_0\rangle \neq 0$ [25]. One can construct the trial wave function by filling the lowest energy orbitals of a mean field Hamiltonian which can be constructed in a way similar to the VMC case described in the previous section. The pseudo-partition function of a system with a Hamiltonian $\mathcal{H}$ can be defined as [21]

$$\mathcal{Z} = \langle\Psi_{\mathrm{T}}|e^{-\beta\mathcal{H}}|\Psi_{\mathrm{T}}\rangle = \langle\Psi_{\mathrm{T}}|(e^{-\Delta\tau\mathcal{H}})^{2T}|\Psi_{\mathrm{T}}\rangle, \tag{3.1}$$

where β is discretized into $2T$ time slices with an interval $\Delta\tau$ in the R.H.S. of the Eq.(3.1) given by $\beta = 2T\Delta\tau$. Then the ground-state expectation value of an operator $\mathcal{O}$ can be written as

$$\frac{\langle\Psi_0|\mathcal{O}|\Psi_0\rangle}{\langle\Psi_0|\Psi_0\rangle} = \lim_{T\to\infty} \frac{\langle\Psi_{\mathrm{T}}|(e^{-\Delta\tau\mathcal{H}})^{T}\mathcal{O}(e^{-\Delta\tau\mathcal{H}})^{T}|\Psi_{\mathrm{T}}\rangle}{\mathcal{Z}}. \tag{3.2}$$

Generally an interacting Hamiltonian $\mathcal{H}$ consists of a one-body term defined as $\mathcal{H}_{\mathcal{K}}$ which is written in terms of two creation and annihilation operators, i.e, $c^{\dagger}c$ as the kinetic term in the Hubbard Hamiltonian. In addition to the one body term there can exist also a two-body term $\mathcal{H}_{\mathcal{V}}$ which is the term describing the interaction between the particles and written in terms of 4 creation and annihilation operators such as $c^{\dagger}cc^{\dagger}c$ as in the interaction part of the Hubbard Hamiltonian. These terms $\mathcal{H}_{\mathcal{K}}$ and $\mathcal{H}_{\mathcal{V}}$ generally do not commute. In order to simplify this expression one can factorize the propagator $e^{-\beta\mathcal{H}}$ in Eq.(3.1) using the Trotter-Suzuki decomposition [26, 27]. In this case the imaginary-time propagator $e^{-\beta\mathcal{H}}$ can be written as:

$$e^{-\Delta\tau\mathcal{H}} = e^{-\Delta\tau\mathcal{H}_{\mathcal{K}}}e^{-\Delta\tau\mathcal{H}_{\mathcal{V}}} + O(\Delta\tau^2), \tag{3.3}$$

$$e^{-\Delta\tau\mathcal{H}} = e^{-\frac{\Delta\tau}{2}\mathcal{H}_{\mathcal{K}}}e^{-\Delta\tau\mathcal{H}_{\mathcal{V}}}e^{-\frac{\Delta\tau}{2}\mathcal{H}_{\mathcal{K}}} + O(\Delta\tau^3), \tag{3.4}$$

where $O(\Delta\tau^2)$ is the systematic error due to the time discretization in the first case whereas $O(\Delta\tau^3)$ is the error in the second symmetric case. Since there are $2T$ number of slices, the errors are accumulated and the resulting systematic error is at most $O(\Delta\tau)$ in the first case whereas it is at most $O(\Delta\tau)^2$ in the second case. When the second symmetric discretization is used the resulting expression of the partition function can be written as follows

$$\mathcal{Z} = \langle\Psi_T|e^{-\frac{\Delta\tau K}{2}}e^{-\Delta\tau V}e^{-\Delta\tau K}e^{-\Delta\tau V}e^{-\Delta\tau K}....e^{-\Delta\tau V}e^{-\Delta\tau K}e^{-\Delta\tau V}e^{-\frac{\Delta\tau K}{2}}|\Psi_T\rangle. \tag{3.5}$$

The expression of the partition function is composed of exponential terms that are applied to a trial wave function consecutively as it can be seen in the above equation. It can be shown that the application of a term containing an exponential of a one-body operator to a Slater determinant transforms it to another Slater determinant. However, application of an exponential term containing two-body operator to a Slater determinant is much more complicated as it is not given by a single Slater determinant. In order to simplify this operation one can write the interaction term as a superposition of one-body term using the so called Hubbard-Stratonovich transformation [28, 29] namely any two-body operator $\hat{O}$ can be recast as the integration of one-body operators over auxiliary fields such that

$$e^{\frac{1}{2}\hat{O}^2} = \int_{-\infty}^{\infty} d\sigma\Big(\frac{e^{-\frac{1}{2}\sigma^2}}{\sqrt{2\pi}}\Big)e^{\hat{O}\sigma}. \tag{3.6}$$

For the Hubbard model we decompose the Hamiltonian into two terms

$$\mathcal{H}_{\mathcal{K}} = -t \sum_{\langle i,j \rangle, \sigma} \left(c^{\dagger}_{i,\sigma} c_{j,\sigma} + \text{H.c.} \right) - \mu \sum_{i,\sigma} c^{\dagger}_{i,\sigma} c_{i,\sigma}, \tag{3.7}$$

$$\mathcal{H}_{\mathcal{V}} = U \sum_{i} n_{i,\uparrow} n_{i,\downarrow}. \tag{3.8}$$

The most common choices for the HST are by coupling the fields either to the charge or to the density as follows

$$e^{\frac{\gamma}{2}(n_{i,\uparrow} - n_{i,\downarrow})^2} = \int_{-\infty}^{\infty} \frac{dx_i}{\sqrt{2\pi}} e^{-\frac{1}{2}x_i^2 + \sqrt{\gamma} x_i (n_{i,\uparrow} - n_{i,\downarrow})}. \tag{3.9}$$

$$e^{\frac{\gamma}{2}(n_{i,\uparrow} + n_{i,\downarrow} - 1)^2} = \int_{-\infty}^{\infty} \frac{dx_i}{\sqrt{2\pi}} e^{-\frac{1}{2}x_i^2 + \sqrt{\gamma} x_i (n_{i,\uparrow} + n_{i,\downarrow} - 1)}. \tag{3.10}$$

where $\gamma = U\Delta\tau$ in the first case, whereas $\gamma = -U\Delta\tau$ for the second case. Therefore, for positive values of U the second equation involves complex expressions. Hirsch pointed out that since the occupation numbers are only 0 or 1 for fermions, one can introduce Ising-like discrete fields, $x_i = \pm 1$ [30], such that

$$\prod_i e^{-\Delta\tau U n_{i,\uparrow} n_{i,\downarrow}} = \prod_i \frac{1}{2} e^{\frac{-\Delta\tau}{2}(n_{i,\uparrow} + n_{i,\downarrow})} \sum_{x_i = \pm 1} e^{x_i \gamma (n_{i,\uparrow} - n_{i,\downarrow})}, \tag{3.11}$$

$$\prod_i e^{-\Delta\tau U n_{i,\uparrow} n_{i,\downarrow}} = \prod_i \frac{1}{2} e^{\frac{-\Delta\tau U}{2}(n_{i\uparrow} + n_{i\downarrow} - 1)} \sum_{x_i = \pm 1} e^{x_i \gamma (n_{i\uparrow} + n_{i\downarrow} - 1)}.$$

where $\cosh\gamma = e^{\frac{\Delta\tau|U|}{2}}$. After this operation the partition function is written as

$$\mathcal{Z} = \sum_{x=\pm 1} \langle \Psi_T | e^{-\frac{\Delta\tau K}{2}} e^{-\Delta\tau V^x_{2T}} e^{-\Delta\tau K} e^{-\Delta\tau V^x_{2T-1}} e^{-\Delta\tau K} .... e^{-\Delta\tau V^x_2} e^{-\Delta\tau K} e^{-\Delta\tau V^x_1} e^{-\frac{\Delta\tau K}{2}} | \Psi_T \rangle. \tag{3.12}$$

where V^x_t indicates the HF transformed one-body potential at tth time slice with set of fields $x = \{x^1_t, x^2_t, ...x^N_t\}$ for each lattice sites. The summation over the auxiliary fields $\{x^j_i\}$ are performed by the Monte Carlo sampling. For AFQMC, the sampling is done via Markov chains which include local field-flip operations. By defining the propagator as

$$\mathbf{P}_x(t,0) = e^{-\frac{\Delta\tau K}{2}} e^{-\Delta\tau V^x_t} e^{-\frac{\Delta\tau K}{2}} ... e^{-\frac{\Delta\tau K}{2}} e^{-\Delta\tau V^x_2} e^{-\frac{\Delta\tau K}{2}} e^{-\frac{\Delta\tau K}{2}} e^{-\Delta\tau V^x_1} e^{-\frac{\Delta\tau K}{2}}. \tag{3.13}$$

one can write the single particle Green's function as

$$G^t_{j,i} = \frac{\langle \Psi_T | \mathbf{P}_x(2T,t) c_i^\dagger c_j | \mathbf{P}_x(t,0) | \Psi_T \rangle}{\langle \Psi_T | \mathbf{P}_x(2T,0) | \Psi_T \rangle}. \tag{3.14}$$

which allows us to calculate all the ratios of determinants and all relevant observables in an efficient way [21]. Now the partition function can be written as

$$\mathcal{Z} = \sum_{x=\pm 1} \langle \Psi_T | \mathbf{P}_x(2T,0) | \Psi_T \rangle \tag{3.15}$$

In order to calculate the ground state expectation value of any operator $\mathcal{A}$ we compute

$$\frac{\langle \Psi_T | \mathcal{A} | \Psi_T \rangle}{\mathcal{Z}} = \frac{\sum_{x=\pm 1} \langle \Psi_T | \mathbf{P}_x(2T,T) \mathcal{A} \mathbf{P}_x(T,0) | \Psi_T \rangle}{\sum_{x=\pm 1} \langle \Psi_T | \mathbf{P}_x(2T,0) | \Psi_T \rangle}, \tag{3.16}$$

In AFQMC applications it is possible that $\langle \Psi_T | \mathbf{P}_x(2T,0) | \Psi_T \rangle$ is negative which results in so called negative sign problem. In this case the expectation values of the operators will be weighted also with the sign. Therefore, expectation value of an operator will be calculated as

$$\langle \mathcal{A} \rangle = \frac{\langle A_x S_x \rangle}{\langle S_x \rangle}. \tag{3.17}$$

where S_x is the sign of $\langle \Psi_T | \mathbf{P}_x(2T,0) | \Psi_T \rangle$. For the Hubbard model AFQMC suffers from the negative-sign problem when $U > 0$, if the particle-hole symmetry is broken. However, in several interesting cases one can choose an appropriate HST transformation suitable for the model and study the ground state of the model of interest with no sign problem. For this thesis, in the case of negative-U Hubbard model we have used the transformation defined as 3.10 in which case we use real auxiliary fields. Indeed, in the case of the attractive Hubbard model, there is no sign problem whenever the number of up-spin particles equals the one of the down-spin particles [21].

3.1 First Order Langevin Dynamics

Molecular Dynamics simulations are very useful tools to simulate classical many-body systems consisting of N classical particles in a volume V by integrating the

Newton's equation of motion [31, 32]. The First order Langevin Dynamics (LD) can be used to simulate N classical particles in a finite volume at temperature T, the so called NVT ensemble [31]. Langevin equations are a set of stochastic differential equations defined as follows

$$\frac{d\mathbf{R}(t)}{dt} = \mathbf{f}(\mathbf{R}(t)) + \eta(t), \tag{3.18}$$

with $\mathbf{R}(t) = \{x_1, x_2, x_3....x_N\}$ being the coordinates of the particles and $\mathbf{f}(\mathbf{R}(t))$ being the classical force calculated as

$$f_i = -\frac{\partial V(\mathbf{R})}{\partial x_i},$$

and $\eta(t)$ is a random noise mimicking the interaction of particles with the heat bath. The average value of the noise vanishes and its components do not correlate with each other and within different times such that

$$\langle \eta_i(t) \rangle = 0 \quad \text{and} \quad \langle \eta_i(t)\eta_j(t') \rangle = 2T\delta_{i,j}\delta(t-t'). \tag{3.19}$$

It is very well known that after some equilibration time the system will converge to the Boltzmann distribution [21]

$$P(\mathbf{R}) = \frac{1}{\mathcal{Z}} e^{-\frac{V(\mathbf{R})}{T}}, \tag{3.20}$$

where $\mathcal{Z}$ is the partition function defined as:

$$\mathcal{Z} = \int d\mathbf{R} e^{-\frac{V(\mathbf{R})}{T}}. \tag{3.21}$$

3.1.1 Accelerated Langevin Dynamics

One can accelerate the integration scheme of the stochastic differential equations by means of a covariance matrix coupling the degrees of freedom and in this case the equation of motion will be written as follows

$$\frac{d\mathbf{R}(t)}{dt} = \mathbf{S}^{-1}\mathbf{f}(\mathbf{R}(t)) + \eta(t), \tag{3.22}$$

where S is the acceleration matrix that for practical reasons of efficiency has to be chosen as close as possible to the Hessian matrix whereas $\eta(t)$ is a random noise similar to the previous non-accelerated dynamics with the following properties:

$$\langle \eta_i(t) \rangle = 0 \quad \text{and} \quad \langle \eta_i(t)\eta_j(t') \rangle = 2TS^{-1}_{i,j}\delta(t-t'). \tag{3.23}$$

For obvious numerical reasons we need to discretize the differential equation described in Eq.(3.22). Therefore, the discretized Langevin equation with $\mathbf{R} = \{x_1, x_2, ..., x_L\}$ is written as

$$\mathbf{R}_{n+1} = \mathbf{R}_n + \Delta \mathbf{S}^{-1}\mathbf{f}_n + \sqrt{2T\Delta}\mathbf{z}_n. \tag{3.24}$$

where $\mathbf{z}_n = S^{-1/2}z_n$, and z_n as normally distributed random numbers. $S^{-1/2}$ is obtained after diagonalizing the inverse matrix as follows

$$U^{\dagger}S^{-1}U = \Lambda \quad \text{therefore} \quad S^{-1/2} = U\Lambda^{1/2}. \tag{3.25}$$

As it can be seen the dicretization results in an error which dominates as $\sqrt{\Delta}$ as $\Delta \to 0$, however, the error in the probability distribution scales as Δ [21]. Therefore, we expect an error of the order of Δ for the physical quantities we measure.

3.2 Path Integration via Accelerated Molecular Dynamics on the Holstein Model

The Holstein model is one of the simplest models including electron-phonon coupling, however, without taking into account the electron-electron correlation. It is known that at half filling this model is describing polarons namely electrons with the cloud of phonons [10]. The Hamiltonian is

$$H = -t\sum_{<ij>\sigma}(c^{\dagger}_{i\sigma}c_{j\sigma} + h.c) + g\sum_i \hat{X}_i n_i + \sum_i \Big(\frac{Mw_0^2\hat{X}_i^2}{2} + \frac{1}{2M}\hat{P}_i^2\Big). \tag{3.26}$$

and we can decompose the Hamiltonian as a kinetic term

$$\hat{K} = -t\sum_{<ij>\sigma}(c^{\dagger}_{i\sigma}c_{j\sigma} + h.c) + \sum_i \frac{1}{2M}\hat{P}_i^2, \tag{3.27}$$

and a potential term as

$$\hat{V} = g\sum_{i} n_i \hat{X}_i + \frac{Mw_0^2}{2}\hat{X}_i^2. \tag{3.28}$$

The non-symmetric decomposition of the propagator can be written as follows:

$$\mathcal{Z} = \langle \Psi_T | e^{-\Delta\tau\hat{K}} e^{-\Delta\tau\hat{V}} e^{-\Delta\tau\hat{K}} e^{-\Delta\tau\hat{V}} e^{-\Delta\tau\hat{K}} .... e^{-\Delta\tau\hat{V}} e^{-\Delta\tau\hat{K}} e^{-\Delta\tau\hat{V}} e^{-\Delta\tau\hat{K}} | \Psi_T \rangle. \tag{3.29}$$

We decompose also the kinetic part into pure electronic and pure phononic part as follows:

$$e^{-\Delta\tau(-t\sum_{<ij>\sigma}(c^{\dagger}_{i\sigma}c_{j\sigma}+h.c)+\sum_i \frac{1}{2M}\hat{P}_i^2)} = e^{-\Delta\tau(-t\sum_{<ij>\sigma}(c^{\dagger}_{i\sigma}c_{j\sigma}+h.c))} e^{-\Delta\tau(\sum_i \frac{1}{2M}\hat{P}_i^2)}. \tag{3.30}$$

We also define the electronic propagator as follows

$$e^{-\Delta\tau\hat{K}_{el}} = e^{-\Delta\tau(-t\sum_{<ij>\sigma}(c^{\dagger}_{i\sigma}c_{j\sigma}+h.c))}. \tag{3.31}$$

Now inserting position identities, $\int dX|X\rangle\langle X| = 1$, inside the partition function we obtain

$$\begin{aligned}\mathcal{Z} = \int dX_1 dX_2 ... dX_{T+1} \langle\Psi_T||X_{T+1}\rangle\langle X_{T+1}| e^{-\Delta\tau\hat{K}_{el}} e^{-\frac{\Delta\tau}{2M}\hat{P}^2} e^{-\Delta\tau\hat{V}} |X_T\rangle\langle X_T| e^{-\Delta\tau\hat{K}_{el}} \\ e^{-\frac{\Delta\tau}{2M}\hat{P}^2} e^{-\Delta\tau\hat{V}} |X_{T-1}\rangle\langle X_{T-1}| e^{-\Delta\tau\hat{K}_{el}} e^{-\frac{\Delta\tau}{2M}\hat{P}^2} e^{-\Delta\tau\hat{V}} ....|X_3\rangle\langle X_3| \\ e^{-\Delta\tau\hat{K}_{el}} e^{-\frac{\Delta\tau}{2M}\hat{P}^2} e^{-\Delta\tau\hat{V}} |X_2\rangle\langle X_2| e^{-\Delta\tau\hat{K}_{el}} e^{-\frac{\Delta\tau}{2M}\hat{P}^2} e^{-\Delta\tau\hat{V}} |X_1\rangle\langle X_1||\Psi_T\rangle.\end{aligned} \tag{3.32}$$

In this way we have inserted T+1 position identities for T number of time slices. From now on by letting M=1, one of the terms corresponding to the pure phononic part is evaluated as

$$\langle X| e^{-\frac{\Delta\tau}{2}\hat{P}^2} |X'\rangle = \int \frac{dk}{2\pi} \langle X| e^{-\frac{\Delta\tau}{2}\hat{P}^2} |k\rangle\langle k|X'\rangle, \tag{3.33}$$

with $\int \frac{dk}{2\pi}|k\rangle\langle k| = 1$ and since $\langle X|k\rangle = e^{ikX}$ we have the following expression

$$\int \frac{dk}{2\pi} e^{ik(X-X')} e^{-\Delta\tau k^2/2} = \int \frac{dk}{2\pi} e^{-(\sqrt{\frac{\Delta\tau}{2}}k - \frac{1}{\sqrt{2\Delta\tau}}i(X-X'))^2} e^{-\frac{(X-X')^2}{2\Delta\tau}}, \tag{3.34}$$

by completing the squares as above and evaluating the shifted Gaussian integral we obtain

$$\langle X| e^{-\frac{\Delta\tau}{2}\hat{P}^2} |X'\rangle = \sqrt{\frac{1}{2\pi\Delta\tau}} e^{-\frac{1}{2}\frac{(X-X')^2}{\Delta\tau}}. \tag{3.35}$$

When the electron-phonon coupling is included, the wave function used is the tensor product of electronic and phononic wave functions such that $\langle \Psi_T| = \Big(\langle \Psi_T^e| \otimes \langle \Psi_T^{ph}\Big)|$. At the boundaries we assign a trial wave function for phonon variables such that $\langle \Psi_T^{ph}|X_{T+1}\rangle = 1$, and also $\langle X_1|\Psi_T^{ph}\rangle = 1$. With this in mind the total partition function can be written as follows

$$\begin{aligned}\mathcal{Z} = \int dX_1 dX_2 ... dX_{T+1} \langle \Psi_T^e| e^{-\Delta\tau \hat{K}_{el}} \sqrt{\frac{1}{2\pi\Delta\tau}} e^{-\frac{1}{2}\sum_j \frac{(X_{T+1}^j - X_T^j)^2}{\Delta\tau}} e^{-\Delta\tau\sum_j \frac{w^2 (X_T^j)^2}{2}} \\ e^{-\Delta\tau g \sum_i X_T^j n_j} \sqrt{\frac{1}{2\pi\Delta\tau}} e^{-\frac{1}{2}\sum_j \frac{(X_T^j - X_{T-1}^j)^2}{\Delta\tau}} e^{-\Delta\tau \hat{K}_{el}} e^{-\Delta\tau\sum_j \frac{w^2 (X_{T-1}^j)^2}{2}} e^{-\Delta\tau g \sum_j X_{T-1}^j n_j} \\ \sqrt{\frac{1}{2\pi\Delta\tau}} e^{-\frac{1}{2}\sum_j \frac{(X_{T-1}^j - X_{T-2}^j)^2}{\Delta\tau}} e^{-\Delta\tau \hat{K}_{el}} .... e^{-\Delta\tau \frac{w^2 \sum_j (X_2^j)^2}{2}} e^{-\Delta\tau g \sum_j X_2^j n_j} \sqrt{\frac{1}{2\pi\Delta\tau}} \\ e^{-\frac{1}{2}\sum_j \frac{(X_3^j - X_2^j)^2}{\Delta\tau}} e^{-\Delta\tau \hat{K}_{el}} e^{-\Delta\tau \frac{w^2 \sum_j (X_1^j)^2}{2}} e^{-\Delta\tau g \sum_j X_1^j n_j} \sqrt{\frac{1}{2\pi\Delta\tau}} e^{-\frac{1}{2}\sum_j \frac{(X_2^j - X_1^j)^2}{\Delta\tau}} e^{-\Delta\tau \hat{K}_{el}} |\Psi_T^e\rangle.\end{aligned} \tag{3.36}$$

this expression can be written in more compact way as follows

$$\begin{aligned}\mathcal{Z} = \mathcal{C} \int [dX] \exp\Big[-\frac{1}{2}\sum_{l,m,j} A_{l,m} X_l^j X_m^j\Big] \langle \Psi_T^e| e^{-\Delta\tau \hat{K}_{el}} e^{-\Delta\tau g \sum_i X_L^j n_j} e^{-\Delta\tau \hat{K}_{el}} \\ e^{-\Delta\tau g \sum_j X_{L-1}^j n_j} e^{-\Delta\tau \hat{K}_{el}} .... e^{-\Delta\tau g \sum_j X_2^j n_j} e^{-\Delta\tau \hat{K}_{el}} e^{-\Delta\tau g \sum_j X_1^j n_j} e^{-\Delta\tau \hat{K}_{el}} |\Psi_T^e\rangle\end{aligned} \tag{3.37}$$

where

$$[dX] = \prod_{j,l} dX_l^j \tag{3.38}$$

and

$$\mathcal{C} = \Big(\frac{1}{2\pi\Delta\tau}\Big)^{\frac{NT}{2}} \tag{3.39}$$

and the matrix A is defined as follows

$$A_{l,m} = \frac{1}{\Delta\tau}[2\delta_{l,m} - \delta_{l,m+1} - \delta_{m,l+1}] + \Delta\tau w_0^2 \delta_{l,m} \tag{3.40}$$

It can be seen that there are Gaussian terms coupling the phonon fields at different time slices. This system can be imagined as a polymer with components attached each other via spring with some spring constant. The spring constant is increasing as the imaginary time step decreases and as the number of time slices increases. Therefore, any tiny change in any phonon field will not change the overall system in a significant way. Therefore, simulating such a stiff system with a MC integration scheme might not be the most efficient way because within the standard MC the phonon field updates can have only small local changes around each site and time slice. It is also possible to propose many moves in many time slices at once [33]. However, this scheme is very expensive since it requires the computation of determinants from scratch, implying that it is not possible to compute the ratio of determinants in a cheap way via Eq.(3.14). Here we propose to update all phonon fields at once using the accelerated Langevin dynamics by the computation of the forces [34] as formulated in Eq.(3.24). As described above, the difficulty of sampling the partition function in our problem is due to the harmonic part which we formulated as the A matrix above. Therefore, we have chosen the acceleration matrix, defined as S in Eq.(3.24) to coincide with the matrix A in Eq.(3.40) .

After all, we have $T{+}1$ time slices and for each time slice we have N number of phonon fields. Therefore, we would like to calculate the corresponding forces which are defined as

$$f_t^j = \partial_{X_t^j} \ln(\mathcal{W}(\sigma)) \tag{3.41}$$

where f_t^j is the force corresponding to tth time slice and jth site at this time slice, whereas X_t^j is the phonon field at tth time slice and jth site, and $\mathcal{W}(\sigma)$ is the integrand in Eq.(3.37). The forces include a purely phononic term which can be calculated very easily by differentiating the harmonic part of the partition function, or by the A matrix defined above. In addition to this term, there is also another term coming from the electronic part of the partition function. One can calculate this term of the forces and any other electronic correlations very easily via Eq.(3.14). After the calculation of all forces for all lattice sites and the time slices, the fields are updated according to the Eq.(3.24). The expectation values of purely phononic variables such as potential and kinetic energies are calculated as

$$\langle \frac{w^2 X^2}{2} \rangle = \sum_{i=2}^{T-1} \frac{w^2 X_i^2}{2} \tag{3.42}$$

and the kinetic energy at a particular time slice is given by

$$-\frac{\partial}{\partial \Delta\tau} \langle X | e^{-\Delta\tau p^2/2} | X' \rangle = -\frac{\partial}{\partial \Delta\tau} \Big[\sqrt{\frac{1}{2\pi\Delta\tau}} e^{-\frac{1}{2}\frac{(X-X')^2}{\Delta\tau}} \Big] \tag{3.43}$$

$$\langle \frac{p^2}{2} \rangle = \Big[\frac{1}{2\Delta\tau} - \frac{1}{2} (\frac{X-X'}{\Delta\tau})^2 \Big] \tag{3.44}$$

3.2.1 Test Projector Molecular Dynamics on Holstein Model: Charge Structure Factor at Half Filling

It is known that the tight-binding square lattice model with nearest-neighbour couplings has perfect nesting properties, i.e., there exists a vector $\mathbf{Q} = (\pi, \pi)$ connecting opposite sides of the Fermi surface. As soon as a tiny amount of electron-electron or electron-phonon correlation is switched on a gap opens up. For the pure Holstein model it is expected that an infinitesimally amount of electron-phonon coupling will lead the system to be charge ordered. Therefore, measuring the charge structure factor at the nesting vector can be a relevant check to test our newly formulated projector molecular dynamics algorithm. The charge structure factor (SF) is defined as

$$S_{cdw}(\mathbf{Q}) = \frac{1}{N} \sum_{i,j} e^{i\mathbf{Q}.(\mathbf{r}_i - \mathbf{r}_j)} n_i n_j \tag{3.45}$$

By observing the iteration step (one iteration means computation of all forces at every time slice for every sites and updating all the phonon fields at once) we can observe the effect of the acceleration scheme in our LD algorithm. With this in mind, we can monitor our results of the structure factor for $w/t = 1$ and electron-phonon coupling strength $g/t = 2.0$ and $g/t = 1.0$ at $\Delta\tau = 0.1$ as a function of the iteration steps. In figure 3.1 the convergence of SF is reported. The two behaviours of the SF with and without acceleration matrix show that the acceleration scheme fastens the convergence of SF and also significantly decreases the auto-correlation time.

One important source of systematic error on the observables is given by the LD time discretization. In figure 3.2 one can observe the convergence of SF for different MD time steps. It can be seen that the convergence is fastened as one increases the Δ_{MD} as expected. In figure 3.3 the SF values as a function of MD step are reported. The error due to discretization of LD equation turned out to be less than few percent. Moreover this source of systematic error can be easily controlled because the extrapolation to the zero MD step is very well behaved and smooth.

The same formulation of the pure Holstein model can be simulated via finite temperature Determinant Quantum Monte Carlo (DQMC) technique in which the imaginary time propagation provides quantities of interest at a fixed temperature in the grand canonical ensemble instead of projecting the ground state of the system. A very fist application of this technique was done in ref. [35] on the Hubbard model and then later many studies have been done via this algorithm also for the Holstein [33] and Hubbard-Holstein models [17, 18]. The connection between DQMC and our projector MD/MC algorithm is that as the temperature is decreased, i.e. imaginary time propagation is increased, the results of these techniques should converge to the same values. With this in mind, we compared our results of the structure factor with the one of Scalettar et al. for $w/t = 1$ and electron-phonon coupling strength $g/t = 2.0$ and $g/t = 1.0$ at $\Delta\tau = 0.1$. Indeed figure 3.4 shows the inverse temperature dependence of the structure factor on an 8x8 cluster. One can observe the rapid convergence of our projector algorithm to the zero temperature limit of the DQMC algorithm.

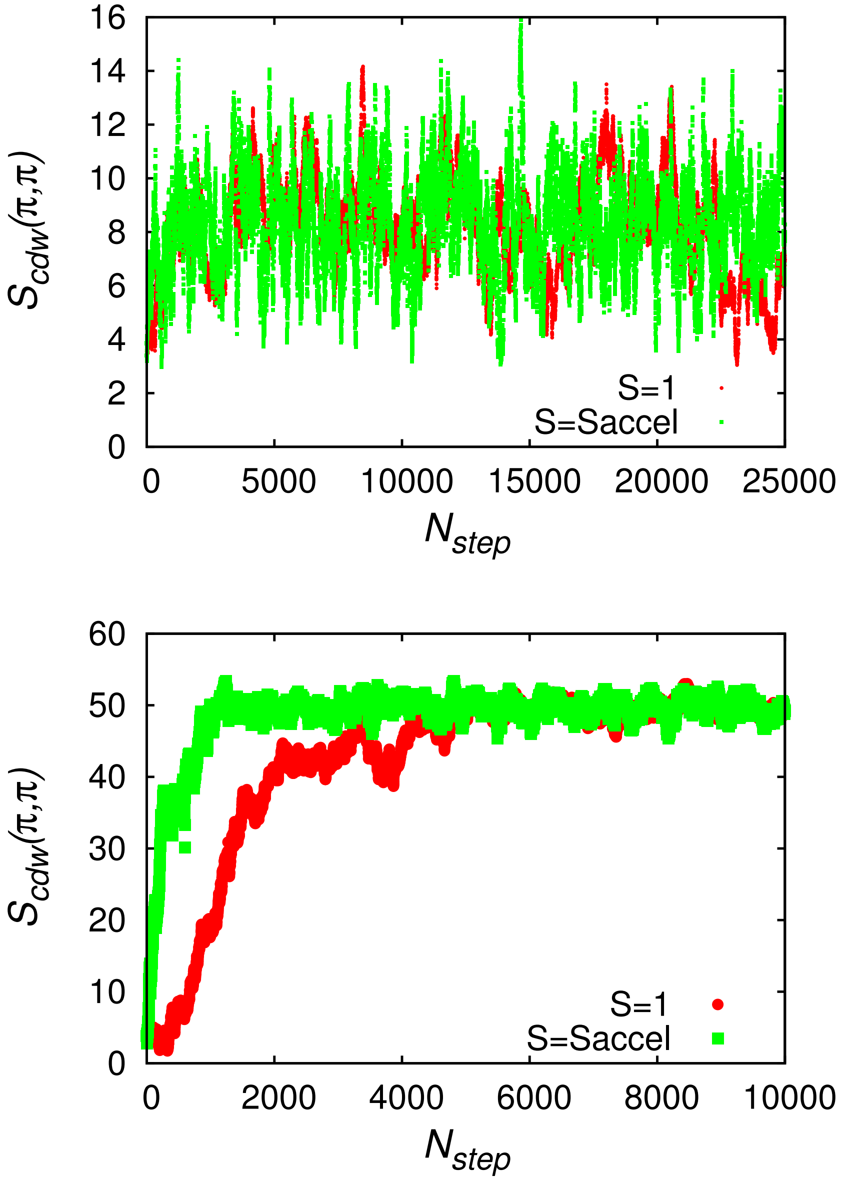

Figure 3.1: Charge structure factor as a function of MD iteration step for Δ_{MD}=0.025 and $\Delta\tau$=0.1 for g=1(up) and g=2(down) with and without acceleration matrix on the 8x8 cluster

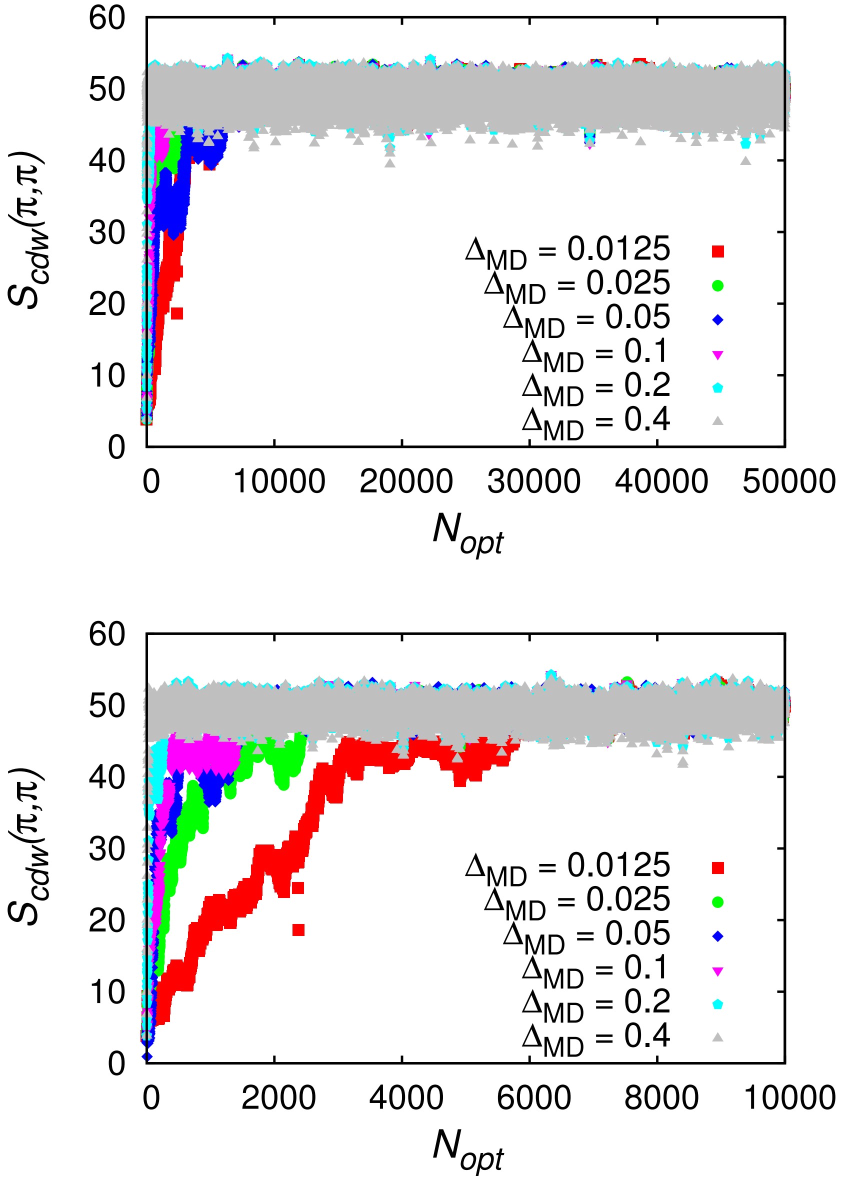

Figure 3.2: Charge structure factor as a function of MD step for different values of Δ_{MD} at $\Delta\tau$=0.1 for g=2 on the 8x8 cluster. The upper figure shows all MD iterations while the lower panel represents a zoom over the first 10000 ones.

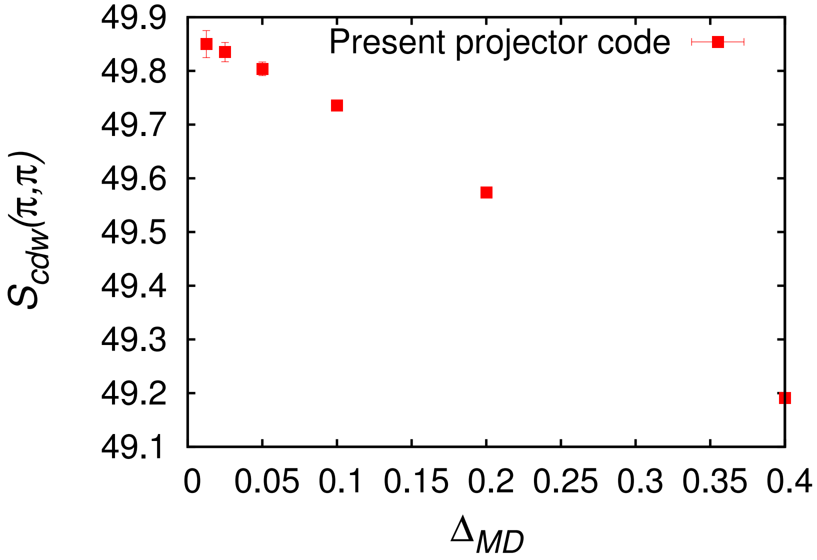

Figure 3.3: Charge structure factor as a function of MD step for g =2 at $\Delta\tau$=0.1 and β =16 on the 8x8 cluster

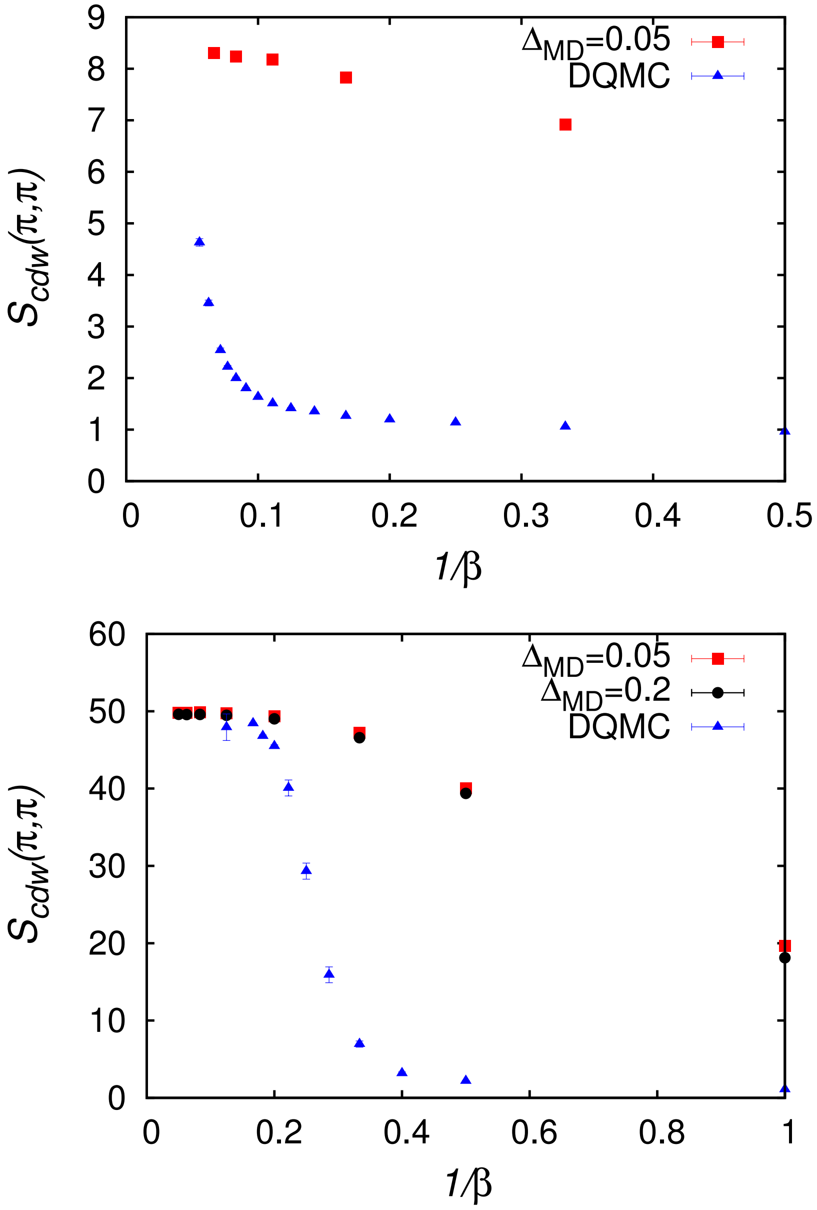

Figure 3.4: Charge structure factor as a function of $1/\beta$ for g=1(up) and g=2(down) for different values of Δ_{MD} compared with finite temperature determinant Monte Carlo (DQMC) calculation estimates on the 8x8 cluster

3.3 Sign Problem Free Hubbard-Holstein Model

In the previous section the electron-electron interaction is not included in the Hamiltonian. Now we are at the point of introducing the electron-electron correlation via the onsite Hubbard interaction as follows

$$H = -t \sum_{<ij>\sigma} (c^{\dagger}_{i\sigma} c_{j\sigma} + h.c) + \frac{U}{2} \sum_j (n_j - 1)^2 + g \sum_j \hat{X}_j (n_j - 1) + \frac{w_0}{2} \sum_j \left(\hat{X}_j^2 + \hat{P}_j^2 \right). \tag{3.46}$$

We can define electronic and phononic kinetic parts as

$$\hat{K} = -t \sum_{<ij>\sigma} (c^{\dagger}_{i\sigma} c_{j\sigma} + h.c), \tag{3.47}$$

$$\hat{K}_{ph} = \frac{w_0}{2} \sum_j \hat{P}_j^2, \tag{3.48}$$

whereas the potential term of pure electronic, mixed and pure phononic as

$$\hat{V} = \frac{U}{2} \sum_j (n_j - 1)^2, \tag{3.49}$$

$$\hat{V}_{eph} = \sum_j \hat{X}_j (n_j - 1), \tag{3.50}$$

$$\hat{V}_{ph} = \frac{w_0}{2} \sum_j \hat{X}_j^2. \tag{3.51}$$

This time with the usual decomposition we obtain an expression of the single-time propagator as resulting with an error $\mathcal{O}(\Delta\tau)$

$$\mathcal{P} = e^{-\Delta\tau \hat{K}} e^{-\Delta\tau \hat{K}_{ph}} e^{-\Delta\tau \hat{V}} e^{-\Delta\tau \hat{V}_{eph}} e^{-\Delta\tau \hat{V}_{ph}}. \tag{3.52}$$

By using the HST transformation defined in Eq.(3.6) the interaction can be transformed as follows

$$e^{-\Delta\tau \frac{U}{2} (n_j - 1)^2} = \int_{-\infty}^{\infty} d\sigma \Big(\frac{e^{-\frac{1}{2}(\sigma^j)^2}}{\sqrt{2\pi}} \Big) e^{i\sqrt{\Delta\tau U}\sigma^j (n_j - 1)}. \tag{3.53}$$

After this operation the whole partition function can be written as

$$\begin{aligned}\mathcal{Z} = \int dX_1 dX_2..dX_{T+1} \langle \Psi_T | x_{T+1} \rangle \langle x_{T+1} || e^{-\Delta\tau K} \int_{-\infty}^{\infty} d\sigma_T \Big(\frac{e^{-\sum_j \frac{1}{2}(\sigma_T^j)^2}}{\sqrt{2\pi}} \Big) \\ e^{i\sqrt{\Delta\tau U}\sum_j (n_j-1)\sigma_T^j} e^{-\Delta\tau p^2/2} e^{-\Delta\tau g \sum_j \hat{X}_T^j (n_j-1)} e^{\frac{w_0}{2}\sum_j (\hat{X}_T^j)^2} |x_T\rangle\langle x_T| e^{-\Delta\tau K} \\ \int_{-\infty}^{\infty} d\sigma_{T-1} \Big(\frac{e^{-\sum_j \frac{1}{2}(\sigma_{T-1}^j)^2}}{\sqrt{2\pi}} \Big) e^{i\sqrt{\Delta\tau U}\sum_j (n_j-1)\sigma_{T-1}^j} e^{-\Delta\tau p^2/2} e^{-\Delta\tau g \sum_j \hat{X}_{T-1}^j (n_j-1)} \\ e^{\frac{w_0}{2}\sum_j (\hat{X}_{T-1}^j)^2} ...|x_2\rangle\langle x_2| e^{-\Delta\tau K} \int_{-\infty}^{\infty} d\sigma_1 \Big(\frac{e^{-\sum_j \frac{1}{2}(\sigma_1^j)^2}}{\sqrt{2\pi}} \Big) e^{i\sqrt{\Delta\tau U}\sum_j (n_j-1)\sigma_1^j} e^{-\Delta\tau p^2/2} \\ e^{-\Delta\tau g \sum_j \hat{X}_1^j (n_j-1)} e^{\frac{w_0}{2}\sum_j (\hat{X}_1^j)^2} |x_1\rangle\langle x_1 || \Psi_T \rangle.\end{aligned} \tag{3.54}$$

which can be written in a compact way as follows

$$\begin{aligned}\mathcal{Z} = \int [dX] \int [d\sigma] \exp\Bigg[-\frac{1}{2} \sum_{l,m,j} \Big(A_{l,m} X_l^j X_m^j + \delta_{l,m} (\sigma_l^j)^2 \Big) \Bigg] \\ \times \langle \Psi_T | \prod_{l=1}^{T} \Bigg\{ \exp\Bigg[\sum_j \Big(-\Delta\tau g X_l^j + i\sqrt{U\Delta\tau}\sigma_l^j \Big) (n_j - 1) \Bigg] \exp(-\Delta\tau K) \Bigg\} | \Psi_T \rangle,\end{aligned} \tag{3.55}$$

where

$$[dX] = \prod_{j,l} dX_j^l, \tag{3.56}$$

$$[d\sigma] = \prod_{j,l} d\sigma_j^l, \tag{3.57}$$

are defining the integration variables over phonon and electron fields. And

$$A_{l,m} = \frac{1}{w_0 \Delta\tau} [2\delta_{l,m} - \delta_{l,m+1} - \delta_{m,l+1}] + \Delta\tau w_0 \delta_{l,m}. \tag{3.58}$$

is the matrix defining the pure phononic part of the partition function expression as for the pure Holstein model described in the previous section. It is easy to show that the pure phononnic part can be diagonalized exactly with the expression as follows:

$$\sum_{l,m} A_{l,m} X_l^j X_m^j = \sum_{n=1}^{T} E_n (X_n^j)^2, \tag{3.59}$$

where

$$X_n^j = \sqrt{\frac{1}{T+1}} \sum_{l=1}^{T} \sin(w_n l) X_l^j, \tag{3.60}$$

and the eigenvalues

$$E_n = \frac{1}{w_0}(2 - 2\cos(w_n)) + \Delta\tau w_0, \tag{3.61}$$

with

$$w_n = \frac{\pi}{T+1} n. \tag{3.62}$$

One can see that in the Eq.(3.55) both the electronic and phononic fields are coupled to the density. In order to simplify this expression one can combine these terms as follows

$$\bar\sigma_j^l = \sigma_j^l + \frac{ig\Delta\tau}{\sqrt{U\Delta\tau}} X_j^l. \tag{3.63}$$

The simplified expression after this shift can be written as follows

$$\mathcal{Z} = \int [dX] \int [d\bar\sigma] \exp\left[-\frac{1}{2} \sum_{l,m,j} \left(A_{l,m} X_l^j X_m^j + \delta_{l,m}((\bar\sigma_l^j)^2 + \frac{2ig\Delta\tau}{\sqrt{U\Delta\tau}} \bar\sigma_l^j X_j^l - \frac{g^2\Delta\tau}{U}(X_j^l)^2) \right) \right] \times \langle \Psi_T | \prod_{l=1}^{T} \left\{ \exp\left[\sum_j \left(i\sqrt{U\Delta\tau}\,\bar\sigma_l^j \right)(n_j - 1) \right] \exp\left(-\Delta\tau K\right) \right\} |\Psi_T\rangle. \tag{3.64}$$

However, this operation will lead a complex shift in the boundaries of the integral as $\int_{-\infty + \frac{ig\Delta\tau}{\sqrt{U\Delta\tau}} X_j^l}^{\infty + \frac{ig\Delta\tau}{\sqrt{U\Delta\tau}} X_j^l}$. According to the Cauchy theorem the integration of any function that is analytical inside a contour C is zero [36], namely:

$$\oint_C f(z) dz = 0. \tag{3.65}$$

where C is a closed contour over which the function $f(z)$ is integrated. The partition function in Eq.(3.64) is analytical since there is no pole in the contour $C = C1 + C2 + C3 + C4$ shown in the Figure 3.5. The shifted integration can be moved back to the real axis in the case the integration $\int_{C2+C4} \int [dX] \int [d\bar\sigma] [....] \to 0$ as $R \to \infty$. This condition is satisfied as long as the propagator is positive definite and since the Gaussian term of the order of $\int_{C2+C4} \int [dX] \int [dy] \exp(-R^2/2)[....]$ will suppress the other contributions as $R \to \infty$ leading the overall integration over the y-axis to be zero on $C2 + C4$ shown in Figure 3.5. With this in mind now we can shift all the $[d\bar\sigma]$ integrations to the real axis with real valued $\bar\sigma$ variables.

By defining

$$A' = A - \frac{g^2\Delta\tau}{U} I, \tag{3.66}$$

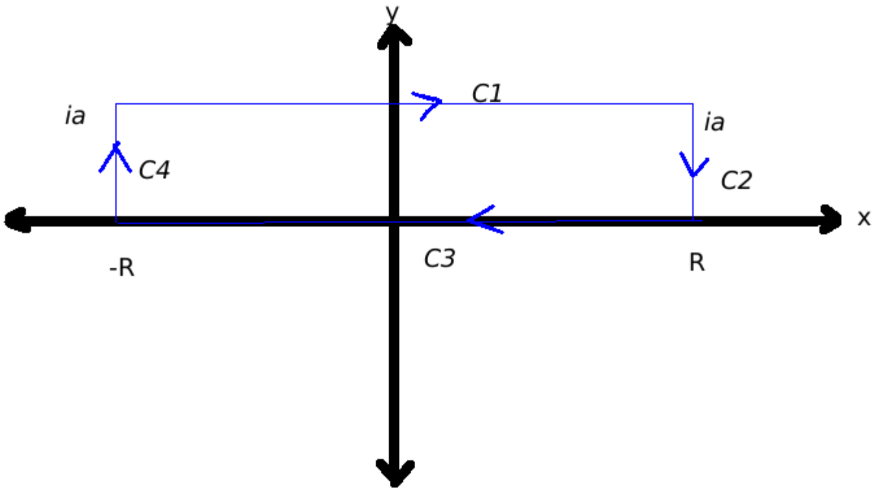

Figure 3.5: Schematic contour integration of a function integrated over a closed contour $C = C1 + C2 + C3 + C4$. The shift $\int_{-\infty+\frac{ig\Delta\tau}{\sqrt{U\Delta\tau}}X_j^l}^{\infty+\frac{ig\Delta\tau}{\sqrt{U\Delta\tau}}X_j^l}$ corresponds to the integrals in the imaginary y-axis with $ia = \frac{ig\Delta\tau}{\sqrt{U\Delta\tau}}X_j^l$.

the partition function can be rearranged as follows

$$\mathcal{Z} = \int [dX] \int [d\bar{\sigma}] \exp\Bigg[-\frac{1}{2}\sum_{l,m,j}\Big(A'_{l,m}X_l^j X_m^j + \delta_{l,m}((\bar{\sigma}_l^j)^2 + \frac{2ig\Delta\tau}{\sqrt{U\Delta\tau}}\bar{\sigma}_l^j X_j^l\Big)\Bigg]$$
$$\times\langle\Psi_T| \prod_{l=1}^{T}\Bigg\{\exp\Bigg[\sum_j \Big(i\sqrt{U\Delta\tau}\bar{\sigma}_l^j\Big)(n_j-1)\Bigg]\exp\left(-\Delta\tau K\right)\Bigg\}|\Psi_T\rangle. \tag{3.67}$$

Any Gaussian integral including complex quantities can be evaluated as follows

$$\int \exp\Big(-\frac{1}{2}\mathbf{x}.\mathbf{A}'.\mathbf{x} + i\mathbf{J}.\mathbf{x}\Big)d\mathbf{x} = \sqrt{\frac{(2\pi)^N}{\det\left(A'\right)}}\exp\Big(-\frac{1}{2}\mathbf{J}.\mathbf{A}'^{-1}.\mathbf{J}\Big). \tag{3.68}$$

where $\mathbf{X}$ is an N dimensional vector such that $\mathbf{X} = \{X_i^j\}$ and $\mathbf{J} = \frac{2g\Delta\tau}{\sqrt{U\Delta\tau}}\bar{\sigma}$ with $\bar{\sigma} = \{\bar{\sigma}_i^j\}$ where i, j indicating time slice and the site index respectively. Likewise, after rearranging the terms in the exponential, one can integrate over the phononic fields X and obtain the following expression of the partition function

$$\begin{aligned}\mathcal{Z} = C(\Delta\tau)\int[d\bar{\sigma}]\exp\Bigg[-\frac{1}{2}\sum_{l,m,j}\Big(P_{l,m}\bar{\sigma}_l^j\bar{\sigma}_m^j\Big)\Bigg]\\ \times\langle\Psi_T|\prod_{l=1}^{T}\Bigg\{\exp\Bigg[\sum_j\Big(i\sqrt{U\Delta\tau}\bar{\sigma}_l^j\Big)(n_j-1)\Bigg]\exp\left(-\Delta\tau K\right)\Bigg\}|\Psi_T\rangle,\end{aligned} \tag{3.69}$$

where

$$C(\Delta\tau) = \sqrt{\frac{(2\pi)^{NT}}{\det\left(A'\right)^T}}, \tag{3.70}$$

$$P_{l,m} = \delta_{l,m} + \frac{\Delta\tau g^2}{U}[A']^{-1}_{l,m}, \tag{3.71}$$

$$A' = A - \frac{g^2\Delta\tau}{U}I, \tag{3.72}$$

$$[A']^{-1}_{l,m} = \frac{2}{T+1}\sum_{n=1}^{T}\sin\left(w_n l\right)\sin\left(w_n m\right)(E_n - \frac{g^2\Delta\tau}{U})^{-1}, \tag{3.73}$$

$$\det\left(A'\right) = \prod_{n=1}^{T}(E_n - \frac{g^2\Delta\tau}{U}). \tag{3.74}$$

After all this operations we have a very simple expression for the overall partition function. As it can be seen, whenever the matrix $P_{l,m}$ is positive definite we have a convergent expression for the partition function. This condition is satisfied as long as

$$U \geq \frac{g^2}{w_0} \tag{3.75}$$

One can also observe that after a particle-hole transformation defined in the previous chapter we have

$$\begin{aligned}\mathcal{Z} = C(\Delta\tau)\int[d\bar{\sigma}]\exp\Bigg[-\frac{1}{2}\sum_{l,m,j}\Big(P_{l,m}\bar{\sigma}_l^j\bar{\sigma}_m^j\Big)\Bigg]\\ \times\langle\Psi_T|\prod_{l=1}^{T}\Bigg\{\exp\Bigg[\sum_j\Big(i\sqrt{U\Delta\tau}\bar{\sigma}_l^j\Big)(n_{\uparrow j}-n_{\downarrow j})\Bigg]\exp\left(-\Delta\tau K\right)\Bigg\}|\Psi_T\rangle.\end{aligned} \tag{3.76}$$

which results in spin-up and spin-down parts of the partition function to be complex conjugate of each other. Therefore, at half-filling this property will allow us to have always positive weights. In this way, we will be able to perform calculations without experiencing sign problem. In case some order is included in the trial wave function, this should also satisfy the condition that the spin-up part will be the complex conjugate of the spin down part. Otherwise the sign problem will affect the scheme. Antiferromagnetic order satisfies the previous condition since after the particle hole transformation, we will obtain the required condition to avoid the sign problem.

3.3.1 Test Sign Free Projector Molecular Dynamics on Pure Hubbard Model at Half Filling

Before investigating the ground state properties of the Hubbard-Holstein model one should perform some benchmark calculations in order to test the correctness of our newly formulated approach. As emphasized in the case of the pure Holstein model, the discretization of MD equations results in an error of the order of the time step. Therefore, one should perform an extrapolation to the zero time step which is the limit of unbiased sampling. In here, we would like to perform benchmark calculations for the pure Hubbard model by comparing them with AFQMC calculations which are not affected by the time step errors.

Figure 3.6 shows the kinetic energy, double occupation and the magnetization of the pure Hubbard model at U =4 on the 12x12 lattice as a function of the MD discretization time step for $\Delta\tau$ =0.1 and β =12. The Δ_{MD} =0 limit was simulated by purely MC method described in the very first section of the Chapter. It can be seen that we are able to simulate the pure Hubbard model with the extra cost of $\Delta_{MD} \to 0$ extrapolation. With this confidence, we can add the electron-phonon coupling and perform ground state calculations for the Hubbard-Holstein model which we will analyze in the upcoming chapters in detail.

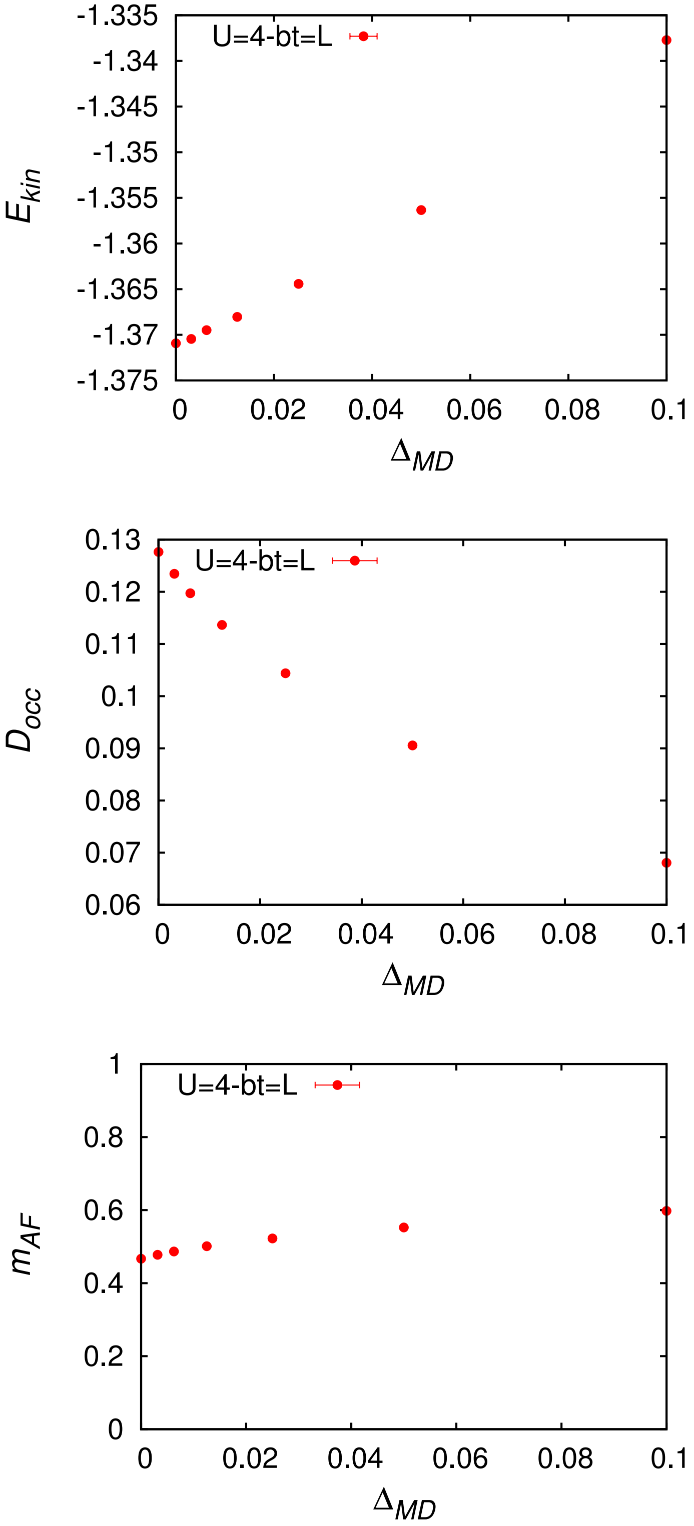

Figure 3.6: Kinetic energy, double occupation and magnetization at U=4 of pure Hubbard model as a function of MD step on the 12x12 cluster. The Δ_{MD} =0 values are obtained by AFQMC sampling.

Chapter 4

Twist Averaging and Finite-Size Errors in the Negative-U Hubbard Model

4.1 Twist Averaging Boundary Conditions (TABCs) for Lattice Models

Due to the computational cost, numerical simulations are done with finite number of particles. However, the main aim is usually to understand the thermodynamic properties of the systems. For example, for the simulation of electronic systems, different number of particles are used in order to reach the thermodynamic limit and extrapolate the observables of interest as a function of the system size. However, this task can be very difficult especially in the weak coupling ($|U|/t \ll 8$) regime because in this limit allowed finite number of momenta plays a crucial role, therefore, the results obtained with conventional periodic-boundary conditions (PBC) may significantly depend on the system size which makes the extrapolations to the thermodynamic limit very difficult. Due to this well known drawback of PBC numerical techniques dealing with fermions are facing a big and challenging limitation. Thermodynamic limit extrapolations of the models with simple Fermi surface, such as the half-filled Hubbard model as it is perfectly nested, can be thought as less severe but, at weak coupling, even this regime of interest can be very challenging.

Twist-averaged boundary conditions (TABCs) for Monte Carlo simulations have been introduced in order to control the finite size effects for the first time in continuum systems [37] and then adopted for lattice model [38, 39, 40, 41, 42, 43]. Brillouin zone integration is done via TABCs, therefore, physical quantities are estimated by averaging them over several twisted-boundary conditions [44], rather than limiting the calculation to a single set of k-points, such as PBC. It has been shown that within TABCs approach one can substantially reduce finite-size effects [37, 40, 41, 42, 43] and, within QMC, the cost of performing TABCs is the same as performing several independent calculations with different twists. Thus performing TABCs is particularly useful and appealing within QMC and, quite recently, is becoming widely used in order to study the properties of strongly correlated systems.

This approach has been used also for continuum models as reported in the reference [37]. Likewise, on a system defined on a lattice, by indicating the coordinates of the lattice site by $\mathbf{R}_i = (x_i, y_i)$ and the corresponding creation operators. Twisted-boundary conditions correspond to impose [44]:

$$\begin{aligned} c^{\dagger}_{\mathbf{R}_i+\mathbf{L_x}\sigma} &= e^{i\theta^{\sigma}_{x}} c^{\dagger}_{\mathbf{R}_i\sigma}, \\ c^{\dagger}_{\mathbf{R}_i+\mathbf{L_y}\sigma} &= e^{i\theta^{\sigma}_{y}} c^{\dagger}_{\mathbf{R}_i\sigma}, \end{aligned} \tag{4.1}$$

where $\mathbf{L_x} = (L, 0)$ and $\mathbf{L_y} = (0, L)$ are the vectors that define the periodicity of the square lattice; θ^{σ}_{x} and θ^{σ}_{y} are two phases in the interval $(-\pi, \pi)$ determining the twists along the x and the y directions. The number of sites N is given by $N = L^2$. In order to preserve time-reversal invariance and translational invariance of the BCS pairs, one can impose that $\theta^{\uparrow} = -\theta^{\downarrow}$ in both directions. The expectation value of any operator $\mathcal{A}$ in TABCs can be calculated by

$$\langle \mathcal{A} \rangle = \frac{1}{N_{\mathrm{TABC}}} \sum_{\theta} \frac{\langle \Psi_\theta | \mathcal{A}_\theta | \Psi_\theta \rangle}{\langle \Psi_\theta | \Psi_\theta \rangle}. \tag{4.2}$$

where $\theta = (\theta^{\sigma}_{x}, \theta^{\sigma}_{y})$, $\mathcal{A}_\theta$ is the operator corresponding to $\mathcal{A}$ under the applied boundary condition Eq. (4.1), N_{TABC} is the number of twist angles in the whole Brillouin zone, and $|\Psi_\theta\rangle$ is the uncorrelated wave function $|\Psi_T\rangle$ for VMC or for AFQMC, constructed by imposing a phase as in Eq. (4.1) to the trial wave function $|\Psi_{\mathrm{T}}\rangle$ as well as to the Hamiltonian of the system. However, one should note that all the wave functions with different θ share the same variational parameters, thus, while performing the stochastic optimization scheme for VMC described in Chapter 2 we average stochastically all the logarithmic derivatives resulting from different twisted wave functions. Also one should note that the two-body part and also the Jastrow correlator are not affected by the applied phase. In order to perform TABCs, we typically take $N_{\mathrm{TABC}} = 1088$ points in the Brillouin zone.

Recently, by using finite-temperature determinant quantum Monte Carlo without TABCs, the convergence of physical quantities to the thermodynamic limit have been examined for the canonical ensemble (CE) and the grand-canonical ensemble (GCE) [45],. It has been shown that finite size scaling via GCE provides a convergence faster than CE. One of the reason can be that due to the fluctuation of the particle number, the fermi surface of the system in the thermodynamic limit can be constructed, i.e., Gibbs-free energy at $U = 0$ coincides with the one in the thermodynamic limit [38]. Due to the fact that at zero temperature one occupies only the electronic states within the given Fermi surface, and therefore, it is extremely important for fermionic systems to allow an integration over many momenta, this mimics the thermodynamic limit. Therefore, while doing TABCs we will consider Brillouin zone integration also in the GCE.

4.2 Finite Size Errors in 2D Negative-U Hubbard Model

The achievements of numerical simulations are constantly increasing with very big impact on theoretical and experimental condensed matter physics as they allow reliable solutions of correlated models which cannot be solved analytically [46] and also providing accurate benchmark results about very important physical problems such as the emergent collective properties of quantum many-body systems, like Bose-Einstein condensation (BEC) and superconductivity. An interesting aspect of the numerical simulations is that it is possible to compare directly the results of the simulations with clean and realistic representations of Hubbard-like lattice models obtained for instance with ultracold atoms trapped in optical lattices [47, 48, 49, 50].

One of the simplest models describing the electrons subject to an attractive interaction is the negative-U Hubbard model. This model is clearly relevant for describing the standard mechanism of superconductivity within the Bardeen-Cooper-Schrieffer (BCS) theory [51, 52, 53]. There is a huge amount of literature about both the ground state and the finite temperature properties of this important model. However, we will mention a few of them related to the purpose of this work. At finite temperatures, the phase diagram of the model have been investigated by quantum Monte Carlo [54, 55, 56, 57, 58] and also there are dynamical-mean-field theory calculations [59, 60] to study the BEC to BCS crossover. Normal (non-superconducting) state properties have been studied via finite-temperature Monte Carlo calculations [61], by focusing mainly on the BCS-BEC crossover, and a work [62] was published investigating the zero temperature quantum critical point between a metal and a superconductor. There are also variational Monte Carlo (VMC) calculations at zero temperature where the ground-state properties of the model as a function of the interaction strength for several electron fillings [63, 64] having been studied.

The finite size effects are mostly pronounced at zero temperature and at weak coupling, therefore, it is very important to explore efficient ways to reduce these errors and benchmark them systematically. What we will do in this thesis is to assess with some confidence the behavior of the superconducting order parameter in this regime.

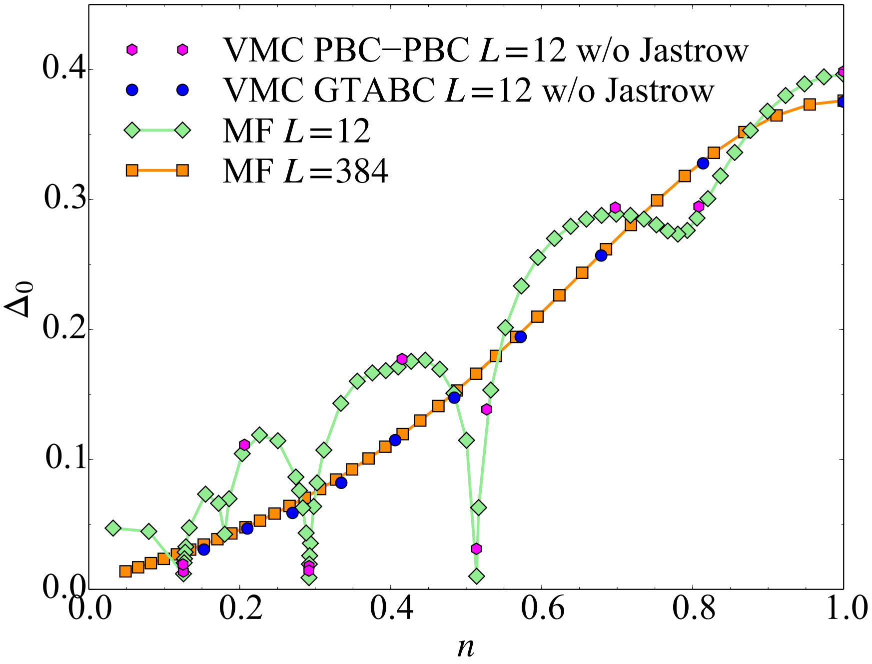

Figure 4.1: s-wave variational parameter Δ_0 as a function of n at $U = -2$. MF calculations are performed on $L = 12$ and $L = 384$ clusters, and VMC calculations are done in GCE without Jastrow correlator on $L = 12$ with PBC and TABCs. The error bars in the VMC results are smaller than the symbol sizes. (S.Karakuzu et al.,98,075156 (2018))

4.2.1 Size effects in mean-field approximation

Before investigating the finite-size effects in correlated systems, it is instructive to study the finite-size effects within the single-particle theory. For this purpose, we treat the attractive Hubbard model in Eq. (3.7) within the self-consistent mean-field approximation by decoupling the interaction term into the s-wave pairing terms.

$$\begin{aligned} c^\dagger_{i\uparrow}c^\dagger_{i\downarrow} &= \langle c^\dagger_{i\uparrow}c^\dagger_{i\downarrow}\rangle + \delta c^\dagger_{i\uparrow}c^\dagger_{i\downarrow}, \\ c_{i\downarrow}c_{i\uparrow} &= \langle c_{i\downarrow}c_{i\uparrow}\rangle + \delta c_{i\downarrow}c_{i\uparrow}. \end{aligned} \tag{4.3}$$

this approximation will allow the Hubbard Hamiltonian to be written as in the Eq.(2.25) with $\Delta = |U|\langle c^\dagger_{i\uparrow}c^\dagger_{i\downarrow}\rangle = |U|\langle c_{i\downarrow}c_{i\uparrow}\rangle$. One can write Eq.(2.25) in momentum space

$$\mathcal{H}_{\rm MF} = \sum_{\mathbf{k}\sigma} \epsilon_{\mathbf{k}} c^\dagger_{\mathbf{k}\sigma}c_{\mathbf{k}\sigma} + \Delta \sum_{\mathbf{k}} (c^\dagger_{\mathbf{k}\uparrow}c^\dagger_{-\mathbf{k}\downarrow} + c_{-\mathbf{k}\downarrow}c_{\mathbf{k}\uparrow}). \tag{4.4}$$

where $\epsilon_{\mathbf{k}} = -2t(\cos{(kx)} + \cos{(ky)}) - \mu_{BCS}$. After diagonalizing the equation via the transformation below [65]

$$\begin{aligned} \phi^{\dagger}_{\mathbf{k}\uparrow} &= u_{\mathbf{k}} c^{\dagger}_{\mathbf{k}\uparrow} + v_{\mathbf{k}} c_{-\mathbf{k}\downarrow}, \\ \phi^{\dagger}_{\mathbf{k}\downarrow} &= u_{\mathbf{k}} c^{\dagger}_{\mathbf{k}\downarrow} - v_{\mathbf{k}} c_{-\mathbf{k}\uparrow}. \end{aligned} \tag{4.5}$$

with the constraint that $u^2_{\mathbf{k}} + v^2_{\mathbf{k}} = 1$, one can show that the self-consistency equation can be written as

$$\frac{1}{|U|} = \frac{1}{L^2} \sum_{\mathbf{k}} \frac{1}{2E_{\mathbf{k}}}. \tag{4.6}$$

$$n = \frac{1}{L^2} \sum_{\mathbf{k}} \Big(1 - \frac{\epsilon_{\mathbf{k}}}{E_{\mathbf{k}}}\Big). \tag{4.7}$$

where $E_{\mathbf{k}} = \sqrt{\Delta^2 + \epsilon^2_{\mathbf{k}}}$.

In figure 4.1 the s-wave superconducting order parameter Δ_0 is shown as a function of electron density n where $n = 1$ corresponds to the half filling within the mean-field approximation at $U = -2$ for $L = 12$ and $L = 384$. It has been confirmed that the order parameter does not depend on the system size for $L \geqslant 384$, implying that by using $L = 384$ we have already converged to the thermodynamic limit. On the contrary, significant size effect, i.e., the oscillatory dependence on n is observed for $L = 12$ which shows that we are far from the thermodynamic limit for this cluster size.

One can obtain the same results by using the VMC and setting the Jastrow correlator $\mathcal{J}$ in Eq. (2.30) to be unity, i.e., $v_{i,j} = 0$. We have performed the VMC calculations on $L = 12$ and $L = 12$ with 32×32 twist angles in the whole Brillouin zone. One should note that, for the latter case, the number of the momenta in the Brillouin zone coincides with that for $L = 384$. We have shown that the results obtained by VMC in GCE without Jastrow part indeed well agree with those retained with the mean-field ones.

4.2.2 s-wave variational parameter

It is known that the mean-field calculations do not take into account the correlations between the electrons. However, we can improve the accuracy for treating the electron correlations by including the Jastrow correlations in Eq. (2.30). In the figure 4.2 we have plotted the superconducting variational parameter Δ_0 as a function of the electron density n within VMC for the clusters of size $L = 12$ and $L = 16$ with different boundary conditions and in different ensembles. We can see that when we use the fixed system size of $L = 12$, the results with a single boundary condition show oscillatory dependencies on n, as in the mean-field approximation for $L = 12$. On the contrary, within TABCs in both ensembles, the oscillatory dependencies are significantly smoothed. Is has been also shown that if we further increase the system size to $L = 16$, a sizable decrease of Δ_0 is observed in CE especially for the low-density regime, while the change in GCE is almost negligible, implying that by using the GCE our results show smaller size effects.

After confirming the significant reduction of the finite-size effects, we show in Fig. 4.3 how the Jastrow correlator affects the magnitude of the optimal variational parameter. By using the same system size of $L = 12$ with the same number of twist angles, the Jastrow correlator reduces the magnitude of the s-wave variational parameter by more than a factor of two for $n = 1$. Even when the electron density n is small, the reduction of the variational parameter is not negligible, showing the importance of the inclusion of the electron correlations. Note that, this systematic comparison of the variational wave function with and without Jastrow correlator for the entire doping range has been made possible only with TABCs, because the results with a single boundary condition exhibit oscillatory behaviours both in the mean-field approximation and the VMC.

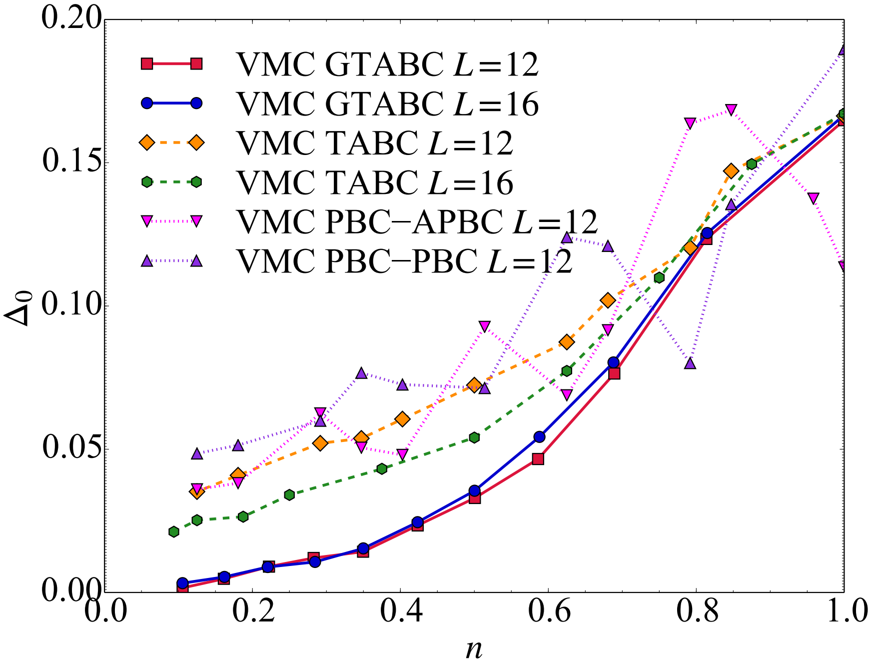

Figure 4.2: s-wave variational parameter Δ_0 as a function of n at $U = -2$ calculated by VMC. The system size and boundary conditions used are indicated in the figure. Here, GTABC represents the grand-canonical twist-averaged boundary conditions, TABC the canonical twist-averaged boundary conditions, PBC-APBC the PBC in one direction and APBC in the other, and PBC-PBC the PBC in the both directions. The error bars are smaller than the symbol sizes. (S.Karakuzu et al., 98,075156 (2018))

4.2.3 Pairing correlation function

Due to the fact that the wave function Ansatz explicitly breaks the U(1) symmetry, we have observed a finite order or equivalently finite variational parameters in the mean-field approximation or in the VMC calculations in finite-size systems. In order to compare the results with the ones of the numerically exact AFQMC, one has to calculate a correlation function because order parameters are zero by symmetry. In order to examine the long-range superconducting correlation, we define the s-wave pairing correlation function

$$\phi^2(L) = \frac{1}{2N}\sum_i \left\langle \Delta_i^\dagger \Delta_{i+j} + \text{H.c.} \right\rangle , \tag{4.8}$$

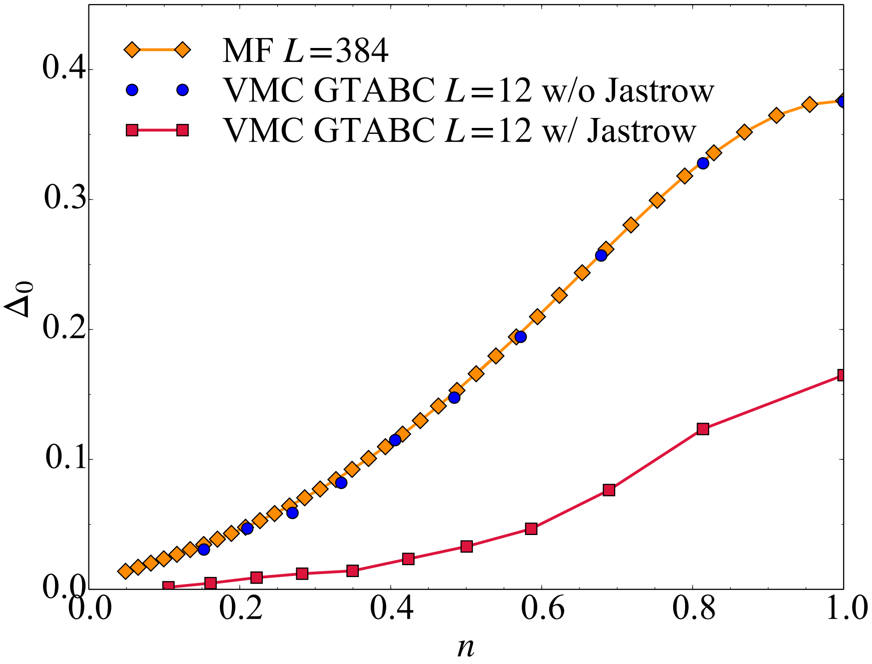

Figure 4.3: s-wave variational parameter Δ_0 as a function of n at $U = -2$. The results for MF on $L = 384$ and VMC on $L = 12$ with and without Jastrow correlator in GCE with TABCs are shown. The error bars in the VMC results are smaller than the symbol sizes. (S.Karakuzu et al., 98,075156 (2018))

where $\Delta_i^\dagger = c_{i\uparrow}^\dagger c_{i\downarrow}^\dagger$ and $i+j$ indicates the site that has the largest distance from site i for a given periodic system of system size $N = L^2$.

In the figure 4.4 we have shown the calculated pairing correlation function with VMC for various boundary conditions. As in the case of the variational parameter discussed in the previous section, strong finite-size effects are observed for $L = 12$ with single boundary condition. By further increasing the system size to $L = 16$, TABCs with CE reduce the oscillatory dependence on n. By changing the ensemble to GCE, the size effects are further reduced.

We have performed careful finite-size-scaling analyses for the pairing correlation function for $U = -2, -3$, and -4 at half filling and at quarter filling in Figs. 4.5 and 4.6, respectively. It can be seen that even at half filling it is almost impossible to extrapolate the pairing correlation in the case of single boundary conditions since the qualitative dependence on L changes as the system size grows

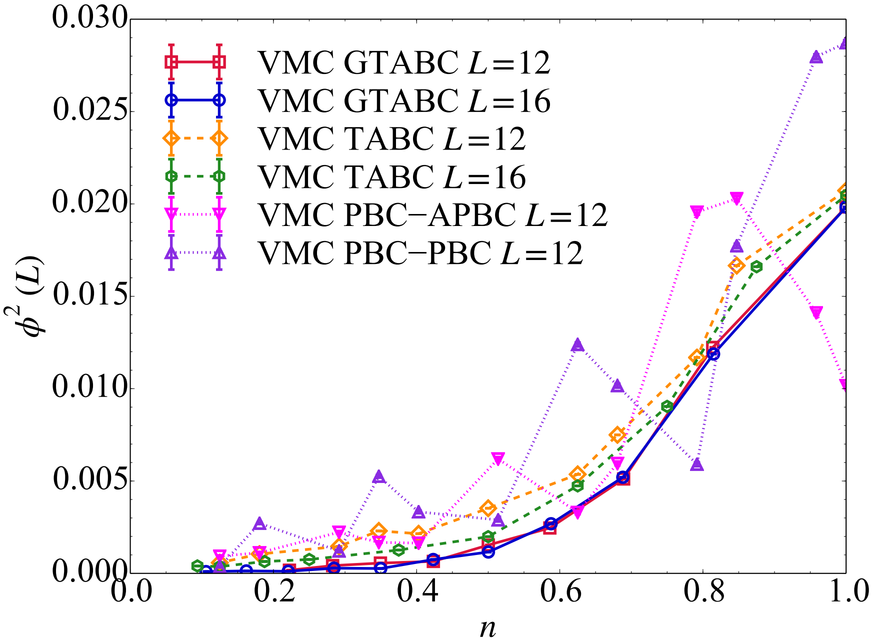

Figure 4.4: Pairing correlations ϕ^2 as a function of n at $U = -2$ calculated by VMC. The system size and boundary conditions used are indicated in the figure. The abbreviations are the same as those in Fig. 4.2. (S.Karakuzu et al., 98,075156 (2018))

especially when the value of $|U|$ is small. Moreover, it is evident that the TABCs with GCE represents the best available technique, much better than all the other approaches based on CE. In particular, at quarter filling, severe system-size dependencies of the correlation function are observed, implying that the finite-size scaling with a single PBC is almost impossible within the feasible cluster sizes. The extrapolated thermodynamic values of the superconducting correlations calculated by VMC in GCE via TABCs are reported as follows: 0.01994(4) for $U = -2$, 0.0497(4) for $U = -3$, and 0.0758(5) for $U = -4$ at half filling, and 0.00095(25) for $U = -2$, 0.0143(1) for $U = -3$, and 0.0378(4) for $U = -4$ at quarter filling.

Figure 4.7 shows the pairing correlations obtained with AFQMC for $L = 8$ and $L = 12$ as well as VMC in GCE on $L = 12$. As in the case of VMC, the results with the single PBC shows significant size effects, efficiently reduced by TABCs also within AFQMC. At variance with VMC, AFQMC results in the vicinity of the half filling shows the value of ϕ^2 becomes larger than that at half filling.

This behaviour has been observed in the early QMC study on the attractive Hubbard model [66], where the model can be mapped to the repulsive Hubbard model under the magnetic field (see also Sec. 4.2.4) and can be attributed to the spin-flop transition in the strong-coupling limit.

We show the finite-size scaling of the pairing correlation at half filling and at quarter filling calculated by AFQMC in Figs. 4.8 and 4.9, respectively. As in the case of VMC, the TABCs with GCE provide the better finite-size scaling than the single boundary condition one also in the case of AFQMC calculations. At half filling, the extrapolated values of ϕ^2 to the thermodynamic limit are 0.0098(3) for $U = -2$, 0.0222(6) for $U = -3$, and 0.0368(2) for $U = -4$.

At quarter filling, however, it can be seen that the system-size dependencies of the correlation function are much problematic for single boundary and they prevent us to perform a systematic extrapolation the thermodynamic limit. Remarkably this is possible within the TABC approach. We have done the same extrapolation also for the AFQMC calculations. The thermodynamic values of superconducting correlations are given as 0.0009(3) for $U = -2$, 0.0088(1) for $U = -3$, and 0.0266(2) for $U = -4$.

4.2.4 Attractive-repulsive mapping and order parameters

The attractive and repulsive routes of the Hubbard model are related to each other and they can be mapped to each other via the particle-hole transformation [67]

$$\begin{aligned} \tilde{c}_{i\uparrow} &\to c_{i\uparrow}, && (4.9) \\ \tilde{c}_{i\downarrow} &\to (-1)^{x_i+y_i} c^{\dagger}_{i\downarrow}. && (4.10) \end{aligned}$$

With the help of this mapping we can compare the results of the pairing correlation function $\phi(L)^2$ of the negative-U Hubbard model with those of the transverse spin-spin correlation function in the positive-U Hubbard model. Indeed, in terms of the newly defined operators $\tilde{c}_{i\sigma}$, $\tilde{c}^{\dagger}_{i\sigma}$ and $\tilde{n}_{i\sigma} = \tilde{c}^{\dagger}_{i\sigma}\tilde{c}_{i\sigma}$, the Hamiltonian can be written as $\mathcal{H} = \tilde{\mathcal{H}} - \mu N$, where

$$\begin{aligned}\tilde{\mathcal{H}} &= -t \sum_{\langle i,j\rangle,\sigma} \left(\tilde{c}_{i\sigma}^{\dagger} \tilde{c}_{j\sigma} + \text{H.c.} \right) + |U| \sum_i \tilde{n}_{i\uparrow} \tilde{n}_{i\downarrow} \\ &- \sum_i \left[(\mu - U)\tilde{n}_{i\uparrow} - \mu \tilde{n}_{i\downarrow} \right], \end{aligned} \tag{4.11}$$

whereas $\phi^2(L)$ can be written as the transverse spin-spin correlation function

$$\begin{aligned} M_{xy}^2(L) &= \frac{1}{2N} \sum_i (-1)^{x_j+y_j} \left\langle S_i^+ S_{i+j}^- + \text{H.c.} \right\rangle \\ &= \frac{1}{N} \sum_i (-1)^{x_j+y_j} \left\langle S_i^x S_{i+j}^x + S_i^y S_{i+j}^y \right\rangle, \end{aligned} \tag{4.12}$$

where $S_i^+ = \tilde{c}_{i\uparrow}^{\dagger} \tilde{c}_{i\downarrow}$, $S_i^- = (S_i^+)^{\dagger}$, $S_i^x = (S_i^+ + S_i^-)/2$, and $S_i^y = (S_i^+ - S_i^-)/2\mathrm{i}$. Similarly, the charge-charge correlation in the attractive Hubbard model can be mapped to the longitudinal spin-spin correlation in the repulsive Hubbard model. In the present study, however, the charge-charge correlations are not considered as they will not dominate over the pairing correlations for large distances away from the half filling.

Since the attractive Hubbard model with $\mu = U/2$ (the half-filled case) corresponds to the repulsive Hubbard model with zero magnetic field, the SU(2) symmetric staggered magnetization M_0 in the thermodynamic limit can be estimated from $M_{xy}(L)$ through the relation

$$M_0 = \sqrt{\frac{3}{2} \lim_{L\to\infty} M_{xy}^2(L)}, \tag{4.13}$$

where the factor 3/2 within the square root is multiplied to complement the contribution from the longitudinal spin-spin correlation which is not included in $M_{xy}^2(L)$. The estimated values of M_0 are as follows: 0.122(1) for $|U| = 2$, 0.183(2) for $|U| = 3$, and 0.2347(4) for $|U| = 4$. For $|U| = 2$ and 4, these values are in agreement with the previous study [43].

At quarter filling, the CDW order (the staggered magnetization along z axis under the mangetic field in the repulsive case) disappears. Therefore we define the s-wave order parameter as

$$\Phi_s = \sqrt{\lim_{L\to\infty} \phi^2(L)}. \tag{4.14}$$

Table 4.1: Comparison of the s-wave superconducting (antiferromagnetic) order parameter M_0 defined in Eq. (4.13) for the attractive (repulsive) Hubbard model at half filling ($n = 1$). The number in each parenthesis in this work indicates the uncertainty due to the extrapolation to the thermodynamic limit. DMET stands for density-matrix-embedding theory. (S.Karakuzu et al., 98,075156 (2018))

	$n = 1$		
$\lvert U\rvert/t$	2	3	4
VMC (this work)	0.1729(1)	0.2731(7)	0.3371(7)
AFQMC (this work)	0.122(1)	0.183(2)	0.2347(4)
AFQMC [43]	0.119(4)	–	0.236(1)
AFQMC [46]	0.094(4)	–	0.236(1)
DMET [46]	0.133(5)	–	0.252(9)

Table 4.2: Comparison of the s-wave superconducting order parameter Φ_s defined in Eq. (4.14) for the attractive Hubbard model at quarter filling ($n = 0.5$). The number in each parenthesis in this work indicates the uncertainty due to the extrapolation to the thermodynamic limit. (S.Karakuzu et al., 98,075156 (2018))

	$n = 0.5$		
$\lvert U\rvert/t$	2	3	4
VMC (this work)	0.031(4)	0.1196(6)	0.194(1)
AFQMC (this work)	0.030(4)	0.094(1)	0.163(1)

The estimated values of Φ_s from the extrapolated values of $\phi^2(L)$ are as follows: 0.030(4) for $|U| = 2$, 0.094(1) for $|U| = 3$, and 0.163(1) for $|U| = 4$.

Finally, the extrapolated values of the order parameters to the thermodynamic limit at half filling ($n = 1$) and at quarter filling ($n = 0.5$) are summarized in Table 4.1 and Table 4.2, respectively.

4.3 Conclusions and discussions

To conclude, finite-size effects on the s-wave order parameter and the pairing correlation function have been examined for the attractive Hubbard model with VMC and AFQMC methods. TABCs in GCE can reduce the size effects and provide smooth extrapolation to the thermodynamic limit. TABCs in GCE also enables to systematically examine the effect of the Jastrow correlator as a function of doping. It has been shown that the Jastrow correlator in VMC significantly reduces the magnitude of the s-wave variational parameter already in the entire doping range at $U = -2$.

We have presented the comparison of the pairing correlation functions for different values of Hubbard interaction U obtained by VMC and by numerically exact AFQMC. It has been found that the VMC provides good agreements with the AFQMC for finite doping. At half filling, there is an "accidental" SU(2) symmetry in the sense that it can be broken by a small perturbation such as the next-nearest-neighbor hopping t'. Since the wavefunction breaks this accidental SU(2) symmetry due to the inclusion of the s-wave pairing and the Jastrow correlator, the agreement between the VMC and AFQMC is not excellent as compared to the doped cases. The explicit breaking of the symmetry in the wave function also explains the reason that the spin-flop transition observed in AFQMC is not present in VMC.

However, defining the SU(2)-invariant variational wavefunction is in turn very difficult, if not practically impossible. For example, even if one prepares the antisymmetric part $|\Psi_{\mathrm{T}}\rangle$ so that the order parameters to be SU(2) symmetric by adding both s-wave pairing and CDW variational parameters, the Jastrow correlator $\mathcal{J}$ breaks the symmetry. Besides the symmetry consideration, one might be able to improve the quality of the variational wave function, for example, by further taking into account the backflow correlations, as in repulsive Hubbard models [68, 69].

The method for reducing the finite-size effects in the ground state developed in this thesis is applicable for any correlated lattice models. The calculation in GCE will be particularly useful for systematically investigating the doping dependence of the d-wave superconductivity in the repulsive Hubbard model with parameters relevant for cuprates. Furthermore, the strong reduction of the order parameter in the entire doping range due to the Jastrow correlator suggests that the electron-correlation effects beyond the mean-field approximation might not be negligible even in the weakly attracting fermions in the low-electron-density regime. This implies that the method will be also promising to study the ground-state properties of dilute electron systems. Such systems may include $TiSe_2$ in the series of transition metal dichalcogenides [70], where its electronic state is in vicinity of the semimetal-semiconductor transition and considered to be a candidate of excitonic insulators, in which coherent electron-hole pairs are formed and condensate spontaneously [71, 72].

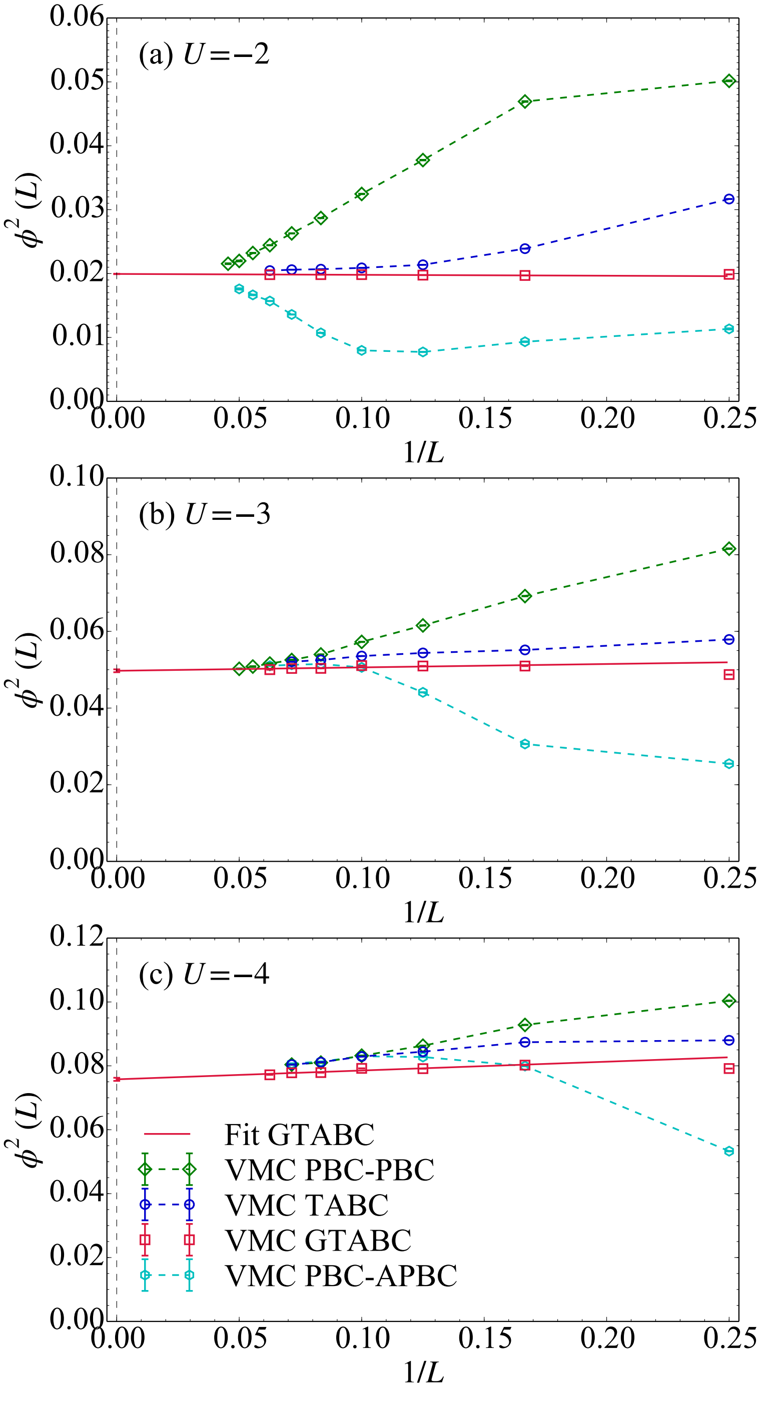

Figure 4.5: Finite-size scalings of the pairing correlation $\phi^2(L)$ for (a) $U = -2$, (b) $U = -3$, and (c) $U = -4$ by VMC at half filling with different boundary conditions. The solid lines are the fit to the GTABC data. The extrapolated value to the thermodynamic limit $\lim_{L\to\infty} \phi^2(L)$ is indicated at $1/L = 0$ for each panel. The abbreviations are the same as those in Fig. 4.2. (S.Karakuzu et al., 98,075156 (2018))

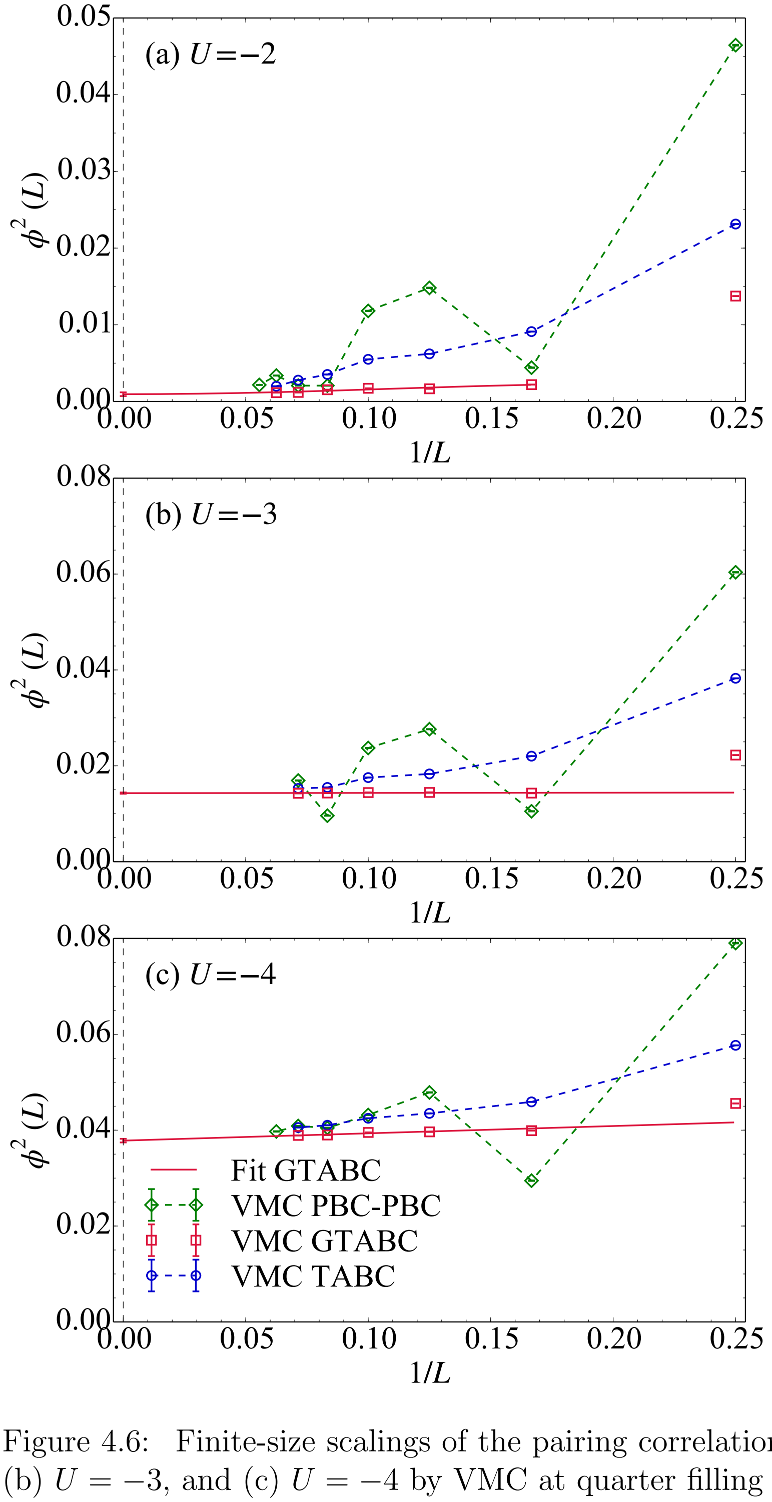

Figure 4.6: Finite-size scalings of the pairing correlation $\phi^2(L)$ for (a) $U = -2$, (b) $U = -3$, and (c) $U = -4$ by VMC at quarter filling with different boundary conditions. The solid lines are the fit to the GTABC data. The extrapolated value to the thermodynamic limit $\lim_{L\to\infty} \phi^2(L)$ is indicated at $1/L = 0$ for each panel. The abbreviations are the same as those in Fig. 4.2. (S.Karakuzu et al., 98,075156 (2018))

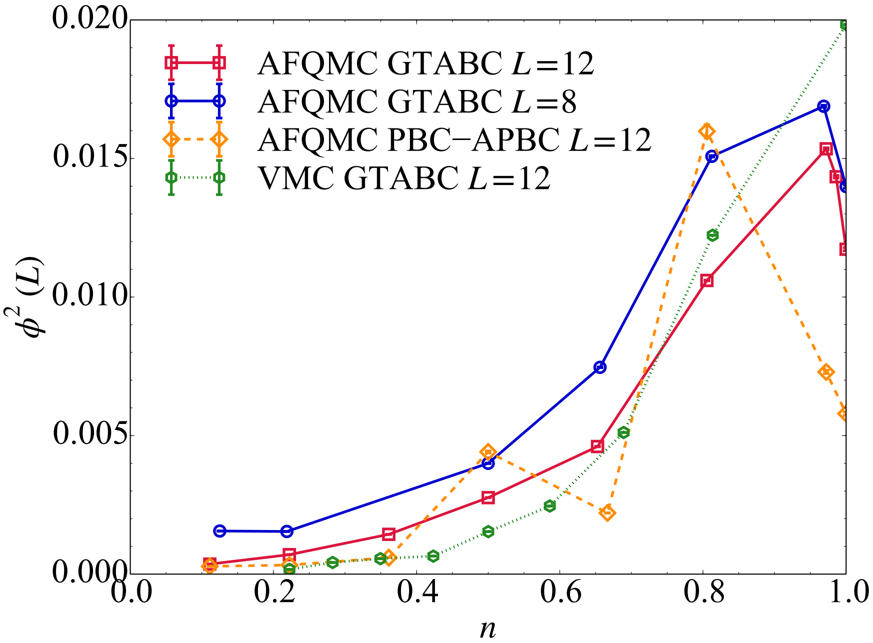

Figure 4.7: Pairing correlation ϕ^2 as a function of n at $U = -2$ by AFQMC and VMC. The system size and boundary conditions are indicated in the figure. The abbreviations are the same as those in Fig. 4.2. (S.Karakuzu et al., 98,075156 (2018))

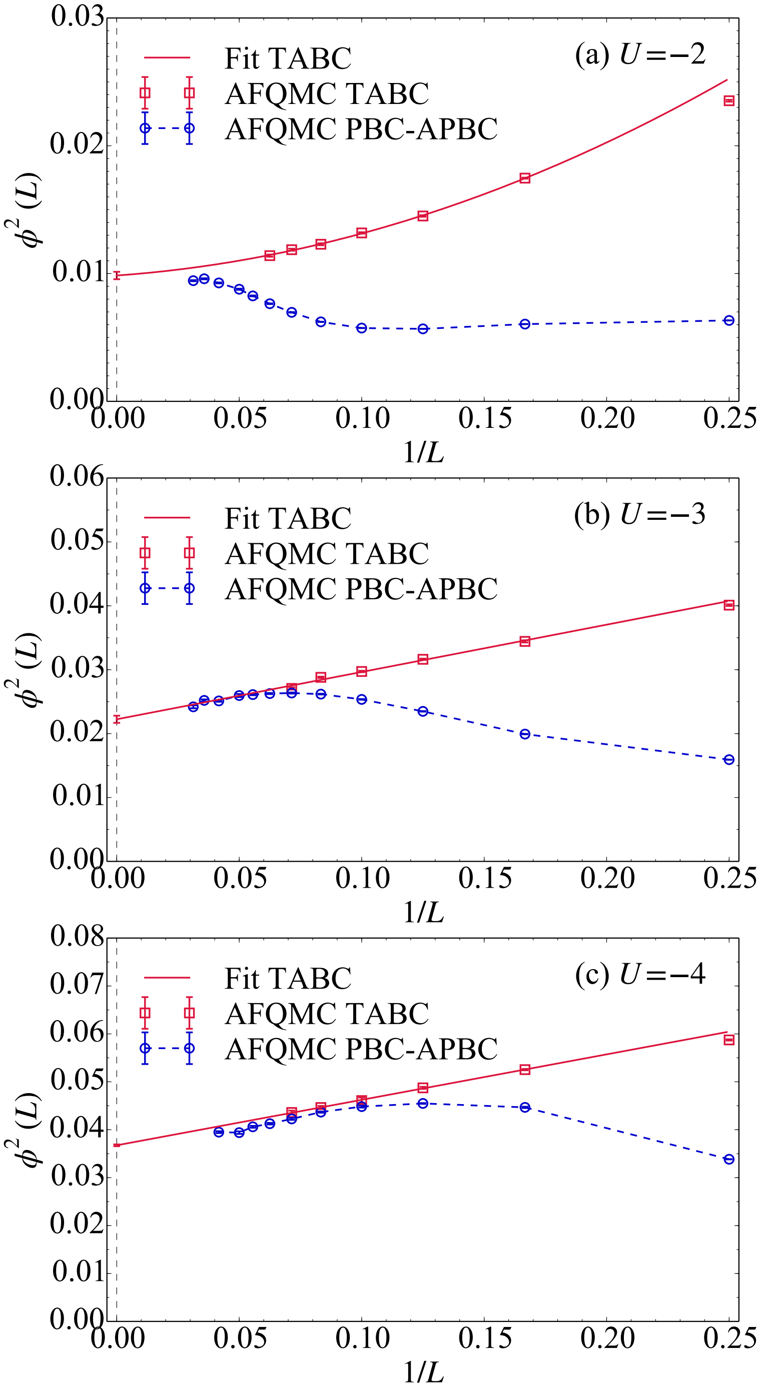

Figure 4.8: Finite-size scalings of the pairing correlation $\phi^2(L)$ for (a) $U = -2$, (b) $U = -3$, and (c) $U = -4$ by AFQMC at half filling with different boundary conditions. The solid lines are the fit to the TABC data. The extrapolated value to the thermodynamic limit $\lim_{L\to\infty} \phi^2(L)$ is indicated at $1/L = 0$ for each panel. The abbreviations are the same as those in Fig. 4.2. (S.Karakuzu et al., 98,075156 (2018))

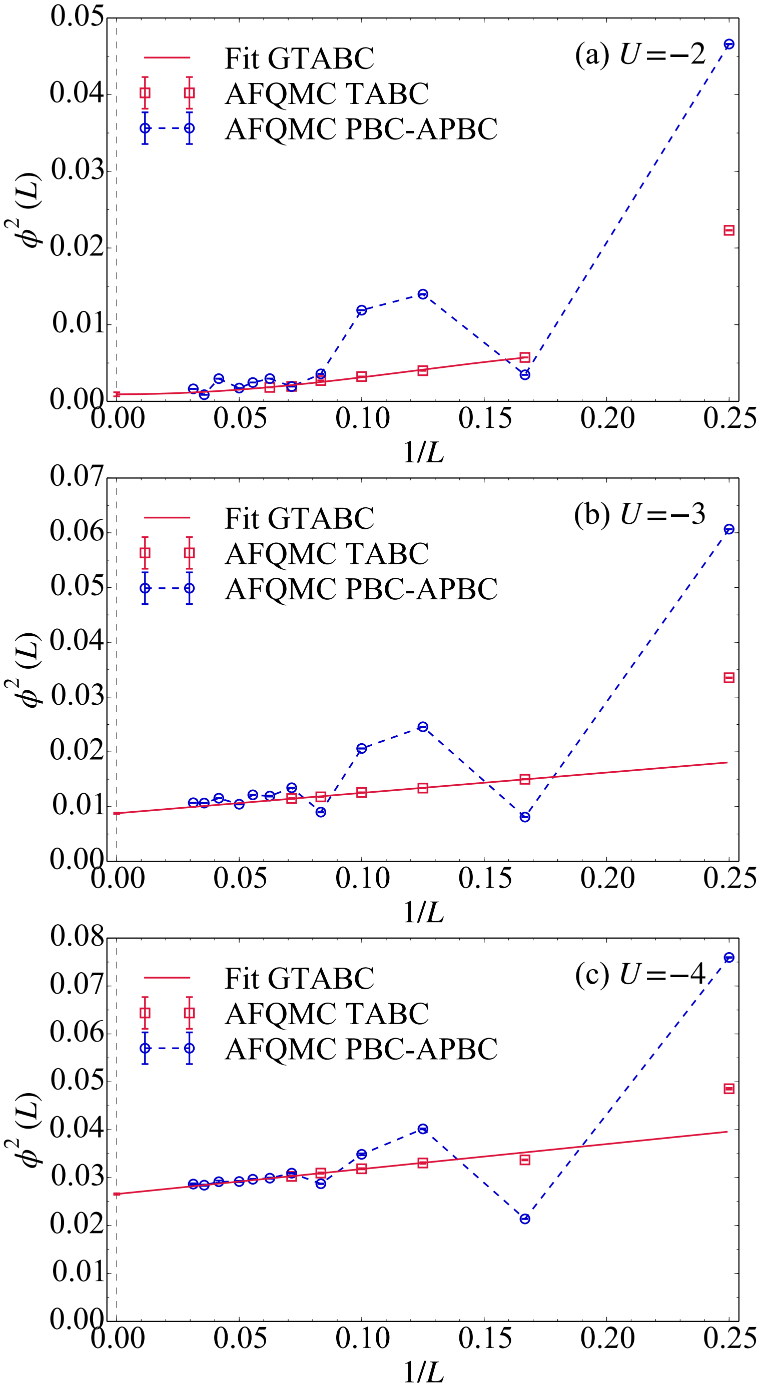

Figure 4.9: Finite-size scalings of the pairing correlation $\phi^2(L)$ for (a) $U = -2$, (b) $U = -3$, and (c) $U = -4$ by AFQMC at quarter filling with different boundary conditions. The solid lines are the fit to the GTABC data. The extrapolated value to the thermodynamic limit $\lim_{L\to\infty} \phi^2(L)$ is indicated at $1/L = 0$ for each panel. The abbreviations are the same as those in Fig. 4.2. (S.Karakuzu et al., 98,075156 (2018))

Chapter 5

Hubbard-Holstein Model by VMC

Previous perturbation theory studies and Monte Carlo calculations on the 1D Holstein model suggest that the ground state of the Holstein model displays CDW order for any non-zero electron-phonon coupling when $\omega_0/t < \infty$ [35, 73]. On the other hand, several studies using density-matrix renormalization group (DMRG) and Monte Carlo techniques have suggested that there exists a gapless phase with superconducting correlations for small values of the electron-phonon coupling and finite phonon energies, and it has been shown that this phase persists also when the values of U/t is finite, namely for the Hubbard-Holstein model [74, 75, 76, 77, 78, 79]. In addition to these studies, in the limit of infinite dimensions, dynamical mean-field theory (DMFT) has been employed to investigate the competition between superconductivity and CDW order [80, 81, 16, 82], the effect of phonons in the vicinity of the Mott transition [83, 15], the verification of the Migdal-Eliashberg theory [14], the polaron formation, and the existence of the isotope effect [84, 85, 86]. However, the Hubbard-Holstein model in two-dimensions has been very little studied in the past, especially due to the sign problem that the exact quantum Monte Carlo techniques suffer from [87, 17, 18] as explained in detail in the 3rd chapter. Therefore, the Hubbard-Holstein model has been mainly considered within mean-field approaches [88, 89, 12, 90] or by using perturbative

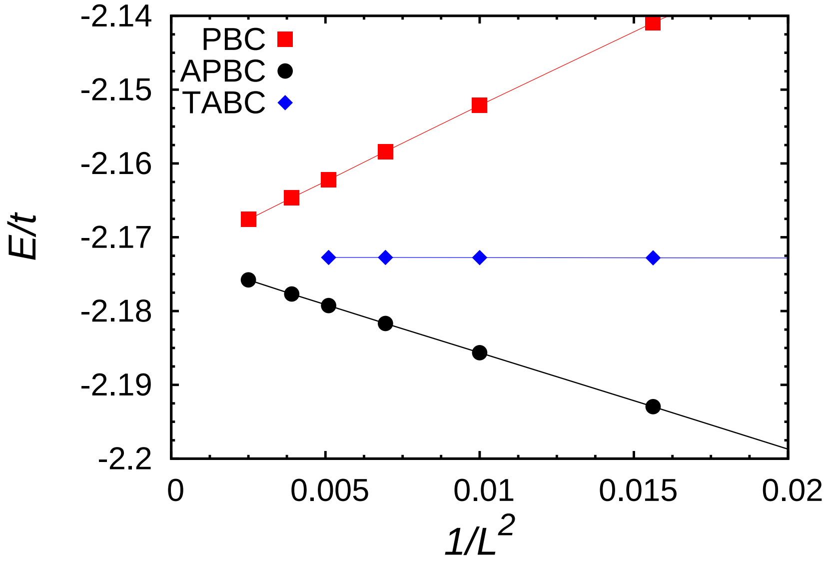

Figure 5.1: Size scaling of the energy per site at half filling (with $\omega_0/t = 1$, $\lambda/t = 0.98$, and $U = 0$) for periodic-periodic (PBC), periodic-antiperiodic (APBC), and twisted average (TABC) boundary conditions. Error bars are smaller than the size of the symbols. (S.Karakuzu et al., 96,205145 (2017))

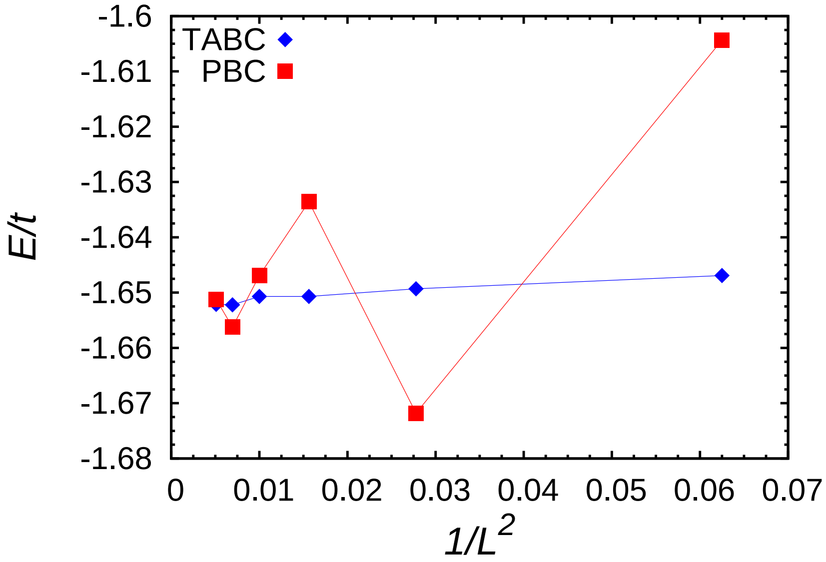

Figure 5.2: Size scaling of the energy per site at quarter filling (with $\omega_0/t = 1$, $\lambda/t = 2$, and $U = 0$) for periodic-periodic (PBC) and twisted average (TABC) boundary conditions. Error bars are smaller than the size of the symbols. (S.Karakuzu et al., 96,205145 (2017))

methods [91, 92]. There is also a work done by using the Variational Monte Carlo (VMC) method to study the interplay between electron-electron and electron-phonon interactions in the Su-Schrieffer-Heeger (SSH) model [93]. More recently, Ohgoe and Imada used the VMC approach to investigate the ground-state phase diagram of the Hubbard-Holstein model at half filling and at finite doping [13]. Similar variational wave functions have been used to study the electron-phonon coupling in multi-band models [94].

One of the important features of the phase diagram of the Hubbard-Holstein model is that it displays transition between a charge densiry wave (CDW) (bi-polaronic) and a Mott insulator at half filling and also the exciting possibility that a metallic/superconducting phase may exist in between these two phases [95, 96]. In the antiadiabatic limit, namely when $\omega_0/t \to \infty$, the Holstein model can be mapped to the negative-U Hubbard model. Due to this property of the model one can expect a direct transition between an antiferromagnetic (Mott) insulator, that is stable for $U > \lambda$, and a CDW insulator, that is stable for $U < \lambda$. However, in this limit, as explained in the previous Chapter, the CDW state is degenerate with an s-wave superconductor, due to the SU(2) pseudo-spin symmetry of the negative-U Hubbard model. In some studies the properties of the transition between the two insulating states and the possibility of an intermediate phase have been investigated. In one dimension, it has been reported that there exists a metallic phase, with strong superconducting correlations, by DMRG studies [76, 77, 78]. It has also been shown that this intermediate region broadens with increasing the phonon energy (up to $\omega_0/t \approx 5$). On the other hand, the DMFT calculations showed some results which are contradicting with the ones of DMRG, claiming that there exists either a direct transition between CDW and Mott insulator [16] or this intermediate phase is very tiny [82]. Not only in 1D but also in 2D the situation is not clear with the current studies yet. One of the few calculations on 2D Hubbard-Holstein model has been done in Refs. [17, 18], in which they report some evidence for the existence of an intermediate metallic region at finite temperatures at half filling. Unfortunately, away from half filling it is almost hopeless to perform reliable calculations due to the sign problem which is very severe, such that it prevents one from drawing conclusions. Therefore, in this thesis we would like to propose some other approaches to tackle the problem. The VMC technique is one of the possibilities for which one needs to define suitable wave functions as explained in the previous chapter. In this aspect, Ohgoe and Imada have recently proposed the "many-variable" VMC wave function which includes also phonon degrees of freedom [13, 97], and they showed the evidence of a metallic (with weak superconducting correlations) phase between the CDW and the Mott insulator at half filling. They also pointed out the presence of phase separation when doping the CDW insulator, whereas, the ground state is found to be uniform when doping the metallic phase.

In this thesis, in order to reduce finite-size effects to reach much faster the thermodynamic limit, as explained in the 3rd chapter, we employ canonical TABC with an average over $N_\theta = 576$ points in the Brillouin zone in order to evaluate the expectation value of the Hamiltonian or any other operator. In Fig. 5.1, we show the size scaling of the energy per site when applying the TABC procedure at half filling for $U = 0$, $\lambda/t = 0.98$, and $\omega_0/t = 1$, and we have compared the results obtained by TABC with the standard cases with periodic-periodic and periodic-antiperiodic boundary conditions. In all three cases, the optimized variational wave functions have $\Delta_{\text{SC}} \neq 0$ (and $\Delta_{\text{CDW}} = \Delta_{\text{AF}} = 0$) and the extrapolated values are all consistent (within few error-bars), and the obtained ground state energy for all of the cases is $E/t = -2.1725(1)$. Away from half filling, as shown also in the previous chapter, size effects become even more pronounced and it is very crucial to use TABC to extract accurate values of the observables in the thermodynamic limit. In Fig. 5.2, we show the case at quarter filling when $U = 0$, $\lambda/t = 2$, and $\omega_0/t = 1$. As one can see, the periodic-periodic boundary conditions give scattered results. However, by averaging over twisted boundary conditions, we obtain rather smooth extrapolation to $E/t = -1.652(1)$. Also in the case of the Hubbard-Holstein model we would like to emphasize the importance of using TABC rather than using fixed boundary conditions, since the latter ones imply huge size effects and require large clusters to reach accurate results in the thermodynamic limit. With this useful tool in hand we are going to examine the ground state properties of the model by considering relatively small clusters in our numerical simulation, with nevertheless small finite-size errors.

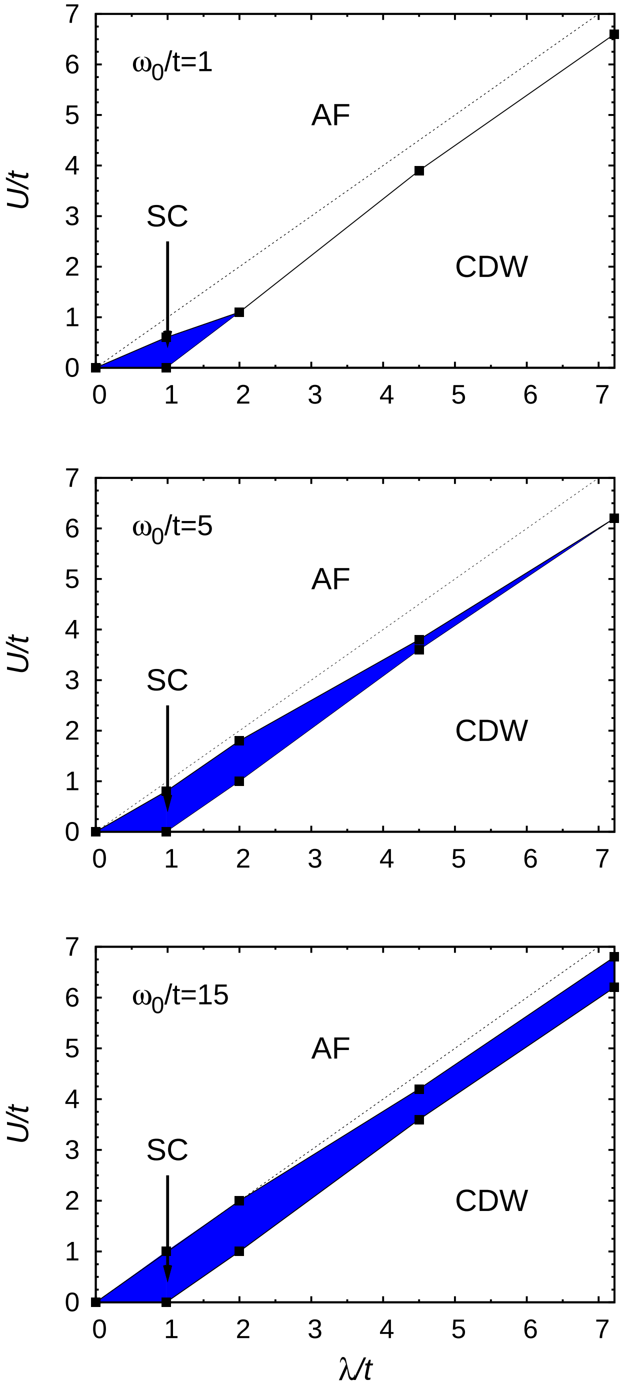

Figure 5.3: Ground-state phase diagram in the $(\lambda/t, U/t)$ plane for the Hubbard-Holstein model at $\omega_0/t = 1$ (upper panel), $\omega_0/t = 5$ (middle panel), and $\omega_0/t = 15$ (lower panel). Antiferromagnetic (AF), charge-density-wave (CDW), and superconducting (SC) phases are present, the latter one being marked in blue. The calculations have been performed on the 12×12 cluster with TABC. The dotted line $U = \lambda$ is also marked for reference. (S.Karakuzu et al., 96,205145 (2017))

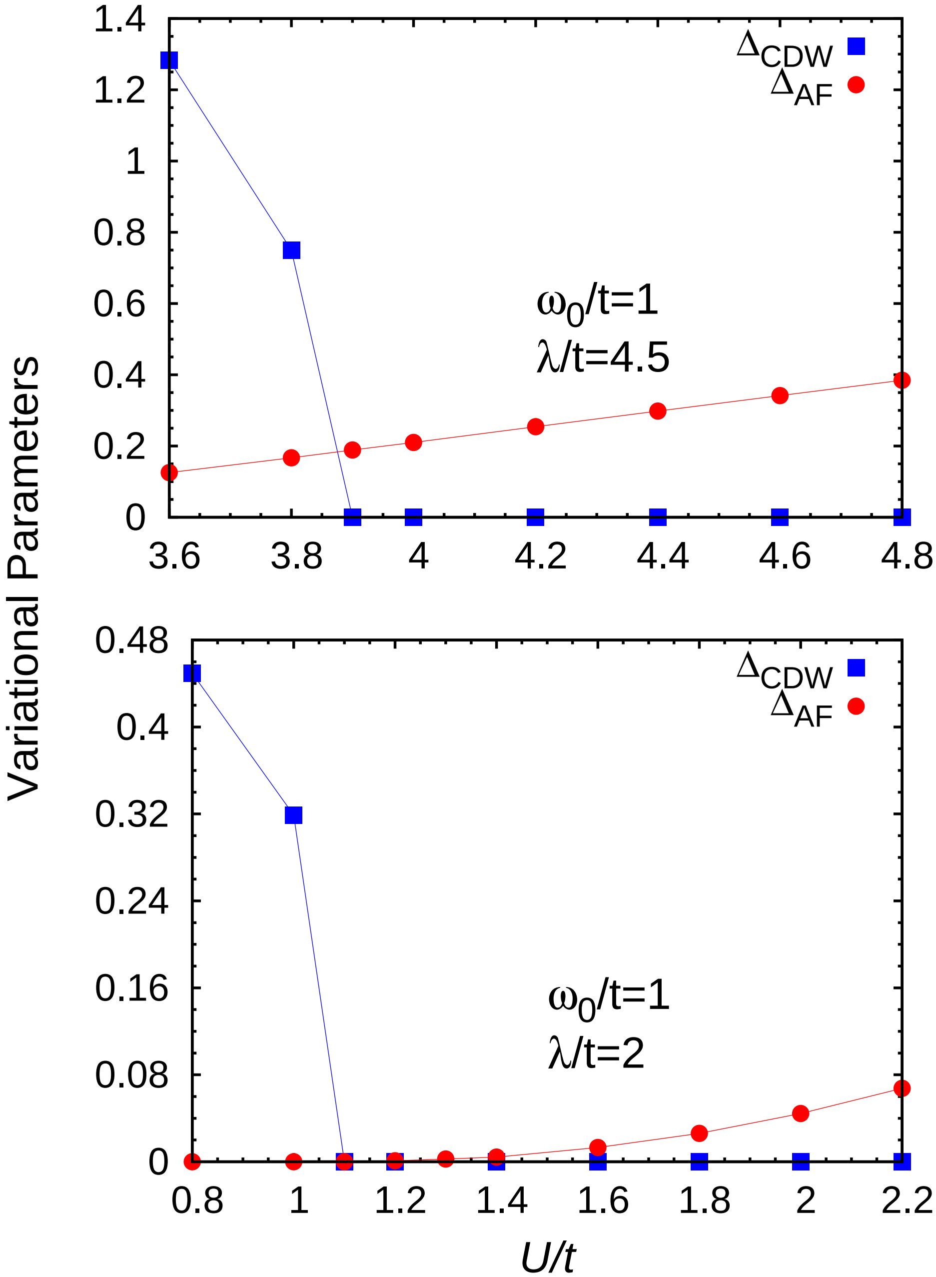

Figure 5.4: Antiferromagnetic and charge-density-wave parameters for the case with $\omega_0/t = 1$. The case with $\lambda/t = 4.5$ (upper panel), where a first-order phase transition between these two insulators is present, and $\lambda/t = 2$ (lower panel), where a continuous phase transition takes place, are reported. The calculations have been performed on the 12×12 cluster with TABC and error bars are smaller than the size of the symbols.(S.Karakuzu et al., 96,205145 (2017))

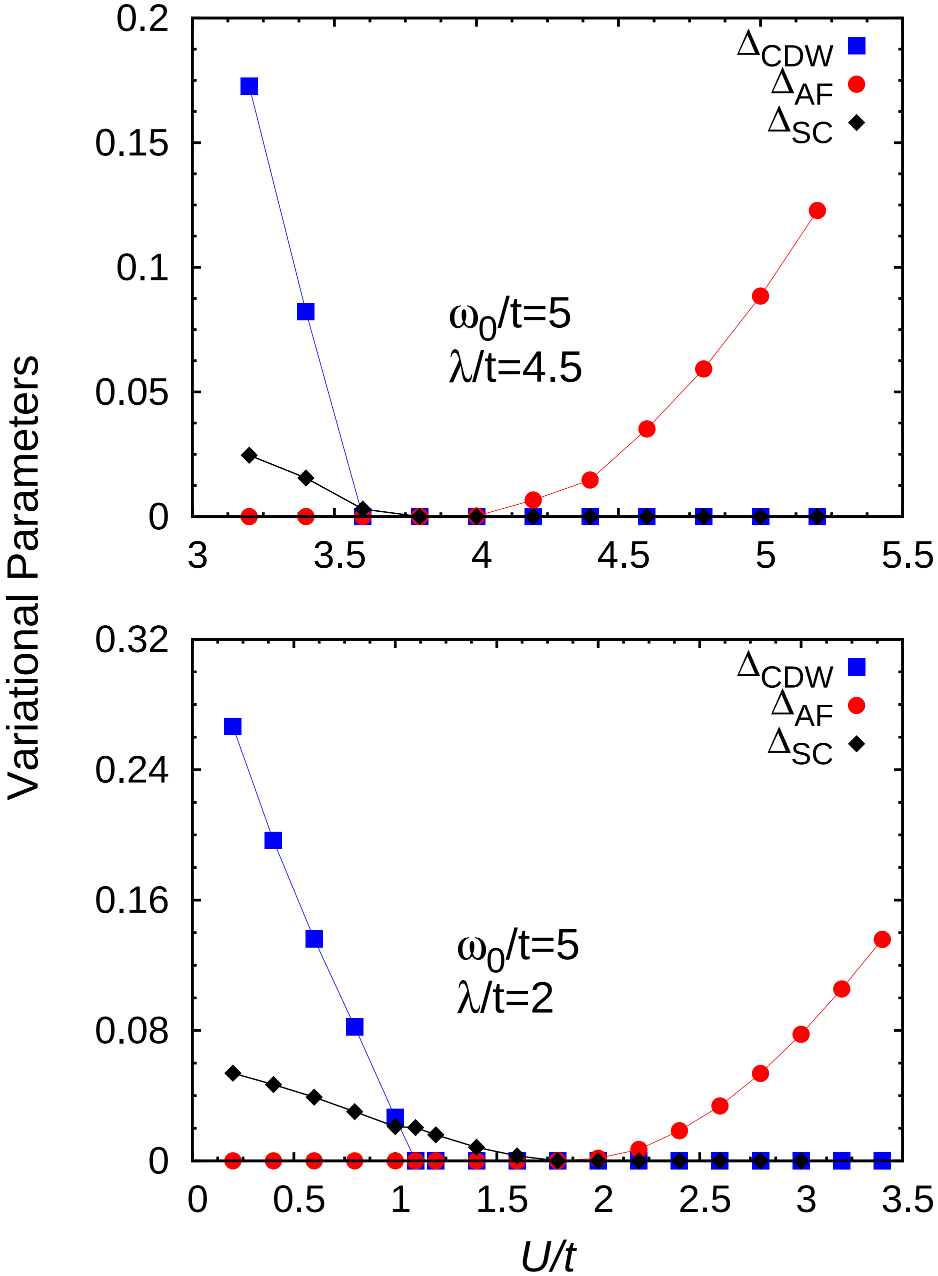

Figure 5.5: The same as in Fig. 5.4 for $\omega_0/t = 5$. Here, also the superconducting parameter is reported. (S.Karakuzu *etal.*,96,205145 (2017))

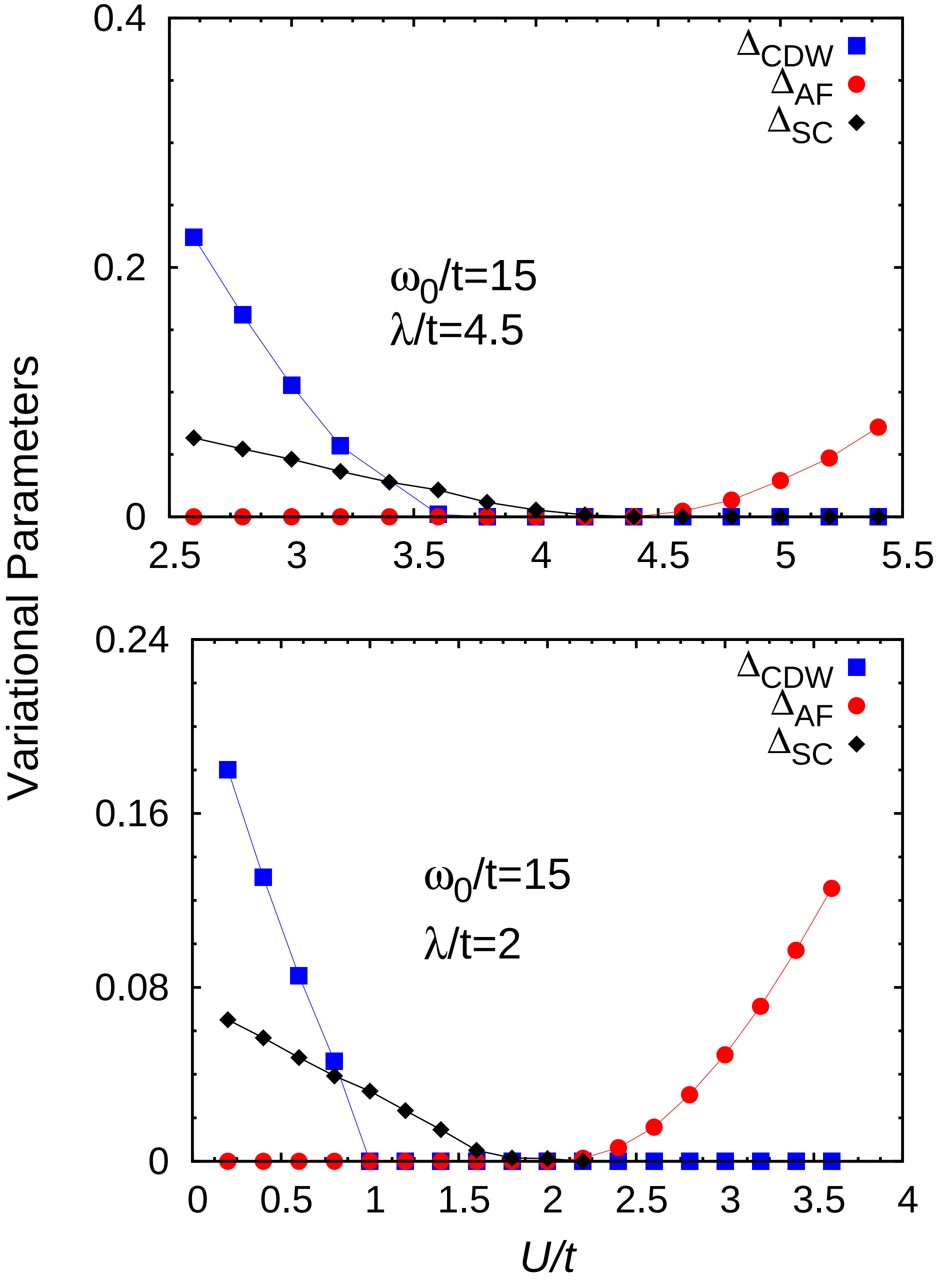

Figure 5.6: The same as in Fig. 5.5 for $\omega_0/t = 15$.(S.Karakuzu et al., 96,205145 (2017))

5.1 Results For The Half-filled case

In this section, we would like to show our numerical results for the half-filled case $n = N_e/N = 1$ and then move to the doped region with $n < 1$. In Fig. 5.3, we report the ground-state phase diagram of the Hubbard-Holstein model for three values of ω_0/t, i.e., $\omega_0/t = 1$, 5, and 15, at half filling. As it is shown in the plot, we represent the phase diagram by three different phases. When the electron-electron interaction is large compared to the electron-phonon coupling, the ground state has long-range antiferromagnetic order so that the uncorrelated part of the electronic wave function has $\Delta_{\text{AF}} \neq 0$. It can be seen that for all the values of the phonon energies this phase is approximately bounded from below) by the line. In one dimension by DMRG [76, 77, 78] and in two dimensions by VMC [13] similar behaviours have been reported. On the other hand, for large electron-phonon coupling, the ground state is a CDW insulator. In this case the system has doubly-occupied sites (doublons) and empty sites (holons) and they form a checkerboard pattern. When this charge modulation occurs a large number of phonons are present on top of doublons, while no phonons are present on empty sites. Due to this phonon cloud and localization the kinetic energy of the electrons are reduced drastically so that they hardly hop around in the lattice. Finally, between these insulators (antoferromagnetic and charge ordered) there exists an intermediate superconducting phase with pairing correlations that grow by increasing ω_0/t. This phase with pairing correlations is limited to a small region for weak couplings. However, for intermediate values of the phonon energy ω_0/t, it expands inside the region where $U < \lambda$. In the case of increasing ω_0/t further, the superconducting correlations get stronger and stronger, eventually filling the whole CDW region. As it is mentioned before when $\omega_0/t \to \infty$ the system maps to the negative-U Hubbard model and therefore, the CDW state returns into the game, being degenerate with the superconducting state due to the emerging SU(2) pseudo-spin symmetry that relates the superconducting and the CDW states as explained. Due to the fact that the density-density Jastrow factor breaks this symmetry the degeneracy between SC and CDW breaks too. Therefore, we cannot recover an exact degeneracy between these two states for very large phonon energies within the VMC approach.

We have found out that for $\omega_0/t = 1$ and large λ/t, the transition between the CDW and the antiferromagnetic insulator is first order, since we are able to stabilize both wave functions even if the stable phase gives the lowest variational energy. For example, the variational parameters Δ_{AF} and Δ_{CDW} across the transition for $\lambda/t = 4.5$ are reported in Fig. 5.4. By decreasing λ/t, the local minima disappear and the transition appears to be continuous. For $\lambda/t = 2$, which approximately corresponds to the tip of the superconducting region, CDW and antiferromagnetic parameters vanish for $U/t \approx 1.2$, see Fig. 5.4. For smaller values of λ/t, a superconducting phase can be stabilized for small enough electron-electron repulsions, with a small but clearly finite pairing term Δ_{SC}. Indeed, we obtain $\Delta_{\mathrm{SC}} = 0.016(1)$ for $U = 0$ and $\Delta_{\mathrm{SC}} = 0.008(1)$ for $U/t = 0.2$, at $\lambda/t = 0.98$.

When we increase the phonon energy, this region of stability for the superconducting phase extends, intruding between the two insulators also when λ/t is large. In Figs. 5.5 and 5.6, we report the behavior of the variational parameters Δ_{AF}, Δ_{CDW}, and Δ_{SC} for $\omega_0/t = 5$ and 15. In the intermediate region, both Δ_{AF} and Δ_{CDW} vanish, whereas Δ_{SC} is finite. Notice that Δ_{SC} is also finite inside the insulating CDW region, which may be ascribed to the fact that superconducting and CDW solutions become degenerate for $\omega_0/t \to \infty$, and, therefore, at the variational level, some energy gain can be obtained by mixing superconductivity and CDW order, even when the phonon energy is large but finite.

5.2 Results For The Doped case

For the doped case we would like to assess the stability toward phase separation. This effect has been found out in the repulsive-U Hubbard model and it has been confirmed by different methods, even though its U dependence is still controversial [98, 99, 100, 101, 102, 103, 104]. In the case of the pure Hubbard model the phase separation occurs when it is more convenient to form hole domains since in this case the energy loss due to the doped holes will be less. Likewise also in the case of the Hubbard-Holstein model we can consider the formation of domains of doublons in order to gain energy. In order to highlight the possible presence of phase separation in the Hubbard-Holstein model, it is very useful to consider the so-called energy per hole [105]:

$$\epsilon(\delta) = \frac{E(\delta) - E(0)}{\delta}, \tag{5.1}$$

where $E(\delta)$ is the energy per site at hole doping $\delta = 1 - n$. For a uniform phase, $\epsilon(\delta)$ has a monotonically increasing behavior with increasing δ from 0 to 1; by contrast, phase separation is marked by the presence of a minimum of $\epsilon(\delta)$ on any finite-size clusters and a flat behavior (up to δ_c, the critical doping below which phase separation occurs) in the thermodynamic limit. These facts can be easily understood by considering that $\epsilon(\delta)$ represents the slope of the line joining $(0, E(0))$ to $(\delta, E(\delta))$ and that, in a stable uniform phase $E(\delta)$ is a convex function, while phase separation implies (after Maxwell construction) a linear behavior of $E(\delta)$ up to δ_c.

The results of the energy per hole are shown in Fig. 5.7. In the lower panel of the figure one can see the behaviour of the energy per hole when $U = 0$, $\omega_0/t = 1$, and different values of λ. When the electron-phonon coupling is small, i.e., when doping the superconducting phase at half filling, the system does not phase separate. In addition to that, the ground state remains superconducting also when the electron density is $n < 1$. The uniform ground state is most evident when ω_0/t is large enough, since the superconducting signal is rather small in the adiabatic limit and increases with ω_0/t. In order to show this feature, we present the results for $\omega_0/t = 15$ in Fig. 5.8. As in the case of the half-filled Hubbard Holstein model, when the electron density is varied, it is very useful to use TABC, since using one boundary condition (periodic in x and antiperiodic in y directions in this case) gives rise to a strongly scattered behavior. On the contrary, when we dope the CDW ordered phase for large values of λ/t, an infinitesimally small hole doping leads to a charge instability, therefore phase separation occurs, and the region of phase separation is increasing with λ. As for the case of an antiferromagnetic phase, also in the presence of CDW order the injection of few mobile holes that damage the charge periodicity is not compensated by a kinetic energy gain. Thus, phase separation appears for sufficiently small hole doping. In Fig. 5.7, we also show the results for $\lambda/t = 2$ and various values of U/t

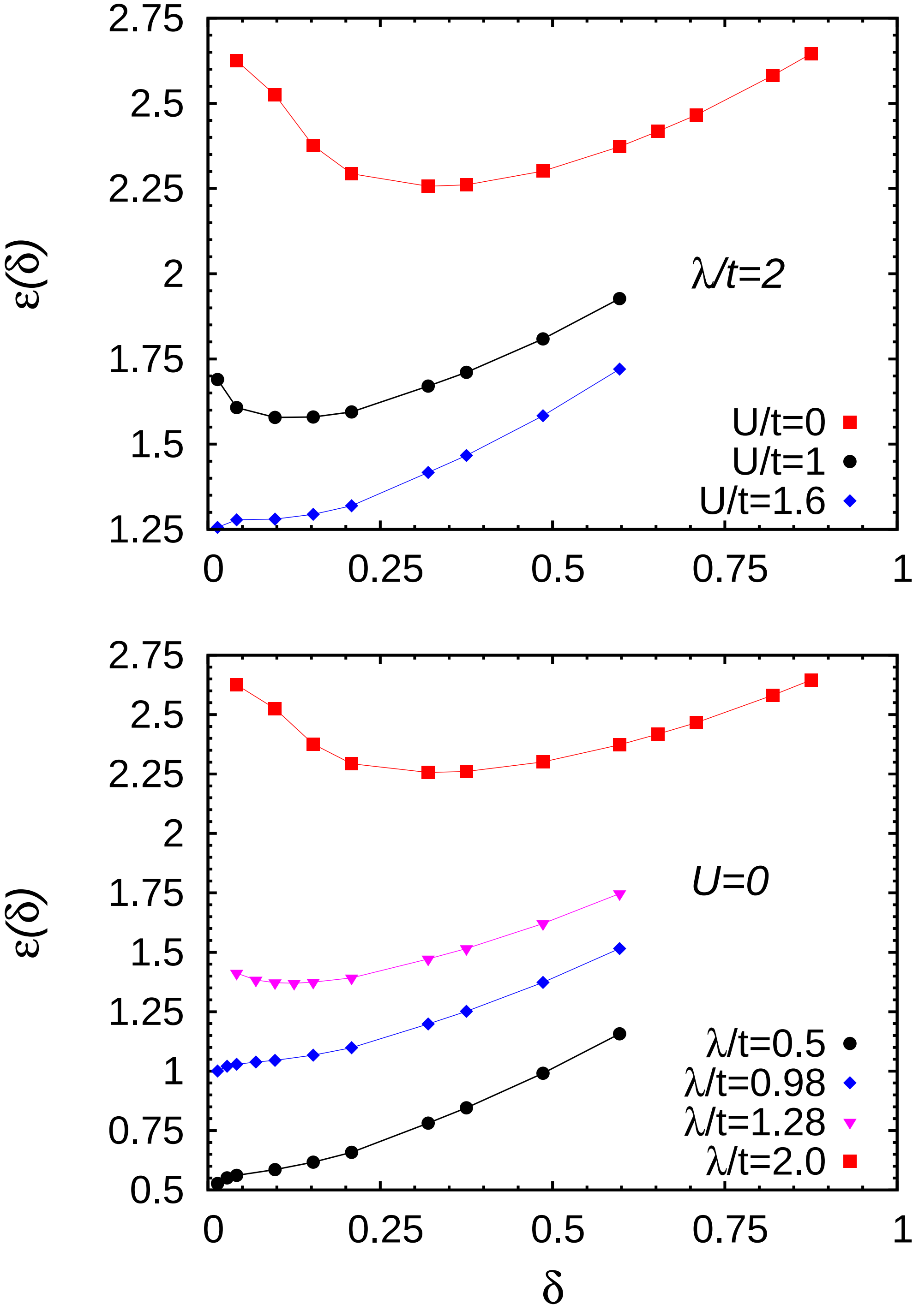

Figure 5.7: Energy per hole of Eq. (5.1) for $\lambda/t = 2$ and various values of U/t (upper panel) and for $U = 0$ and various values of λ/t (lower panel). In both cases $\omega_0/t = 1$ and calculations are performed on the 12×12 cluster with TABC. Error bars are smaller than the size of the symbols.(S.Karakuzu $etal.$,96,205145 (2017))

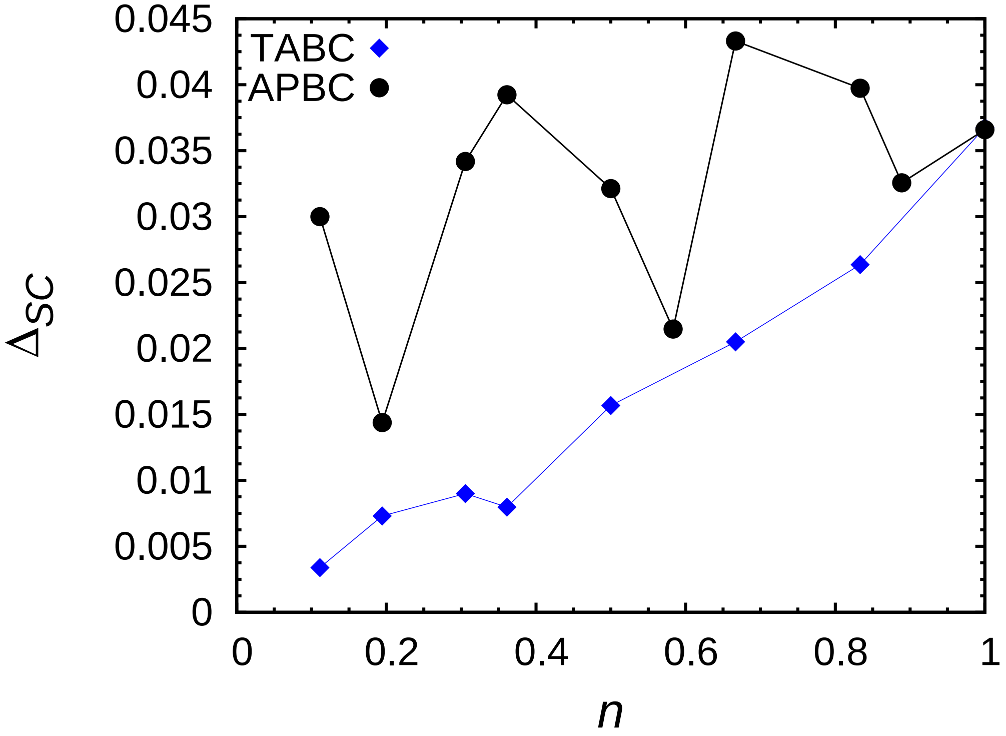

Figure 5.8: Variational parameter Δ_{SC} as a function of the electron density n, computed with periodic-antiperiodic (APBC), and twisted average (TABC) boundary conditions on the 12×12 cluster. Here, $\omega_0/t = 15$ and $\lambda/t = 0.98$. Errorbars are smaller than the size of the symbols.(S.Karakuzu $et al.$,96,205145 (2017))

(upper panel). Here, the electron-electron repulsion opposes to the electron-phonon coupling, leading to a reduction of phase separation until it eventually disappears above a critical value of U/t (by further increasing the electron-electron repulsion, antiferromagnetism settles down at half filling, thus leading again to phase separation, as well known for the positive-U Hubbard model [105]).

In Fig. 5.9, we further show that, at finite values of the phonon energy, the extent of phase separation depends upon the actual values of both U and λ. Indeed, we observe that, for $\omega_0/t = 1$, phase separation is more pronounced for $U/t = 1.38$ and $\lambda/t = 3.38$ than for $U = 0$ and $\lambda/t = 2$, even if both cases would give the same effective interaction $U_{\text{eff}} = U - \lambda$. This fact can be explained by the presence, at half filling, of a larger CDW parameter in the former case with respect to the latter one.

Finally, we would like to compare the energy per hole for $U = 0$ and $\lambda/t = 2$ for different values of ω_0/t, in Fig. 5.10. For all three cases, the ground state at half filling has CDW order (see Fig. 5.3) and, therefore, phase separation is expected to appear away from half filling. However, in the antiadiabatic limit as $\omega_0/t \to \infty$, there is no phase separation, due to the fact that the Holstein model maps to the negative-U Hubbard model, which has a uniform ground state away from half filling. Indeed, we have shown that phase separation reduces as we increase ω_0/t, such that the position of the minimum in the energy per hole shifts toward $\delta = 0$. Within this finding we have reported another indication that our variational approach correctly reproduces the expected physical behavior since the large w_0 limit of the Hubbard-Holstein model is corresponding to the negative-U Hubbard model which has uniform ground state so no phase separation is expected.

5.3 Conclusions

In conclusion, we have done accurate VMC calculations to extract thermodynamic properties of the Hubbard-Holstein model. We have implemented an average

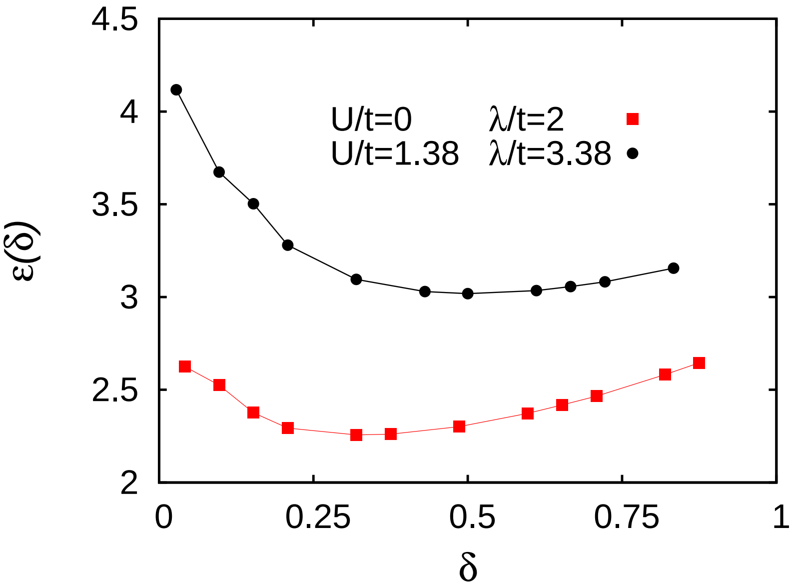

Figure 5.9: Energy per hole of Eq. (5.1) for $U = 0$ and $\lambda/t = 2$, compared with $U/t = 3.38$ and $\lambda/t = 1.38$, that corresponds to the same value of the effective interaction $U_{\text{eff}} = U - \lambda$. In both cases $\omega_0/t = 1$ and calculations are performed on the 12×12 cluster with TABC. Error bars are smaller than the size of the symbols.(S.Karakuzu *etal.*,96,205145 (2017))

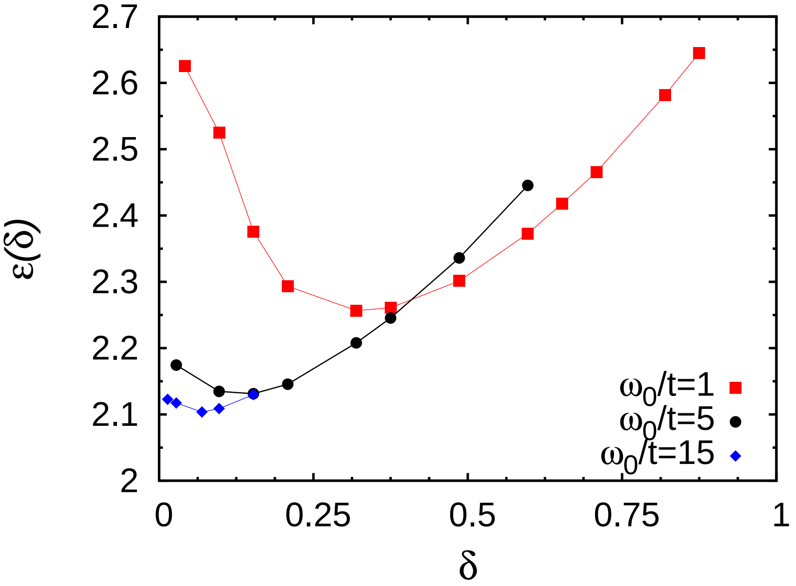

Figure 5.10: Energy per hole of Eq. (5.1) for $U = 0$ and $\lambda/t = 2$ for $\omega_0/t = 1$, 5, and 15. Calculations are performed on the 12×12 cluster with TABC. Error bars are smaller than the size of the symbols.(S.Karakuzu *etal.*,96,205145 (2017))

over canonical twisted boundary conditions in order to decrease the finite-size effects and we have observed a strong reduction of finite-size errors within this approach. At half filling, we have found out that there exists a gapless phase between the CDW and the antiferromagnetic insulator, as also recently reported by different VMC calculations [13]. Moreover, within our approach, thanks to our transparent parametrization of the variational wave functions, we can identify the presence of superconducting correlations in the intermediate phase. When the phonon energy becomes large, pairing correlations gets larger and the region of superconductivity broadens into the region of CDW order. The emergence of superconductivity in the half-filled Hubbard-Holstein model is an example on how two competing tendencies such as antiferromagnetism, favored by electron-electron interaction, and CDW order, favored by electron-phonon coupling may lead to a third stable phase. In addition, we have also studied the effect of doping the system with holes for both regimes where the half-filled ground state has either CDW or superconducting order. In the case of doping a CDW phase we have found out presence of a substantial phase separation region at small dopings and this observation is quite similar to the case of a doped repulsive-U Hubbard [98, 99, 100, 101, 102, 103, 104]. Instead, in the case of doping a superconducting region, the ground state remains uniform with superconducting order. However, we have observed that the superconductivity is found to monotonically decrease as one dopes the system. We remind that size effects are more pronounced away from half filling and therefore, TABC are fundamental to reduce finite-size effects.

One of the main outcome of this work is that, within the Hubbard-Holstein model, superconductivity is rather weak and is suppressed by the electron-electron repulsion and also against electron doping. Indeed, since phonons are coupled to the local electronic density in the Hubbard-Holstein model, the competition between the formation of superconducting pairs and the local Coulomb repulsion U are very direct which almost immediately suppress the superconducting correlations. In addition, superconducting pairing correlations are maximum at half filling and are strongly reduced in the presence of hole doping. A different scenario can be expected within the Su-Schrieffer-Heeger model [11], in which the lattice displacements are coupled to the hopping term. There should be no superconductivity at half filling, since a Peierls insulator should take place for any electron-phonon coupling at $U = 0$ as established in one dimension [106, 107, 19]. However, superconductivity can be expected to emerge upon doping, and it is expected to be also more robust against Coulomb repulsion compared to the Hubbard-Holstein model. Therefore, the Su-Schrieffer-Heeger model would provide a different mechanism for electron pairing. It can provide a more reasonable scenario that is more appropriate for explaining the Cuprate and Iron-pnictide superconductors. Variational investigations can be improved further by the use of backflow terms, that have been introduced before in order to improve the quality of the wave functions in the Hubbard model [68, 69].

Chapter 6

Sign Free Hubbard-Holstein Model by Accelerated First Order Langevin Dynamics at Half Filling

The Hubbard-Holstein model is a very good candidate model to investigate the high temperature superconductivity since it contains both the electron-electron interaction via Hubbard U and the electron-phonon coupling as explained in the previous chapter. At zero temperature the ground state of the Hubbard model is antiferromagnetically ordered for any finite value of U. When the phonons with frequency w_0 are present in the system the effective value of the electron-electron repulsion is reduced as is expected to map onto the Hubbard model with a dynamical effective repulsion with frequency w:

$$U_{eff}(w) = U - \frac{g^2 w_0}{w^2 - w_0^2}. \tag{6.1}$$

In the previous chapter we have investigated this model by using VMC, and published an almost complete description of its phase diagram [41]. However, the reliability of the VMC method depends on the quality of the wave function used in the calculations. It is sometimes possible to be stuck in the local minimas of the energy surface and wrong conclusions may be drawn. In order to obtain more reliable results more accurate methods have been used. There are several works to understand the finite temperature and ground state properties and the phase diagram of the model via exact Monte Carlo calculations. Determinant quantum monte carlo (DQMC) [35, 66] has been widely used for this purpose [17, 18]. However, due to the sign problem, even at half filling, it is almost impossible to study the model in large clusters and make reliable extrapolations to the thermodynamic limit. In this chapter we will examine the ground state properties of the Hubbard Holstein model via a statistically exact auxiliary field projector method combined with molecular dynamics which we developed in the 3rd Chapter. In order to decrease the autocorrelation time we will use first order accelerated Langevin dynamics as also pointed in the 3rd chapter. By using the Cauchy integration we have shown that one can eliminate the sign problem at half filling for $U \geq g^2/w_0$. By defining the dimensionless electron-phonon coupling strength parameter $\lambda = g^2/w_0$ we can examine the ground state properties of the model in the region where there is no sign problem.

It is intuitive to think that, when the Hubbard interaction is large compared to the electron-phonon coupling, the system is antiferromagnetically ordered. On the other hand, when the electron-phonon coupling is large compared to Hubbard interaction, the system is charge ordered. One of the open questions about the Hubbard-Holstein model is whether there is a metallic or a superconducting region when the Hubbard repulsion is of the order of electron-phonon coupling. In the work presented in the previous chapter we have concluded that there is a superconducting region for large w_0 whereas this region gets smaller and smaller as the w_0 decreases. This conclusion is in support with another VMC study by Ohgoe *etal.* [13] and also a DMFT study in 1D system [16]. However, DQMC calculations with finite temperature claim the existence of a large metallic region as the temperature in lowered [17, 18] even when the w_0 is small.

The large phonon frequency limit of the Hubbard-Holstein model maps to the attractive Hubbard model which has been examined in the 4th chapter in details. For this chapter, we would like to examine the small frequency limit of the model to investigate the open question explained in the previous paragraph. Therefore, as a starting point, we fix the value of the phonon frequency w_0=1 for all the simulations considered here.

6.1 Results

In order to access the information about the order parameters we examine the charge and spin structure factor of the model for different values of the Hubbard interaction and the electron-phonon coupling by fixing the projection time $\beta = L$. As defined in the 3rd chapter the charge structure factor is

$$S_{cdw}(\mathbf{Q}) = \frac{1}{N}\sum_{i,j} e^{i\mathbf{Q}.(\mathbf{r}_i - \mathbf{r}_j)} n_i n_j. \tag{6.2}$$

whereas the spin structure factor is

$$S_s(\mathbf{Q}) = \frac{1}{N}\sum_{i,j} e^{i\mathbf{Q}.(\mathbf{r}_i - \mathbf{r}_j)} S_i S_j. \tag{6.3}$$

with the pitching vector $Q = (\pi, \pi)$ at half filling and $S_i = \frac{1}{2}(n_{i\uparrow} - n_{i\downarrow})$ is the value of the spin at site i. In figures Fig. 6.1 and Fig. 6.2 the spin and charge structure factors have been plotted respectively for different values of λ on a 12x12 cluster for U=4. The structure factors at λ=0 for Δ_{MD}=0 have been calculated by AFQMC sampling as explained also in the 3rd Chapter. The abrupt decrease of the spin structure factor has been observed whereas the charge structure factor increases very slowly as λ increased. The same experiment can be done on the antiferromagnetic order parameter of the system:

$$m_{AF}(\mathbf{Q}) = \frac{1}{N}\sum_{i} e^{i\mathbf{Q}.\mathbf{r}_i} S_i. \tag{6.4}$$

In Figure 6.3 the antiferromagnetic order parameter as a function of the molecular dynamics time step Δ_{MD} has been examined for different values of the electron-phonon coupling parameter λ for U=4 on the 12x12 cluster size and for λ =4 with different cluster sizes. The strong reduction of the order parameter has been observed as λ is increased as explained in the previous chapter. On the other hand very smooth and easy extrapolation of the magnetization can be observed at λ =4

Table 6.1: Values of m_{AF} and $S_{\mathrm{CDW}}(\mathbf{Q})$ in the thermodynamic limits, for different values of λ, U/t at $\omega_0 = t$.

	$U/t=1$		$U/t=4$	
λ/U	m_{AF}	$S_{\mathrm{CDW}}(\mathbf{Q})$	m_{AF}	$S_{\mathrm{CDW}}(\mathbf{Q})$
0	0.0280(2)	–	0.238(3)	–
0.25	0.0215(3)	0.838(4)	0.232(2)	0.433(7)
0.50	0.0138(3)	0.862(4)	0.202(4)	0.475(4)
0.75	0.0068(4)	0.890(5)	0.146(2)	0.557(9)
1	0.0009(1)	0.924(5)	0.031(2)	0.83(1)

for different cluster sizes. One can also see the very fast equilibration time as a function of the MD step.

We have investigated the finite size scaling of the magnetization for U=1 and U=4 in figure Fig. 6.4 and Fig. 6.5 respectively. The extrapolated values of the magnetization and charge structure factor in the thermodynamic limit have been sketched in the figure Fig. 6.6 and the corresponding values are in the Table 6.1. It can be seen that as λ is increasing the value of the magnetization decreases whereas the charge structure factor increases. When $U \simeq \lambda$ we observe that the value of the magnetization is almost zero. On the other hand, for any value of U, the charge structure factor increases as λ increases. However, it does not diverge for $U \simeq \lambda$ indicating that there is no coexistence of magnetization and charge order up to U =4. Therefore, we do not observe a first order phase transition between magnetization and charge order for $U \simeq \lambda$. In addition to that, there is a region before the divergence of the charge structure factor, with neither magnetic nor charge ordered correlations which can be attributed to a metallic or superconducting region.

6.2 Conclusion

We have investigated the finite size and thermodynamic properties of the Hubbard-Holstein model without sign problem at half filling for $U \geq \lambda$. We

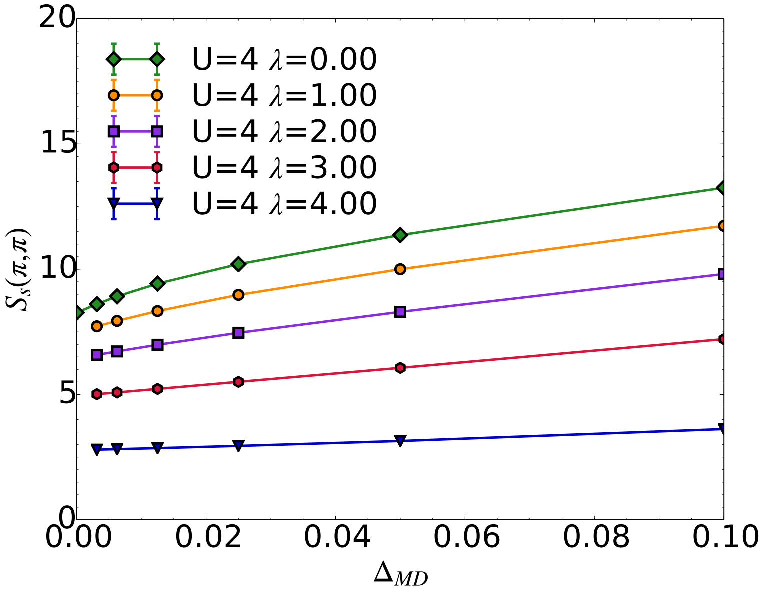

Figure 6.1: Spin structure factor as a function of molecular dynamics time step Δ_{MD} on the 12x12 cluster with periodic boundary conditions for different values of electron-phonon coupling strength λ for U=4. At λ=0 the Δ_{MD}=0 value of the spin structure factor has been calculated by MC.

have found out that a finite λ decreases the effective value of the Hubbard interaction. The total magnetization of a finite system is decreased whereas the charge structure factor of this finite system is increased. In the thermodynamic limit, we observe the decrease of magnetization and the increase of the charge structure factor as λ is increased for both U =1 and U =4. However, we did not observe signature of the divergence of the charge structure factor for $U \geq \lambda$, at least upto U =4. Therefore, there is no signature of a first order transition for these values of Hubbard interaction. Also, we expect a region of metallic or superconducting correlations when $U \simeq \lambda$ extending beyond the $U = \lambda$ line and this region gets more broadened for U =1 compared to U =4.

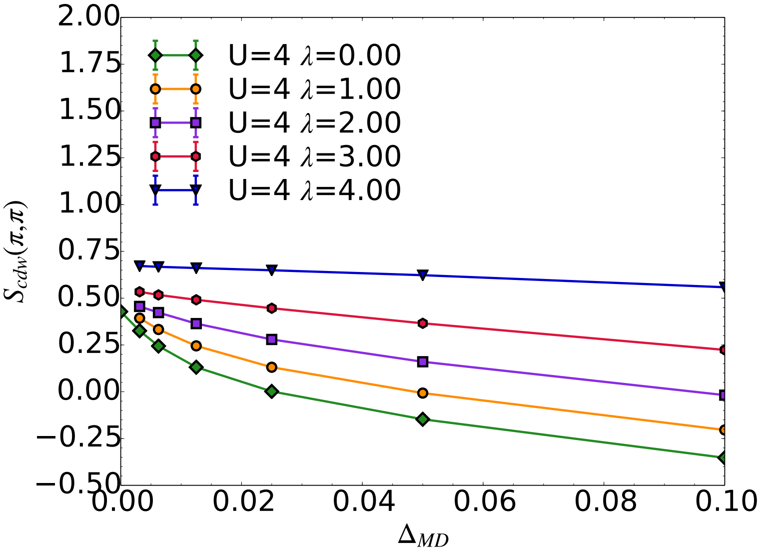

Figure 6.2: Charge structure factor as a function of molecular dynamics time step Δ_{MD} on the 12x12 cluster with periodic boundary conditions for different values of electron-phonon coupling strength λ for U=4.

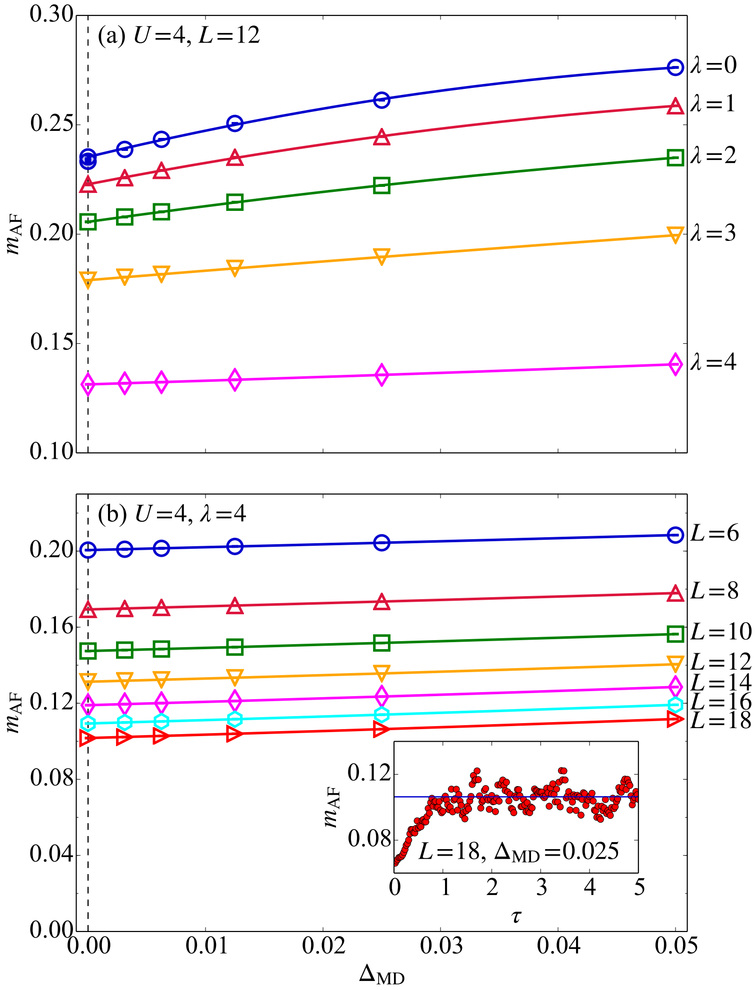

Figure 6.3: Antiferromagnetic order parameters m_{AF} at $U/t = 4$ as a function of the MD time step Δ_{MD} (a) on a 12×12 cluster with periodic boundary conditions at $\beta t = 12$ and different values of the electron-phonon coupling strength λ. The $\lambda = \Delta_{\mathrm{MD}} = 0$ result (filled circle) in (a) is obtained with the standard Monte Carlo algorithm for the Hubbard model, that is clearly consistent with the MD data, extrapolated to $\Delta_{\mathrm{MD}} \to 0$. (b) same as (a) for $\lambda = 4$ with various system sizes $N = L \times L$ with periodic boundary conditions, with $\beta t = L$. The inset shows the equilibration of m_{AF} to its average value (blue line) for the largest cluster as a function of the MD time τ.

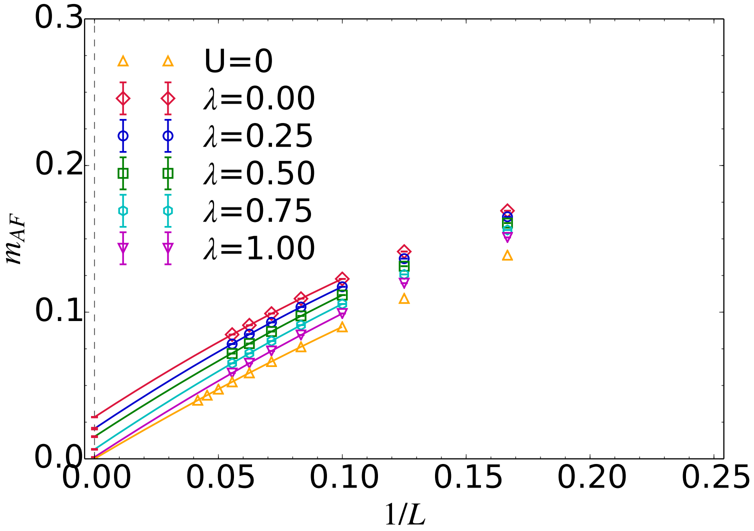

Figure 6.4: Antiferromagnetic order parameters as a function of the linear size of the cluster L with periodic boundary conditions for different values of electron-phonon coupling strength λ for U=1. The U=0 are obtained by the same trial wave function and put as a guide to eye.

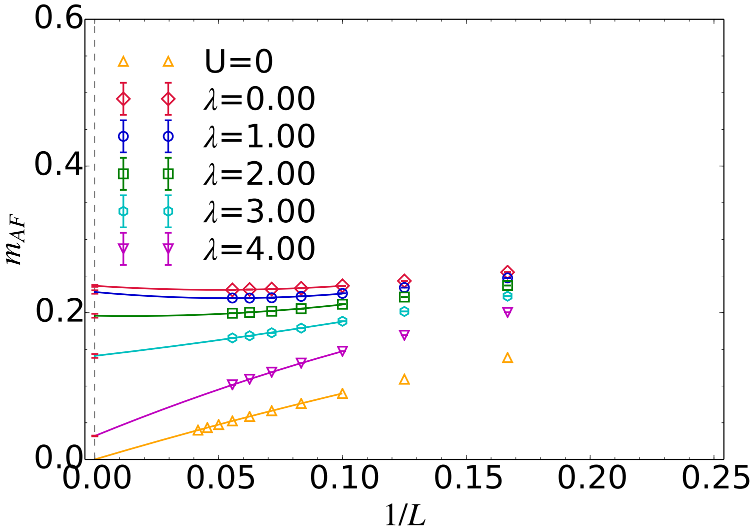

Figure 6.5: Antiferromagnetic order parameters as a function of the linear size of the cluster L with periodic boundary conditions for different values of electron-phonon coupling strength λ for U=4. The U=0 are obtained by the same trial wave function and put as a guide to eye.

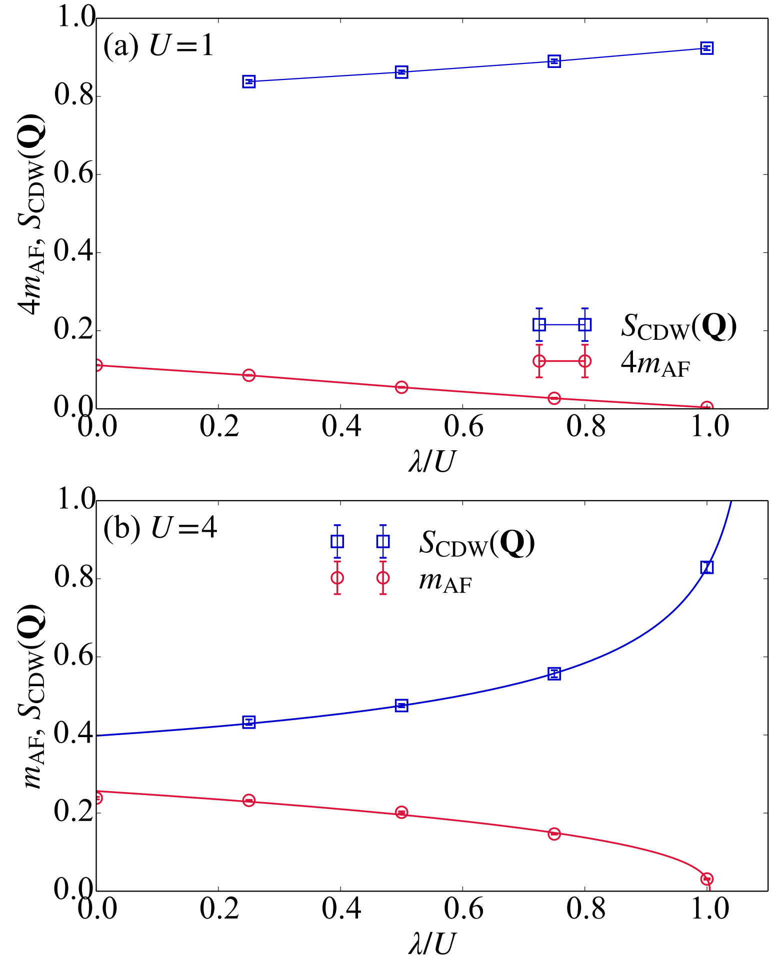

Figure 6.6: Ground state properties of the Hubbard-Holstein model obtained by extrapolating the antiferromagnetic order parameters to the thermodynamic limit for (a) U=1 and (b) U=4. The solid lines in (b) are the fit to m_{AF} and $S_{\mathrm{CDW}}(\mathbf{Q})$ of the form $\gamma\left(\frac{\lambda_{\mathrm{c}}-\lambda}{U}\right)^{\theta}$ with γ, θ, and λ_{c} being the fitting parameters determined by the least-squares method. The parameters are found to be $\gamma = 0.256(8)$, $\theta = 0.39(5)$, and $\lambda_{\mathrm{c}} = \lambda_{\mathrm{c}}^{\mathrm{AF}} = 4.02(2)$ for m_{AF} and $\gamma = 0.407(2)$, $\theta = -0.286(12)$, and $\lambda_{\mathrm{c}} = \lambda_{\mathrm{c}}^{\mathrm{CDW}} = 4.33(4)$ for $S_{\mathrm{CDW}}(\mathbf{Q})$.

Chapter 7

Conclusion

Understanding the mechanism of superconductivity is one of the most important challenges of many theoretical, numerical and experimental physicists. Until now all the efforts of the condensed matter community is still far from the target, unfortunately. Nevertheless, numerical methods and computer simulations can nowadays add something to the understanding of the superconductivity by using appropriate theoretical models. The Hubbard-Holstein model is one of such models including strong correlations which have been found out in many high Tc superconductors like Cuprates and Iron based materials. In addition to that, the model includes also the electron-phonon coupling whose effect is more relevant for BCS type superconductors but still under debate whether it may be important also for strongly correlated superconductors. The Hubbard-Holstein model is a quite simple toy model but still far away and difficult to be treated via analytical methods. Numerical applications are promising in this sense since many models can be tackled and studied with reasonable accuracy. Although there are also some limitations such as finite size effects or difficulties in performing unbiased calculations. In this thesis we have performed quantum Monte Carlo simulations in order to understand the properties of strongly correlated models like the Hubbard and the Hubbard-Holstein models. As common to many numerical methods one has to use finite clusters also in the Monte Carlo simulations. However, the aim is to understand the thermodynamic properties of the model or the system in interest. The extrapolations to the thermodynamics limit via finite system sizes are heavily used in the community to obtain reliable results of the bulk. Here, by using twist-averaging boundary conditions we have eliminated the finite-size errors in the negative-U Hubbard model first. We have shown that the twist-averaging in grand canonical ensemble provides the best size scaling compared to the canonical case for the attractive Hubbard model.

Then, we have investigated the ground state properties of the Hubbard-Holstein model via variational Monte Carlo method by defining an appropriate variational ansatz including the electron-phonon coupling with an appropriate Jastrow correlator and a coherent representation of the phonon wave function. Also in this case we have used twist-averaged boundary conditions but in this case we have found more convenient to remain in the canonical ensemble. The phase diagram of the model has been reported for different phonon frequencies at half filling. One of the most surprising results of this work is the existence of a superconducting region which is sandwiched between antiferromagnetic and charge ordered regions. We have found out the enhancement of superconducting correlations and the extension of this region as the phonon frequency is increased. At finite doping the phase separation has been investigated when a charge ordered state is doped with holes. We have observed that, as the phonon frequency is increased, the phase separation region shrinks, which can be interpreted by stating that the Hubbard-Holstein model is being mapped to the attractive Hubbard model as the phonon frequency is increased. As well known, the attractive Hubbard model has a uniform ground state and does not display phase separation. This result clearly indicate that the variational wave function we constructed represents this limit of the model correctly.

Motivated to establish the ground state properties of the Hubbard-Holstein model we have decided to use an essentially unbiased auxiliary field quantum Monte Carlo method. However, due to the so called large auto-correlation time we have found that it is more appropriate to use the accelerated Langevin dynamics to investigate the ground state of the model. However, the model was affected by the so called sign problem even at half filling, preventing to obtain its bulk properties at zero temperature. We have shown that it is possible to eliminate the sign problem using the Cauchy integration formula at half filling whenever the Hubbard interaction U is larger than or equal to the electron-phonon coupling strength parameter λ, namely when $U \geq \lambda$. As a preliminary calculation, we have fixed the phonon frequency to be relatively small compared to the electronic bandwidth such that w =1. We have observed that the magnetization of the system decreases whereas the charge structure factor increases as we increase λ for a fixed value of the Hubbard interaction U. No signature of first order phase transition between magnetization and charge ordering has been found out at least up to U =4. However, we have observed that there exists a region which has neither magnetic nor charge ordered correlations whenever $U \simeq \lambda$. This region extends beyond the $U = \lambda$ line and extends as the value of the U is decreased.

There are several things which can be done as future work after this thesis. From the technical point of view, one might try to further develop the Langevin dynamics and have more efficient simulations of the strongly correlated models. Obviously, with this highly developed tools we plan to establish the phase diagram of the Hubbard-Holstein model in a wide range of parameters, also considering that out preliminary results show that the superconducting phase may be more extended than the previous expectations. On the other hand, one can study different models such as the so called Su-Schriffer-Heger (SSH) model which was also mentioned in the 5th chapter. This model might be more suited for the description of the superconductivity since the phonon degrees of freedom are coupled to the hopping of the electrons as in the case of the original BCS picture.

Bibliography

[1] A. Abrikosov, L. Gorkov, and I. Dzyaloshinski, *Methods of quantum field theory in statistical physics.* New York, N.Y.: Dover, 1963.

[2] A. Lanzara, P. V. Bogdanov, X. J. Zhou, S. A. Kellar, D. L. Feng, E. D. Lu, T. Yoshida, H. Eisaki, A. Fujimori, K. Kishio, J.-I. Shimoyama, T. Noda, S. Uchida, Z. Hussain, and Z.-X. Shen, "Evidence for ubiquitous strong electron-phonon coupling in high-temperature superconductors," *Nature*, vol. 412, pp. 510 EP –, Aug 2001.

[3] G.-m. Zhao, M. B. Hunt, H. Keller, and K. A. Müller, "Evidence for polaronic supercarriers in the copper oxide superconductors la2-xsrxcuo4," *Nature*, vol. 385, pp. 236 EP –, Jan 1997.

[4] G.-H. Gweon, T. Sasagawa, S. Y. Zhou, J. Graf, H. Takagi, D.-H. Lee, and A. Lanzara, "An unusual isotope effect in a high-transition-temperature superconductor," *Nature*, vol. 430, pp. 187 EP –, Jul 2004.

[5] M. Capone, M. Fabrizio, C. Castellani, and E. Tosatti, "Colloquium: Modeling the unconventional superconducting properties of expanded $A_3\mathrm{c}_{60}$ fullerides," *Rev. Mod. Phys.*, vol. 81, pp. 943–958, Jun 2009.

[6] Y. Takabayashi, A. Y. Ganin, P. Jeglič, D. Arčon, T. Takano, Y. Iwasa, Y. Ohishi, M. Takata, N. Takeshita, K. Prassides, and M. J. Rosseinsky, "The disorder-free non-bcs superconductor cs3c60 emerges from an antiferromagnetic insulator parent state," *Science*, vol. 323, no. 5921, pp. 1585–1590, 2009.

[7] C. de la Cruz, Q. Huang, J. W. Lynn, J. Li, W. R. II, J. L. Zarestky, H. A. Mook, G. F. Chen, J. L. Luo, N. L. Wang, and P. Dai, "Magnetic order close to superconductivity in the iron-based layered lao1-xfxfeas systems," *Nature*, vol. 453, pp. 899 EP –, May 2008.

[8] R. Mitsuhashi, Y. Suzuki, Y. Yamanari, H. Mitamura, T. Kambe, N. Ikeda, H. Okamoto, A. Fujiwara, M. Yamaji, N. Kawasaki, Y. Maniwa, and Y. Kubozono, "Superconductivity in alkali-metal-doped picene," *Nature*, vol. 464, pp. 76 EP –, Mar 2010.

[9] J. Hubbard, "Electron correlations in narrow energy bands," *Proc. R. Soc. London*, vol. 276, no. 1365, pp. 238–257, 1963.

[10] T. Holstein, "Studies of polaron motion: Part i. the molecular-crystal model," *Annals of Physics*, vol. 8, no. 3, pp. 325 – 342, 1959.

[11] W. P. Su, J. R. Schrieffer, and A. J. Heeger, "Solitons in polyacetylene," *Phys. Rev. Lett.*, vol. 42, pp. 1698–1701, Jun 1979.

[12] P. Barone, R. Raimondi, M. Capone, C. Castellani, and M. Fabrizio, "Gutzwiller scheme for electrons and phonons: The half-filled hubbard-holstein model," *Phys. Rev. B*, vol. 77, p. 235115, Jun 2008.

[13] T. Ohgoe and M. Imada, "Competition among superconducting, antiferromagnetic, and charge orders with intervention by phase separation in the 2d holstein-hubbard model," *Phys. Rev. Lett.*, vol. 119, p. 197001, Nov 2017.

[14] P. Werner and A. J. Millis, "Efficient dynamical mean field simulation of the holstein-hubbard model," *Phys. Rev. Lett.*, vol. 99, p. 146404, Oct 2007.

[15] G. Sangiovanni, M. Capone, C. Castellani, and M. Grilli, "Electron-phonon interaction close to a mott transition," *Phys. Rev. Lett.*, vol. 94, p. 026401, Jan 2005.

[16] J. Bauer and A. C. Hewson, "Competition between antiferromagnetic and charge order in the hubbard-holstein model," *Phys. Rev. B*, vol. 81, p. 235113, Jun 2010.

[17] E. A. Nowadnick, S. Johnston, B. Moritz, R. T. Scalettar, and T. P. Devereaux, “Competition between antiferromagnetic and charge-density-wave order in the half-filled hubbard-holstein model,” *Phys. Rev. Lett.*, vol. 109, p. 246404, Dec 2012.

[18] S. Johnston, E. A. Nowadnick, Y. F. Kung, B. Moritz, R. T. Scalettar, and T. P. Devereaux, “Determinant quantum monte carlo study of the two-dimensional single-band hubbard-holstein model,” *Phys. Rev. B*, vol. 87, p. 235133, Jun 2013.

[19] M. Weber, F. F. Assaad, and M. Hohenadler, “Excitation spectra and correlation functions of quantum su-schrieffer-heeger models,” *Phys. Rev. B*, vol. 91, p. 245147, Jun 2015.

[20] M. Hohenadler, F. F. Assaad, and H. Fehske, “Effect of electron-phonon interaction range for a half-filled band in one dimension,” *Phys. Rev. Lett.*, vol. 109, p. 116407, Sep 2012.

[21] F. Becca and S. Sorella, *Quantum Monte Carlo Approaches for Correlated Systems.* Cambridge University Press, 2017.

[22] S. Sorella, “Wave function optimization in the variational monte carlo method,” *Phys. Rev. B*, vol. 71, p. 241103, Jun 2005.

[23] M. Capello, F. Becca, M. Fabrizio, S. Sorella, and E. Tosatti, “Variational description of mott insulators,” *Phys. Rev. Lett.*, vol. 94, p. 026406, Jan 2005.

[24] M. Capello, F. Becca, S. Yunoki, and S. Sorella, “Unconventional metal-insulator transition in two dimensions,” *Phys. Rev. B*, vol. 73, p. 245116, Jun 2006.

[25] S. Sorella, S. Baroni, R. Car, and M. Parrinello, “A novel technique for the simulation of interacting fermion systems,” *EPL (Europhysics Letters)*, vol. 8, no. 7, p. 663, 1989.

[26] H. F. Trotter, “On the product of semi-groups of operators,” *Proc. Am. Math. Soc.*, vol. 10, p. 545, 1959.

[27] M. Suzuki, "Generalized trotter's formula and systematic approximants of exponential operators and inner derivations with applications to man y-body problems," *Comm. Math. Phys.*, vol. 51, no. 2, pp. 183–190, 1976.

[28] J. Hubbard, "Calculation of partition functions," *Phys. Rev. Lett.*, vol. 3, pp. 77–78, Jul 1959.

[29] R. L. Stratonovich *Dokl. Akad. Nauk. SSSR*, vol. 115, p. 1097, 1957.

[30] J. E. Hirsch, "Two-dimensional hubbard model: Numerical simulation study," *Phys. Rev. B*, vol. 31, pp. 4403–4419, Apr 1985.

[31] M. P. Allen and D. J. Tildesley, *Computer Simulation of Liquids.* New York, NY, USA: Clarendon Press, 1989.

[32] D. Frenkel and B. Smit, *Understanding Molecular Simulation.* Orlando, FL, USA: Academic Press, Inc., 2nd ed., 2001.

[33] N. C. Costa, T. Blommel, W.-T. Chiu, G. Batrouni, and R. T. Scalettar, "Phonon dispersion and the competition between pairing and charge order," *Phys. Rev. Lett.*, vol. 120, p. 187003, May 2018.

[34] G. Mazzola and S. Sorella, "Accelerating ab initio molecular dynamics and probing the weak dispersive forces in dense liquid hydrogen," *Phys. Rev. Lett.*, vol. 118, p. 015703, Jan 2017.

[35] J. E. Hirsch and E. Fradkin, "Phase diagram of one-dimensional electron-phonon systems. ii. the molecular-crystal model," *Phys. Rev. B*, vol. 27, pp. 4302–4316, Apr 1983.

[36] G. B. Arfken and H. J. Weber, "7 - functions of a complex variable ii: Calculus of residues," in *Mathematical Methods for Physicists (Fourth Edition)* (G. B. Arfken and H. J. Weber, eds.), pp. 410 – 455, Boston: Academic Press, fourth edition ed., 1995.

[37] C. Lin, F. H. Zong, and D. M. Ceperley, "Twist-averaged boundary conditions in continuum quantum monte carlo algorithms," *Phys. Rev. E*, vol. 64, p. 016702, Jun 2001.

[38] C. Gros, "The boundary condition integration technique: results for the hubbard model in 1d and 2d," *Z. Phys. B: Condens. Matter*, vol. 86, no. 3, pp. 359–365, 1992.

[39] C. Gros, "Control of the finite-size corrections in exact diagonalization studies," *Phys. Rev. B*, vol. 53, pp. 6865–6868, Mar 1996.

[40] T. Koretsune, Y. Motome, and A. Furusaki, "Exact diagonalization study of mott transition in the hubbard model on an anisotropic triangular lattice," *Journal of the Physical Society of Japan*, vol. 76, no. 7, p. 074719, 2007.

[41] S. Karakuzu, L. F. Tocchio, S. Sorella, and F. Becca, "Superconductivity, charge-density waves, antiferromagnetism, and phase separation in the hubbard-holstein model," *Phys. Rev. B*, vol. 96, p. 205145, Nov 2017.

[42] M. Dagrada, S. Karakuzu, V. L. Vildosola, M. Casula, and S. Sorella, "Exact special twist method for quantum monte carlo simulations," *Phys. Rev. B*, vol. 94, p. 245108, Dec 2016.

[43] M. Qin, H. Shi, and S. Zhang, "Benchmark study of the two-dimensional hubbard model with auxiliary-field quantum monte carlo method," *Phys. Rev. B*, vol. 94, p. 085103, Aug 2016.

[44] D. Poilblanc, "Twisted boundary conditions in cluster calculations of the optical conductivity in two-dimensional lattice models," *Phys. Rev. B*, vol. 44, pp. 9562–9581, Nov 1991.

[45] Z. Wang, F. F. Assaad, and F. Parisen Toldin, "Finite-size effects in canonical and grand-canonical quantum monte carlo simulations for fermions," *Phys. Rev. E*, vol. 96, p. 042131, Oct 2017.

[46] J. P. F. LeBlanc, A. E. Antipov, F. Becca, I. W. Bulik, G. K.-L. Chan, C.-M. Chung, Y. Deng, M. Ferrero, T. M. Henderson, C. A. Jiménez-Hoyos, E. Kozik, X.-W. Liu, A. J. Millis, N. V. Prokof'ev, M. Qin, G. E. Scuseria, H. Shi, B. V. Svistunov, L. F. Tocchio, I. S. Tupitsyn, S. R. White, S. Zhang, B.-X. Zheng, Z. Zhu, and E. Gull, "Solutions of the two-dimensional hubbard model: Benchmarks and results from a wide range of numerical algorithms," *Phys. Rev. X*, vol. 5, p. 041041, Dec 2015.

[47] S. Inouye, M. R. Andrews, J. Stenger, H.-J. Miesner, D. M. Stamper-Kurn, and W. Ketterle, “Observation of feshbach resonances in a bose-einstein condensate,” *Nature*, vol. 392, p. 151, Mar 1998. Article.

[48] P. Courteille, R. S. Freeland, D. J. Heinzen, F. A. van Abeelen, and B. J. Verhaar, “Observation of a feshbach resonance in cold atom scattering,” *Phys. Rev. Lett.*, vol. 81, pp. 69–72, Jul 1998.

[49] M. Greiner, C. A. Regal, and D. S. Jin, “Emergence of a molecular bose-einstein condensate from a fermi gas,” *Nature*, vol. 426, pp. 537 EP –, Nov 2003.

[50] I. Bloch, J. Dalibard, and W. Zwerger, “Many-body physics with ultracold gases,” *Rev. Mod. Phys.*, vol. 80, pp. 885–964, Jul 2008.

[51] A. J. Leggett, “Diatomic molecules and cooper pairs,” in *Modern Trends in the Theory of Condensed Matter* (A. Pekalski and J. A. Przystawa, eds.), (Berlin, Heidelberg), pp. 13–27, Springer Berlin Heidelberg, 1980.

[52] R. Micnas, J. Ranninger, and S. Robaszkiewicz, “Superconductivity in narrow-band systems with local nonretarded attractive interactions,” *Rev. Mod. Phys.*, vol. 62, pp. 113–171, Jan 1990.

[53] P. Nozières and S. Schmitt-Rink, “Bose condensation in an attractive fermion gas: From weak to strong coupling superconductivity,” *Journal of Low Temperature Physics*, vol. 59, pp. 195–211, May 1985.

[54] R. T. Scalettar, E. Y. Loh, J. E. Gubernatis, A. Moreo, S. R. White, D. J. Scalapino, R. L. Sugar, and E. Dagotto, “Phase diagram of the two-dimensional negative-u hubbard model,” *Phys. Rev. Lett.*, vol. 62, pp. 1407–1410, Mar 1989.

[55] A. Moreo and D. J. Scalapino, “Two-dimensional negative-u hubbard model,” *Phys. Rev. Lett.*, vol. 66, pp. 946–948, Feb 1991.

[56] J. M. Singer, M. H. Pedersen, T. Schneider, H. Beck, and H.-G. Matuttis, “From bcs-like superconductivity to condensation of local pairs: A numerical study of the attractive hubbard model,” *Phys. Rev. B*, vol. 54, pp. 1286–1301, Jul 1996.

[57] J. Singer, T. Schneider, and M. Pedersen, “On the phase diagram of the attractive hubbard model: Crossover and quantum critical phenomena,” *The European Physical Journal B - Condensed Matter and Complex Systems*, vol. 2, pp. 17–30, Mar 1998.

[58] A. Moreo, D. J. Scalapino, and S. R. White, “Quasiparticle gap in a two-dimensional kosterlitz-thouless superconductor,” *Phys. Rev. B*, vol. 45, pp. 7544–7546, Apr 1992.

[59] A. Toschi, M. Capone, and C. Castellani, “Energetic balance of the superconducting transition across the bcs¯bose einstein crossover in the attractive hubbard model,” *Phys. Rev. B*, vol. 72, p. 235118, Dec 2005.

[60] A. Toschi, P. Barone, M. Capone, and C. Castellani, “Pairing and superconductivity from weak to strong coupling in the attractive hubbard model,” *New Journal of Physics*, vol. 7, no. 1, p. 7, 2005.

[61] M. Randeria, N. Trivedi, A. Moreo, and R. T. Scalettar, “Pairing and spin gap in the normal state of short coherence length superconductors,” *Phys. Rev. Lett.*, vol. 69, pp. 2001–2004, Sep 1992.

[62] Y. Otsuka, K. Seki, S. Yunoki, and S. Sorella *arXiv:1803.02001.*

[63] S. Tamura and H. Yokoyama, “Variational monte carlo study of spin-gapped normal state and bcsbec crossover in two-dimensional attractive hubbard model,” *Journal of the Physical Society of Japan*, vol. 81, no. 6, p. 064718, 2012.

[64] H. Yokoyama, “Variational monte carlo studies of attractive hubbard model. inormal-state properties,” *Progress of Theoretical Physics*, vol. 108, no. 1, pp. 59–101, 2002.

[65] A. L. Fetter and J. D. Walecka, *Quantum Theory of Many-Particle Systems.* Boston: McGraw-Hill, 1971.

[66] R. T. Scalettar, E. Y. Loh, J. E. Gubernatis, A. Moreo, S. R. White, D. J. Scalapino, R. L. Sugar, and E. Dagotto, “Phase diagram of the two-dimensional negative-u hubbard model,” *Phys. Rev. Lett.*, vol. 62, pp. 1407–1410, Mar 1989.

[67] H. Shiba, “Thermodynamic properties of the one-dimensional half-filled-band hubbard model. iiapplication of the grand canonical method,” *Progress of Theoretical Physics*, vol. 48, no. 6, pp. 2171–2186, 1972.

[68] L. F. Tocchio, F. Becca, A. Parola, and S. Sorella, “Role of backflow correlations for the nonmagnetic phase of the $t^{\smile}t'$ hubbard model,” *Phys. Rev. B*, vol. 78, p. 041101, Jul 2008.

[69] L. F. Tocchio, F. Becca, and C. Gros, “Backflow correlations in the hubbard model: An efficient tool for the study of the metal-insulator transition and the large-u limit,” *Phys. Rev. B*, vol. 83, p. 195138, May 2011.

[70] C. Monney, E. F. Schwier, M. G. Garnier, N. Mariotti, C. Didiot, H. Cercellier, J. Marcus, H. Berger, A. N. Titov, H. Beck, and P. Aebi, “Probing the exciton condensate phase in 1 t -tise 2 with photoemission,” *New Journal of Physics*, vol. 12, no. 12, p. 125019, 2010.

[71] D. Jérome, T. M. Rice, and W. Kohn, “Excitonic insulator,” *Phys. Rev.*, vol. 158, pp. 462–475, Jun 1967.

[72] B. I. Halperin and T. M. Rice, “Possible anomalies at a semimetal-semiconductor transistion,” *Rev. Mod. Phys.*, vol. 40, pp. 755–766, Oct 1968.

[73] H. Zheng, D. Feinberg, and M. Avignon, “Effect of quantum fluctuations on the peierls dimerization in the one-dimensional molecular-crystal model,” *Phys. Rev. B*, vol. 39, pp. 9405–9422, May 1989.

[74] E. Jeckelmann, “Mott-peierls transition in the extended peierls-hubbard model,” *Phys. Rev. B*, vol. 57, pp. 11838–11841, May 1998.

[75] E. Jeckelmann, C. Zhang, and S. R. White, "Metal-insulator transition in the one-dimensional holstein model at half filling," *Phys. Rev. B*, vol. 60, pp. 7950–7955, Sep 1999.

[76] R. T. Clay and R. P. Hardikar, "Intermediate phase of the one dimensional half-filled hubbard-holstein model," *Phys. Rev. Lett.*, vol. 95, p. 096401, Aug 2005.

[77] M. Tezuka, R. Arita, and H. Aoki, "Phase diagram for the one-dimensional hubbard-holstein model: A density-matrix renormalization group study," *Phys. Rev. B*, vol. 76, p. 155114, Oct 2007.

[78] H. Fehske, G. Hager, and E. Jeckelmann, "Metallicity in the half-filled holstein-hubbard model," *EPL (Europhysics Letters)*, vol. 84, no. 5, p. 57001, 2008.

[79] M. Hohenadler and F. F. Assaad, "Excitation spectra and spin gap of the half-filled holstein-hubbard model," *Phys. Rev. B*, vol. 87, p. 075149, Feb 2013.

[80] J. K. Freericks, M. Jarrell, and D. J. Scalapino, "Holstein model in infinite dimensions," *Phys. Rev. B*, vol. 48, pp. 6302–6314, Sep 1993.

[81] J. K. Freericks and M. Jarrell, "Competition between electron-phonon attraction and weak coulomb repulsion," *Phys. Rev. Lett.*, vol. 75, pp. 2570–2573, Sep 1995.

[82] Y. Murakami, P. Werner, N. Tsuji, and H. Aoki, "Ordered phases in the holstein-hubbard model: Interplay of strong coulomb interaction and electron-phonon coupling," *Phys. Rev. B*, vol. 88, p. 125126, Sep 2013.

[83] M. Capone, G. Sangiovanni, C. Castellani, C. Di Castro, and M. Grilli, "Phase separation close to the density-driven mott transition in the hubbard-holstein model," *Phys. Rev. Lett.*, vol. 92, p. 106401, Mar 2004.

[84] M. Capone and S. Ciuchi, "Polaron crossover and bipolaronic metal-insulator transition in the half-filled holstein model," *Phys. Rev. Lett.*, vol. 91, p. 186405, Oct 2003.

[85] P. Paci, M. Capone, E. Cappelluti, S. Ciuchi, C. Grimaldi, and L. Pietronero, “Polaronic and nonadiabatic phase diagram from anomalous isotope effects,” *Phys. Rev. Lett.*, vol. 94, p. 036406, Jan 2005.

[86] A. Macridin, B. Moritz, M. Jarrell, and T. Maier, “Synergistic polaron formation in the hubbard-holstein model at small doping,” *Phys. Rev. Lett.*, vol. 97, p. 056402, Aug 2006.

[87] Z. B. Huang, W. Hanke, E. Arrigoni, and D. J. Scalapino, “Electron-phonon vertex in the two-dimensional one-band hubbard model,” *Phys. Rev. B*, vol. 68, p. 220507, Dec 2003.

[88] F. Becca, M. Tarquini, M. Grilli, and C. Di Castro, “Charge-density waves and superconductivity as an alternative to phase separation in the infinite-u hubbard-holstein model,” *Phys. Rev. B*, vol. 54, pp. 12443–12457, Nov 1996.

[89] R. Zeyher and M. L. Kulić, “Renormalization of the electron-phonon interaction by strong electronic correlations in high-t_c superconductors,” *Phys. Rev. B*, vol. 53, pp. 2850–2862, Feb 1996.

[90] A. Di Ciolo, J. Lorenzana, M. Grilli, and G. Seibold, “Charge instabilities and electron-phonon interaction in the hubbard-holstein model,” *Phys. Rev. B*, vol. 79, p. 085101, Feb 2009.

[91] E. Berger, P. Valášek, and W. von der Linden, “Two-dimensional hubbard-holstein model,” *Phys. Rev. B*, vol. 52, pp. 4806–4814, Aug 1995.

[92] T. Hotta and Y. Takada, “Effect of electron correlation on phonons in a strongly coupled electron-phonon system,” *Phys. Rev. B*, vol. 56, pp. 13916–13926, Dec 1997.

[93] B. J. Alder, K. J. Runge, and R. T. Scalettar, “Variational monte carlo study of an interacting electron-phonon model,” *Phys. Rev. Lett.*, vol. 79, pp. 3022–3025, Oct 1997.

[94] H. Watanabe, K. Seki, and S. Yunoki, “Charge-density wave induced by combined electron-electron and electron-phonon interactions in $1t-\text{tise}_2$:

A variational monte carlo study," *Phys. Rev. B*, vol. 91, p. 205135, May 2015.

[95] Y. Takada, "Superconductivity in the half-filled hubbard-holstein model in the antiadiabatic region," *Journal of the Physical Society of Japan*, vol. 65, no. 6, pp. 1544–1547, 1996.

[96] Y. Takada and A. Chatterjee, "Possibility of a metallic phase in the charge-density-wave–spin-density-wave crossover region in the one-dimensional hubbard-holstein model at half filling," *Phys. Rev. B*, vol. 67, p. 081102, Feb 2003.

[97] T. Ohgoe and M. Imada, "Variational monte carlo method for electron-phonon coupled systems," *Phys. Rev. B*, vol. 89, p. 195139, May 2014.

[98] A. Macridin, M. Jarrell, and T. Maier, "Phase separation in the hubbard model using the dynamical cluster approximation," *Phys. Rev. B*, vol. 74, p. 085104, Aug 2006.

[99] M. Aichhorn, E. Arrigoni, M. Potthoff, and W. Hanke, "Phase separation and competition of superconductivity and magnetism in the two-dimensional hubbard model: From strong to weak coupling," *Phys. Rev. B*, vol. 76, p. 224509, Dec 2007.

[100] C.-C. Chang and S. Zhang, "Spatially inhomogeneous phase in the two-dimensional repulsive hubbard model," *Phys. Rev. B*, vol. 78, p. 165101, Oct 2008.

[101] T. Misawa and M. Imada, "Origin of high-T_c superconductivity in doped hubbard models and their extensions: Roles of uniform charge fluctuations," *Phys. Rev. B*, vol. 90, p. 115137, Sep 2014.

[102] S. Sorella, "Finite-size scaling with modified boundary conditions," *Phys. Rev. B*, vol. 91, p. 241116, Jun 2015.

[103] L. F. Tocchio, F. Becca, and S. Sorella, "Hidden mott transition and large-u superconductivity in the two-dimensional hubbard model," *Phys. Rev. B*, vol. 94, p. 195126, Nov 2016.

[104] F. Šimkovic, Y. Deng, N. V. Prokof'ev, B. V. Svistunov, I. S. Tupitsyn, and E. Kozik, "Magnetic correlations in the two-dimensional repulsive fermi-hubbard model," *Phys. Rev. B*, vol. 96, p. 081117, Aug 2017.

[105] V. J. Emery, S. A. Kivelson, and H. Q. Lin, "Phase separation in the t-j model," *Phys. Rev. Lett.*, vol. 64, pp. 475–478, Jan 1990.

[106] E. Fradkin and J. E. Hirsch, "Phase diagram of one-dimensional electron-phonon systems. i. the su-schrieffer-heeger model," *Phys. Rev. B*, vol. 27, pp. 1680–1697, Feb 1983.

[107] D. Baeriswyl and K. Maki, "Electron correlations in polyacetylene," *Phys. Rev. B*, vol. 31, pp. 6633–6642, May 1985.